Active-Site Isolation for the Selective Hydrogenation of Acetylene: the Pd-Ga and Pd-Sn Intermetallic Compounds

vorgelegt von
Diplom-Chemiker
Jürgen Osswald
aus Berlin

Fakultät II – Mathematik und Naturwissenschaften
der Technischen Universität Berlin
zur Erlangung des akademischen Grades
Doktor der Naturwissenschaften
-Dr. rer. nat.-
genehmigte Dissertation

Promotionsausschuss:
Vorsitzender: Prof. Dr. Hildebrandt
Berichter/Gutachter: Prof. Dr. Schlögl
Berichter/Gutachter: Prof. Dr. Ressler
Tag der wissenschaftlichen Aussprache: 21.12.05

Berlin 2006
D 83

1 Abstract

Intermetallic compounds of palladium with gallium (PdGa and Pd_3Ga_7) are introduced as selective catalysts for the hydrogenation of acetylene. Both intermetallic compounds are selected as site-isolated palladium catalysts because of the increased average interatomic Pd-Pd distances and decreased Pd-Pd coordination numbers in their structures. Detailed investigations of PdGa and Pd_3Ga_7 by thermal analysis, in situ X-ray diffraction, and in situ X-ray absorption spectroscopy during thermal treatment under various inert or reactive gas atmospheres showed a high thermal stability. The long-range and short-range order structures of the materials remained intact up to temperatures of about 600 K with no phase transitions or decomposition detectable. In addition to high thermal stability, no incorporation of hydrogen in the intermetallic compounds under reducing conditions was detected. Both intermetallic compounds studied exhibit sufficient thermal stability, isolation of Pd centers under reaction conditions, and no incorporation of hydrogen in the bulk. Therefore, besides being interesting model systems, palladium gallium intermetallic compounds may also be promising candidates for application as highly selective hydrogenation catalysts.

The surface properties of PdGa and Pd_3Ga_7 were characterized by X-ray photoelectron spectroscopy, ion scattering spectroscopy, and CO chemisorption. Catalytic activity, selectivity, and long-term stability of PdGa and Pd_3Ga_7 were investigated under both acetylene hydrogenation reaction conditions in absence and in an excess of ethylene in temperature-programmed and isothermal long-term experiments. Compared to Pd/Al_2O_3 and $Pd_{20}Ag_{80}$ reference catalysts, PdGa and Pd_3Ga_7 exhibited a comparable activity per active Pd site, a higher selectivity, and a reduced deactivation with time on stream. The superior catalytic properties are attributed to the isolation of active Pd sites in the crystallographic structure of PdGa and Pd_3Ga_7 according to the active-site isolation concept.

In addition, structural and catalytic properties of ternary intermetallic compounds of palladium with gallium and platinum and of a binary Pd-Sn intermetallic compound were investigated and the results were discussed and evaluated with respect to the Pd-Ga intermetallic compounds and the concept of active-site isolation.

2 Zusammenfassung

Die intermetallischen Verbindungen aus Palladium mit Gallium, PdGa und Pd_3Ga_7, können als Katalysatoren für die selektive Hydrierung von Acetylen eingesetzt werden. Beide intermetallische Verbindungen wurden aufgrund ihrer Besonderheit der strukturell isolierten Pd Atome ausgewählt. Die thermische und strukturelle Stabilität von PdGa und Pd_3Ga_7 wurde mit in situ Röntgendiffraktometrie und Röntgenabsorptionspektroskopie sowie Thermogravimetrie und dynamischer Differenzkalorimetrie in inerter und reaktiver Gasatmosphäre untersucht. Die lokale Umgebung der isolierten Pd Atome und die kristalline Struktur der intermetallischen Verbindungen zeigen eine bemerkenswerte Beständigkeit bis zu 600 K ohne Phasenumwandlungen, Anzeichen einer Zersetzung oder Hinweise auf die Bildung von Hydridphasen. Aus diesem Grund sind PdGa und Pd_3Ga_7 als Modellkatalysatoren für die Hydrierung von Acetylen über isolierte Pd Zentren geeignet.

Die Oberfläche beider intermetallischen Verbindungen wurde mit Röntgenphoto-elektronenspektroskopie und Ionenstreuung charakterisiert. Die Chemisorption von Kohlenstoffmonoxid auf der Oberfläche von PdGa und Pd_3Ga_7 wurde volumetrisch und mittels Infrarotspektroskopie untersucht. Die katalytische Aktivität, Stabilität und Selektivität der Pd intermetallischen Verbindungen in der Acetylenhydrierung wurden durch temperaturprogrammierte und isotherme Experimente bestimmt. Beide Verbindungen, PdGa und Pd_3Ga_7, zeigten eine bemerkenswerte höhere Selektivität, eine ähnliche Aktivität per Pd Zentrum und eine verminderte Deaktivierung unter Reaktionsbedingungen im Vergleich zu einem kommerziellen, geträgerten Palladiumkatalysator sowie einer ungeträgerten silberreichen Palladiumlegierung. Diese exzellenten katalytischen Eigenschaften werden auf die Isolierung der Pd Atome in der Struktur der intermetallischen Verbindungen zurückgeführt.

Desweiteren wurden ternäre intermetallische Verbindungen aus Palladium mit Gallium und Platin, sowie eine intermetallische Verbindung aus Palladium mit Zinn untersucht. Die Ergebnisse der Struktur- und Katalyseuntersuchungen der intermetallischen Verbindungen wurden diskutiert und eine Struktur-Selektivität-Aktivitäts-Korrelation aufgestellt.

3 Table of content

1 Abstract **3**

2 Zusammenfassung **5**

3 Table of content **6**

4 Introduction **8**

4.1 Acetylene hydrogenation 8

4.1.1 Polyethylene 8

4.1.2 Acetylene hydrogenation 8

4.1.3 Technical aspects of industrial acetylene hydrogenation 8

4.2 Palladium 8

4.2.1 Elemental palladium 8

4.2.2 Palladium in heterogeneous hydrogenation reactions 8

4.2.3 Active-site isolation of Pd catalysts 8

4.2.4 Preparation of active-site isolation in Pd catalysts 8

4.3 Motivation 8

4.3.1 Outline of the work 8

5 The Pd intermetallic compounds **8**

5.1 Binary Pd-Ga intermetallic compounds 8

5.1.1 Palladium-gallium phase system 8

5.1.2 Palladium-gallium intermetallic compound PdGa 8

5.1.3 Palladium-gallium intermetallic compound Pd_3Ga_7 8

5.2 Ternary Pt-Pd-Ga intermetallic compounds 8

5.2.1 $PtPd_2Ga_3$ and $PtPd_2Ga_7$ 8

5.3 Binary Pd-Sn intermetallic compound 8

5.3.1 $PdSn_2$ 8

6 Methods and experiments **8**

6.1 Preparation 8

6.2 Thermal analysis 8

6.3 Scanning electron microscopy 8

6.4 X-ray diffraction 8
6.4.1 Theory of X-ray diffraction 8
6.4.2 XRD equipment 8
6.4.3 XRD measurements 8
6.5 X-ray absorption spectroscopy 8
6.5.1 Theory of X-ray absorption 8
6.5.2 XAS measurements 8
6.5.3 Data processing 8
6.6 Surface characterisation with XPS and ISS 8
6.6.1 X-ray photoelectron spectroscopy 8
6.6.2 Ion scattering spectroscopy 8
6.6.3 XPS and ISS measurements 8
6.7 Chemisorption 8
6.7.1 Active surface determination by volumetric measurement of CO chemisorption 8
6.7.2 Infrared absorption spectroscopy 8
6.8 Catalytic studies 8
6.8.1 Gas chromatography 8
6.8.2 Experimental equipment 8
6.8.3 Catalytic measurements and data processing 8
6.9 Chemical etching 8
6.9.1 Chemical etching of PdGa and Pd_3Ga_7 8
6.9.2 Chemical etching of $PdSn_2$ 8

7 Pd-Ga intermetallic compounds 8
7.1 Results 8
7.1.1 Preparation and characterization of PdGa and Pd_3Ga_7 8
7.1.2 Structural and thermal investigations 8
7.1.3 Surface characterization 8
7.1.4 Investigation of the catalytic performance of PdGa and Pd_3Ga_7 8
7.2 Discussion 8
7.2.1 Structural characteristics of PdGa and Pd_3Ga_7 8
7.2.2 Structural investigations during thermal treatment 8
7.2.3 Surface characterization 8
7.2.4 Acetylene hydrogenation on Pd-Ga intermetallic compounds 8

8 Pt-Pd-Ga intermetallic compounds 8
8.1 Results 8
8.1.1 Preparation and characterization of $PtPd_2Ga_3$ and $PtPd_2Ga_7$ 8
8.1.2 Structural investigations during thermal treatment 8
8.1.3 Investigation of the catalytic performance of $PtPd_2Ga_3$ and $PtPd_2Ga_7$ 8
8.2 Discussion 8
8.2.1 Preparation of ternary Pt-Pd-Ga intermetallic compounds 8
8.2.2 Thermal stability and hydride formation 8
8.2.3 Acetylene hydrogenation on $PtPd_2Ga_3$ and $PtPd_2Ga_7$ 8
9 Pd-Sn intermetallic compound 8
9.1 Results 8
9.1.1 Preparation and characterization of $PdSn_2$ 8
9.1.2 Structural investigations during thermal treatment 8
9.1.3 Investigation of the catalytic performance of $PdSn_2$ 8
9.2 Discussion 8
9.2.1 Preparation and structural characteristics 8
9.2.2 Thermal stability and hydride formation 8
9.2.3 Catalytic performance of $PdSn_2$ 8
10 Summary 8
11 Appendix 8
11.1 References 8
11.2 List of figures 8
11.3 List of tables 8
11.4 Publications 8
11.4.1 Patent application 8
11.4.2 Publications 8
11.4.3 Oral presentations 8
11.4.4 Reports 8
11.4.5 Poster 8
11.5 Acknowledgement / Danksagung 8

4 Introduction

4.1 Acetylene hydrogenation

4.1.1 Polyethylene

Polyethylene (PE) is a polymer consisting of a long backbone of covalently linked carbon atoms connected to two hydrogen atoms. Polyethylene is formed by polymerization of n molecules of the monomer ethylene. The chemical formula of polyethylene in its simplest form is $C_{2n}H_{4n+2}$, where n is the degree of polymerization. Different kinds of polyethylene exist depending on the concentration of side chains and of the presence of linked or functional groups like acids or esters [1]. The total production of polyethylene exceeds 40 million tons per year [2]. PE is used in large quantities of non-expensive synthetic material with modest physical properties like stiffness and excellent chemical resistance for nondurable applications which do not require properties like hardness or thermal resistance [1]. Industrial production of polyethylene is performed by two different processes. The Ziegler-Natta process consists of ethylene polymerization using transition metal organic complexes and transition metal chlorides [3]. Other processes are based on supported transition metal oxides like chromium oxide in the so-called Phillips process and metallocene catalysts [4].

4.1.2 Acetylene hydrogenation

Ethylene for the polymerization to polyethylene is produced by cracking of light alkanes in a steam cracker. The ethylene stream has to be purified and one step in the purification process is the selective hydrogenation of acetylene to ethylene.

$C_2H_2 + H_2 \rightarrow C_2H_4$ $\Delta H = -172$ kJ/mol, $\Delta S = -111$ J/K·mol (298 K) [5]

Presence of acetylene in ethylene stream leads to poisoning of the polymerization catalyst because acetylene adsorbs at the active sites for ethylene and blocks the polymerization process. Therefore, the acetylene content in the ethylene feed has to be reduced to the low ppm-range. Hydrogenation of acetylene in the presence of ethylene requires high selectivity to ethylene to prevent hydrogenation of ethylene to ethane [5,6]. Following reactions occur in an acetylene hydrogenation reactor:

$C_2H_2 + H_2 \rightarrow C_2H_4$ (1) hydrogenation of acetylene to ethylene

$C_2H_4 + H_2 \rightarrow C_2H_6$ (2) hydrogenation of ethylene to ethane

$n\ C_2H_2 + \frac{1}{2}n\ H_2 \rightarrow (C_2H_3)_n$ (3) dimerisation and oligomerisation (n= 2, 3, 4, ..)

Main product of reaction (3) is 1,3-butadiene which can be further hydrogenated to so-called C4 hydrocarbons 1-butene, n-butane, cis- and trans-butene. C6-hydrocarbons and the so called green oil of higher hydrocarbons are formed in small quantities. Hydrocarbon deposits and hydrocarbon decomposition with subsequent formation of carbonaceous deposits on the catalyst surface lead to deactivation [6-8].

4.1.3 Technical aspects of industrial acetylene hydrogenation

Ethylene stream from the steam cracker typical consists of ethylene, propylene, ethane, methane, hydrogen, carbon monoxide, propyne, and acetylene. The exact composition depends on the mixture of light alkanes (so-called naphtha) used and the operating parameters of the steam cracker. The ethylene stream for the PE production has to be purified to obtain the pure ethylene. Acetylene hydrogenation reactors are positioned directly after the steam cracker are called front-end reactor. The ethylene composition is relatively low (30-40%) and high hydrogen content leads to a high hydrogen-acetylene ratio (~20-100) which forces the total hydrogenation of acetylene to ethane and additional other unsaturated hydrocarbons to ethane and propane [9,10]. The hydrogenation reactor is positioned at the end of the purification process (so-called tail-end reactor) and the ethylene stream contains mostly ethylene and around 1% acetylene and low hydrogen content with lower hydrogen-acetylene ratio (~1-3) [11,12].

New developments in acetylene hydrogenation use two or more subsequent reaction zones with a low hydrogen-acetylene ratio for a step-wise removal of acetylene and other alkynes or dienes [13]. The operating temperature ranges from 300 K up to 550 K.

4.2 Palladium

4.2.1 Elemental palladium

Palladium as a group VIII noble metal has unique catalytic properties in homogeneous and in heterogeneous reactions. In heterogeneous catalysis palladium is used for oxidation and hydrogenation reactions. One of the most remarkable properties of palladium is the ability to dissociate and dissolve hydrogen. Atomic hydrogen occupies the octahedral interstices between the Pd atoms of the cubic-closed packed metal. Palladium can absorb up to 935 times of its own volume of hydrogen. Depending on hydrogen partial pressure and temperature a so-called α- and β-hydride is formed [14].

Table 1: Some physical properties of palladium [15].

atomic number	46
atomic weight	106.42
atomic diameter	275.2 pm
melting point	1827 K
crystal structure	cubic closed packed
electron configuration	[Kr] $4d^{10}$
electron negativity (Allred & Rochow)	1.4

4.2.2 Palladium in heterogeneous hydrogenation reactions

Like other group VIII metals, palladium can be used for hydrogenation of unsaturated hydrocarbons. Palladium shows the highest selectivity of these metals in heterogeneously catalyzed semi-hydrogenation of alkynes and dienes to the corresponding alkenes [6]. Activity of palladium for hydrocarbon hydrogenation is based on the ability for the dissociative adsorption of hydrogen and chemisorption of unsaturated hydrocarbons. The chemisorption of alkenes and alkynes is based on the interaction of the d-band of the Pd metal with the π-bonding system of the unsaturated hydrocarbons [16,17]. Industrially used

catalysts for acetylene hydrogenation contain relatively low Pd content (< 0.1 wt%) and are supported on metal oxides like alumina. Palladium shows high activity but only limited selectivity and long-term stability for hydrogenation of acetylene. The limited selectivity is mainly due to enhanced ethane formation and the formation of by-products like C4 and higher hydrocarbons. Palladium shows a strong deactivation behavior because of hydrocarbon and carbon deposits. Catalyst deactivation by hydrocarbon and carbon deposits requires a frequent exchange or regeneration of the catalyst in the hydrogenation reactor. Moreover, fresh or regenerated catalysts show high activity and consequently lead to increased ethylene consumption and reduced selectivity. Furthermore, high activity of fresh or regenerated catalysts can lead to overheating ("thermal run away") of the reactor because of the exothermic hydrogenation reaction [7,8].

4.2.3 Active-site isolation of Pd catalysts

The limited selectivity of Pd catalysts in acetylene hydrogenation can be attributed to the presence of ensembles of active sites on the catalyst surface [18-20]. Selectivity can be increased by active-site isolation ("geometric effect"), modification of the electronic structure by alloying or promoting of Pd catalysts ("electronic effect") or by suppressing hydride formation ("kinetic effect").

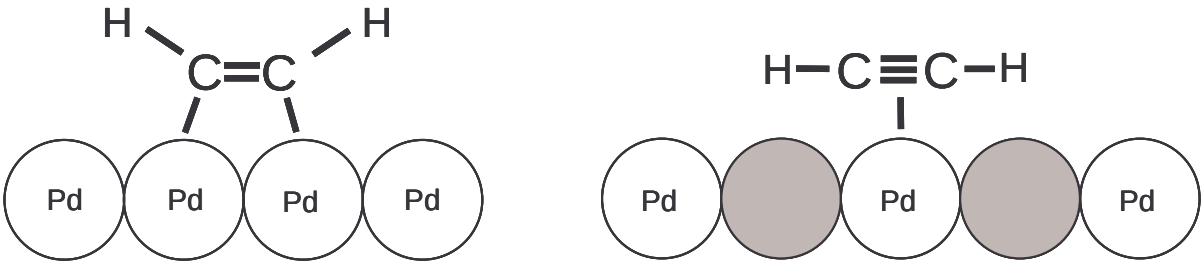

Figure 1: Di-σ bonded acetylene molecule to two neighbouring Pd atoms (left) and a weakly π-bonded acetylene molecule to an isolated Pd atom (right). Only the π-bonded acetylene is hydrogenated in high selectivity to ethylene.

Site-isolation of the active Pd atoms by increasing Pd-Pd distances and reducing Pd-Pd coordination numbers (so-called “geometric effect”) on the catalyst surface influences the adsorption configurations of unsaturated hydrocarbons. The π-bonding system of acetylene and ethylene can bond in several configurations on the Pd surface. Two important configurations are the weak π-bonding on top on a single Pd atom and the di-σ-bonding to two neighboring Pd atoms [21-23]. It was suggested that only weakly π-bonded acetylene can be hydrogenated in high selectivity to ethylene. In contrast, di-σ-bonded acetylene and ethylene molecules and other adsorption configurations lead to considerable formation of ethane under hydrogenation conditions. In recent work it was reported that the di-σ-bonded alkene is the precursor in the alkane formation [24]. Shaikhutdinov and co-workers [25] showed that π-bonded ethylene desorbs already at 200 K under UHV conditions. Only di-σ-bonded ethylene on a palladium surface is stable at higher temperatures and can be hydrogenated to ethane or decompose to carbon deposits [26-28]. The basic principle of active-site isolation is the reduction of multiple adsorption sites resulting in a reduced number of adsorption configurations and intermediates in acetylene hydrogenation and, consequently, in an increased selectivity in acetylene hydrogenation compared to conventional Pd catalysts [29-35].

In addition to a “geometric effect”, an “electronic effect” by modification of the electronic structure of Pd catalysts by alloying or promoting can increase selectivity by changing adsorption and desorption properties, resulting in a replacement of ethylene on the catalyst surface by gaseous acetylene before hydrogenation to ethane occurs [19,36-38].

The presence of Pd hydrides influences the selectivity of the reaction caused by providing the hydrogen for the hydrogenation reaction and therefore, lead to an enhanced ethane formation [39-44]. Alloying or promoting of Pd metal catalysts inhibit hydride formation and dilute the concentration of Pd atoms on the surface. Less Pd on the surface reduces the number of dissociation sites for hydrogen and, consequently, hydrogen concentration on the surface and increases selectivity in acetylene hydrogenation (“kinetic effect“) [42,43,45].

4.2.4 Preparation of active-site isolation in Pd catalysts

Site isolation of Pd atoms in bulk material can be obtained by diluting palladium with a second metal (”alloying“) or by preparation of Pd intermetallic compounds. An additional method is the modification of the Pd catalyst surface, which results in site-isolation of Pd atoms on the surface. These three possibilities of preparation of active site isolation by Pd based alloys, Pd intermetallic compounds or surface modification of Pd catalysts exist and are shortly presented.

Alloying palladium with an additional metal

Different possibilities exist to arrange atoms of two metals in a solid mixture. One is the statistical replacement of metal atoms by another metal and formation of a so-called solid solution. A solid solution of a mixture of two metals is preferably formed by metals with similar atomic radius and the same crystal structure. Palladium forms solid solutions with metals like silver and platinum. A palladium based solid solution is obtained by cooling down of liquid mixture of palladium and an additional metal.

Two metals A and B with different crystal structures and chemical dissimilarity can form a melted mixture. Cooling down of the mixture does not result in solid solution but in mixture of crystals consisting of pure metal A next to crystals consisting of pure metal B. No active-site isolation can be obtained by combination of these kinds of metals. Palladium can form such alloys with chromium as second metal.

Combinations of metals exists which show partial miscibility in particular composition and, therefore, resulting in complex phase diagrams. Interstitial solid solution is another class of alloys where small atoms of an additional element can occupy the interstices between the atoms in a metal structure.

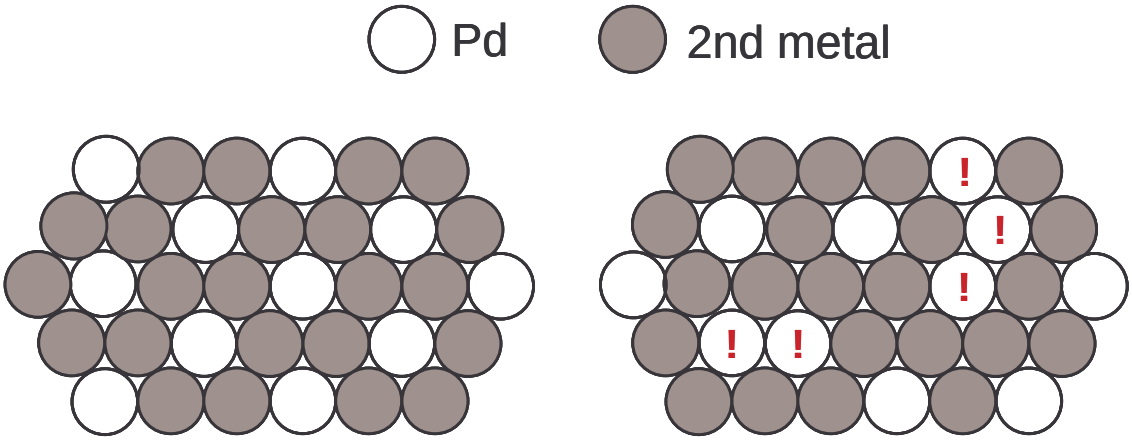

Figure 2: Example of isolated Pd atoms by alternated arrangement of Pd and an additional metal like in Pd intermetallic compounds (left) and an example for random distribution of Pd and a second metal like in a solid solution which does not exclude neighbouring Pd atoms (right).

Complete active-site isolation of Pd atoms can be obtained by an alternated arrangement of Pd atoms and atoms of the co-metal. Site isolation by the use of alloys forming solid solutions is not a sufficient method because of the random distribution of atoms. Random distribution does not result in complete active-site isolation because it allows the presence of neighbouring Pd atoms (Figure 2). In addition, a solid solution from metals with different melting points obtained by cooling down leads to further degradation of site isolation because of non-complete random distribution of the two kinds of metal atoms. The first crystals formed by cooling down of a melted mixture contain more metal with the higher melting point compared to the composition of the melted mixture. The crystals formed at the end of the solidification process contain more of the second metal compared to the metal with the higher melting point.

A sufficient isolation of Pd atoms is difficult to attain without considerably decreasing the concentration of the active Pd constituent in the metal alloy catalyst. The high dilution of Pd with an additional metal results in high selectivity in hydrogenation reaction but also in a decreased activity because of the reduced number of active sites at the catalyst surface. Moreover, surface segregation and ensemble effects may degrade the “numerical” separation of Pd atoms in a metal alloy. Thermal treatment of alloys can result in separation by segregation of the metal atoms. Palladium segregation to the surface leads to ensembles of Pd atoms or a Pd overlayer on the catalyst surface and results in similar catalytic performance like supported Pd catalysts. Segregation of the other metal to the surface leads

to Pd enrichment in the bulk and deactivation of the catalyst [19,46-49]. Alloying is no suitable possibility to obtain active-site isolated Pd catalysts because of the required highly dilution and reduced stability of site isolation during thermal treatment caused by segregation tendencies.

Intermetallic compounds

Intermetallic compounds are formed by the reaction of two or more metals

$n\,A + m\,B \rightarrow A_nB_m \qquad \Delta_{form}G < 0$.

They consist of a particular stoichiometric composition and crystallize in an ordered crystallographic structure. The nature of bonding in intermetallic systems is not well understood yet. Structural properties like stoichiometric composition and ordered crystal structure are due to the partly covalent or ionic character of intermetallic compounds and typically lead to higher structural stability and less segregation compared to alloys. Contribution of covalent or ionic bonding influence the physical properties of the intermetallic compounds and result in reduced ductility and reduced electric conductivity compared to pure metals or alloys consisting of miscible metals. In addition, intermetallic compounds exhibit metal-like Pd-atoms, and, hence, resemble a kind of “diluted” palladium metal.

The structure of intermetallic compounds is preferable based on an alternating arrangement of different types of atoms to increase coordination number to the co-metal. Therefore, Pd intermetallic compounds are suitable to obtain active-site isolation because they allow a higher atomic concentration of Pd atoms (up to 50%) and to a complete site isolation of Pd atoms in a phase pure sample. Moreover, less segregation caused by the high structural stability of intermetallic compounds compared to Pd alloys results in an increased long-term stability under hydrogenation conditions.

Active site isolation by surface modification of Pd catalysts

In addition to the preparation of bulk material consisting of isolated Pd atoms in the structure, active-site isolation in catalysis can be obtained by using palladium catalyst with an additional modification of the catalyst surface. Surface modification can be obtained by impregnation with silanes and further decomposition to Si [27,29], deposition of metal

oxides, [50] or poisoning of Pd catalyst with lead additives similar to Lindlar catalysts [51,52]. However, these modifications may not completely eliminate the presence of ensembles of Pd atoms on the surface. Therefore, the impregnated materials need a very high dispersion on the palladium surface which is associated with a decreased activity similar to Pd based alloys and has to be stable under reaction conditions.

An addition of carbon monoxide to the ethylene feed is an additional possibility to obtain partial active-site isolation and an increased selectivity [5,6,42,53-55]. This effect is based on the strong adsorption of CO molecules on Pd surfaces which leads to blocked Pd sites and diluted unoccupied Pd atoms for acetylene hydrogenation. However, CO has to be present during the entire hydrogenation process in feed in high concentration to obtain high selectivity and has to be removed afterwards.

4.3 Motivation

The motivation of the work presented here is to verify the validity of the concept of active-site isolation as a possible way to obtain catalysts with superior properties like high selectivity and long-term stability in hydrogenation reactions. Therefore, it is desirable to find a material that contains a sufficient amount of Pd together with another less expensive and catalytically less active metal, and exhibits a well-defined crystallographic structure with the Pd atoms sufficiently isolated from each other. Pd intermetallic compounds fulfill these requirements and, hence, are promising candidates for improved hydrogenation catalysts. Pd-Ga intermetallic compounds PdGa and Pd_3Ga_7 were selected because of the increased average interatomic Pd-Pd distances and decreased Pd-Pd coordination numbers in their structures which makes them ideal model system for isolated Pd active sites. Besides being model system for structural activity and selectivity correlations, they may be promising candidates for further application in industrial selective hydrogenation of acetylene.

Industrial application of Pd-Ga intermetallic compounds requires high thermal and structural stability for suitable long-term application in a hydrogenation reactor. Partial replacement of palladium by platinum may increases stability and may lead to improved catalysts. Therefore, the influence of partial replacement of Pd by Pt in PdGa and Pd_3Ga_7 on structural properties and on catalytic performance was investigated by comparably studies of Pd-Ga and Pd-Pt-Ga intermetallic compounds.

Full validation of the concept of active-site isolation in hydrogenation reactions requires the elucidating the role of the inactive metal. Gallium is known to be catalytically inactive in hydrogenation reactions and should not influence the isolated Pd atoms in Pd-Ga intermetallic compounds. Hence, gallium acts as a spacer and forms the matrix to isolate the Pd atoms. In this case, gallium may be substituted by another metal without significant influence on the catalytic properties. A palladium-tin intermetallic compound $PdSn_2$ contains Pd atoms surrounded by tin atoms and was selected to compare the catalytic performance of isolated Pd atoms surrounded by tin or gallium atoms.

4.3.1 Outline of the work

The preparation and characterization of PdGa, Pd_3Ga_7, $PtPd_2Ga_3$, $PtPd_2Ga_7$, and $PdSn_2$ as potential selective hydrogenation catalysts are described.

Pd intermetallic compounds as active-site isolated catalysts require high structural and thermal stability under reaction condition to maintain the isolation of Pd atoms under reaction conditions. Therefore, structural investigations were performed with thermal analysis (TG/DSC), in situ X-ray diffraction (XRD), and in situ X-ray absorption spectroscopy (EXAFS) in inert and reactive gas atmospheres. Hydride formation of Pd catalysts can lead to a decreased selectivity and, therefore, the absence of hydride formation was verified. Thermal treatment in hydrogen containing atmosphere allows detecting incorporation of hydrogen and the formation of hydrides with in situ XRD and in situ EXAFS.

Total surface area, active surface area, and morphology were studied with nitrogen BET, CO chemisorption, and scanning electron microscopy (SEM), respectively. Infrared (IR) investigation of CO chemisorption, X-ray photoelectron spectroscopy (XPS), and ion scattering spectroscopy (ISS) were used to characterize the surface of PdGa and Pd_3Ga_7.

Catalytic performance (i. e. activity, selectivity, and long-term stability) of Pd intermetallic compounds as catalyst for the selective hydrogenation of acetylene was investigated and compared to suitable references. A commercial catalyst palladium supported on alumina and an unsupported silver-rich palladium alloy were used as references.

The structural and catalytic data obtained are discussed and evaluated with respect to the concept of active-site isolation and a further application of Pd intermetallic compounds as potential industrial catalysts.

Cooperation and acknowledgement

The work presented here is the result of a cooperation between the Department of Inorganic Chemistry at the Fritz-Haber-Institute in Berlin and the Max-Planck-Institute for Chemical Physics of Solids in Dresden. The Pd-Ga, Pt-Pd-Ga, and Pd-Sn intermetallic compounds were prepared and fully characterised using methods of solid state chemistry in the group of Prof. Y. Grin in Dresden. Structural in-situ investigations, surface characterisation, catalysis studies, and chemical etching were performed at the Fritz-Haber-Institute. Prof. Y. Grin and his co-workers Rainer Giedigkeit, Dr. Marc Armbrüster and Dr. Kirill Kovnir are gratefully acknowledged.

Fruitful discussions within the research project ATHENA about hydrogenation of unsaturated hydrocarbons on Pd catalysts lead to an improved understanding of the origin of the selectivity of Pd catalysed hydrogenation reactions and are gratefully acknowledged.

5 The Pd intermetallic compounds

5.1 Binary Pd-Ga intermetallic compounds

5.1.1 Palladium-gallium phase system

First investigation of the binary Pd-Ga system was done by Schubert et al. [56,57]. The Pd-Ga system consists of nine intermetallic compounds [58] including the equiatomic compound PdGa, the gallium-rich $PdGa_5$ and Pd_3Ga_7, and the palladium-rich compounds Pd_5Ga_4 to $Pd_{13}Ga_5$. The palladium-rich Pd-Ga intermetallic compound may be high an active catalysts in hydrogenation reactions because of the high Pd content. In order to verify the concept of active-site isolation, only PdGa and the gallium-rich Pd-Ga intermetallic compounds can be used. The structures of $PdGa_5$, Pd_3Ga_7 and PdGa consist of Pd atoms with increased interatomic Pd-Pd distances and a reduced Pd-Pd coordination number. $PdGa_5$ has the lowest palladium content and the shortest Pd-Pd distance is 4.56 Å to four Pd atoms [59]. However, $PdGa_5$ has a low melting point at 473 K. Long-time catalytic operation at temperature next to the melting point of $PdGa_5$ may lead to a structural degradation under hydrogenation condition and, therefore, $PdGa_5$ is not suitable for catalytic application and was not further investigated. A higher structural stability is deduced from the higher melting points of Pd_3Ga_7 (733 K) and of PdGa (1538 K). PdGa and Pd_3Ga_7 were selected because they contain Pd atoms surrounded by Ga atoms in their structure which makes them suitable model systems to verify the concept of active-site isolation.

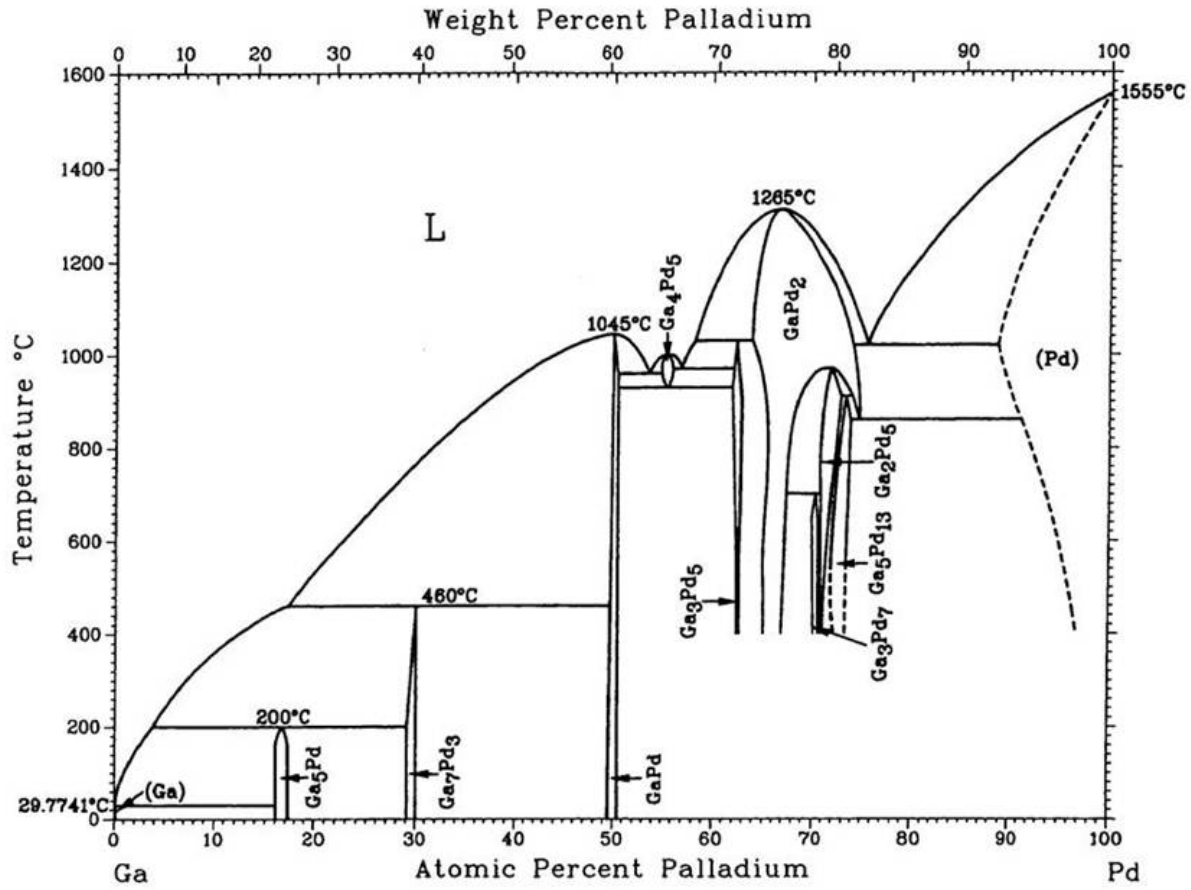

Figure 3: Phase diagram gallium-palladium [58].

5.1.2 Palladium-gallium intermetallic compound PdGa

PdGa [60-62] crystallizes in a FeSi structure type [63] (Table 2). The FeSi structure type can be described as a strongly distorted NaCl structure which leads to an increased coordination number from six to seven. Every Pd atom in PdGa is surrounded by seven (1+3+3) Ga atoms (Figure 4, Table 3) and the shortest Pd-Pd distance in PdGa amounts to 3.01 Å to six Pd atoms.

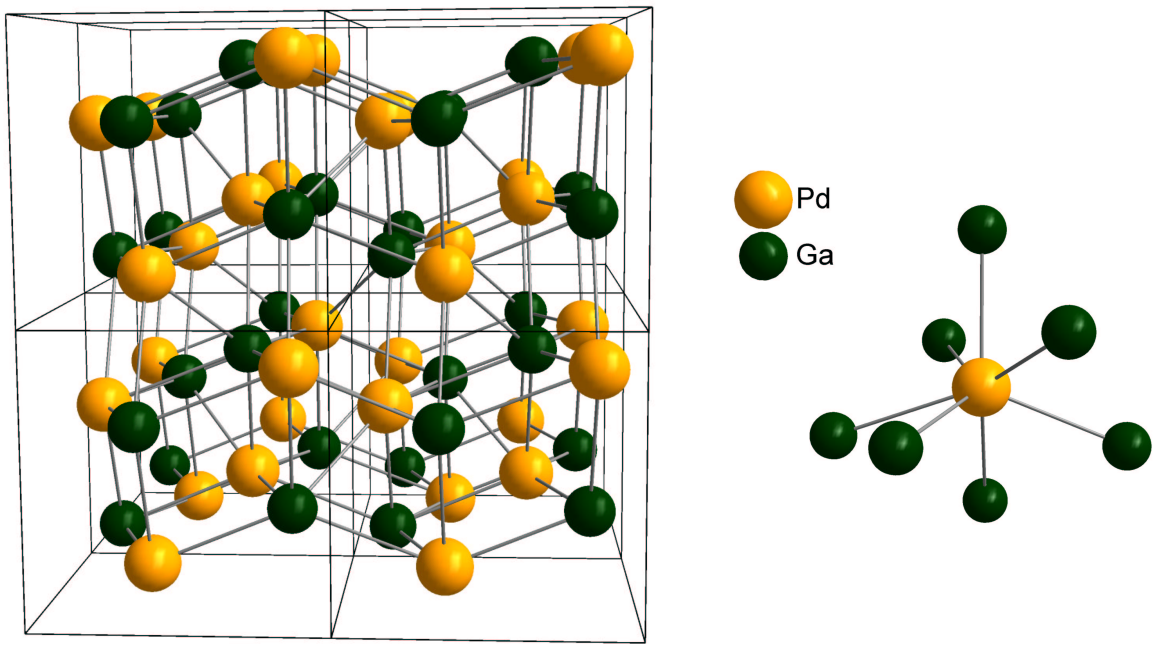

Figure 4 : 2x2x2 unit cell of PdGa and coordination sphere of Pd atoms in PdGa.

5.1.3 Palladium-gallium intermetallic compound Pd_3Ga_7

The gallium-rich Pd_3Ga_7 [57,62,64] crystallizes in a Ir_3Ge_7 [64] structure type and consists of associated Ga tetragonal antiprisms occupied by a Pd atom. The shortest Pd-Ga distances is 2.58 Å and every Pd atom has a coordination sphere of eight (4 + 4) Ga atoms. The presence of Pd-Pd pairs leads to a shortest Pd-Pd distance of 2.73 Å to a single Pd atom. The shortest distance to the next four Pd atoms amounts to 4.27 Å.

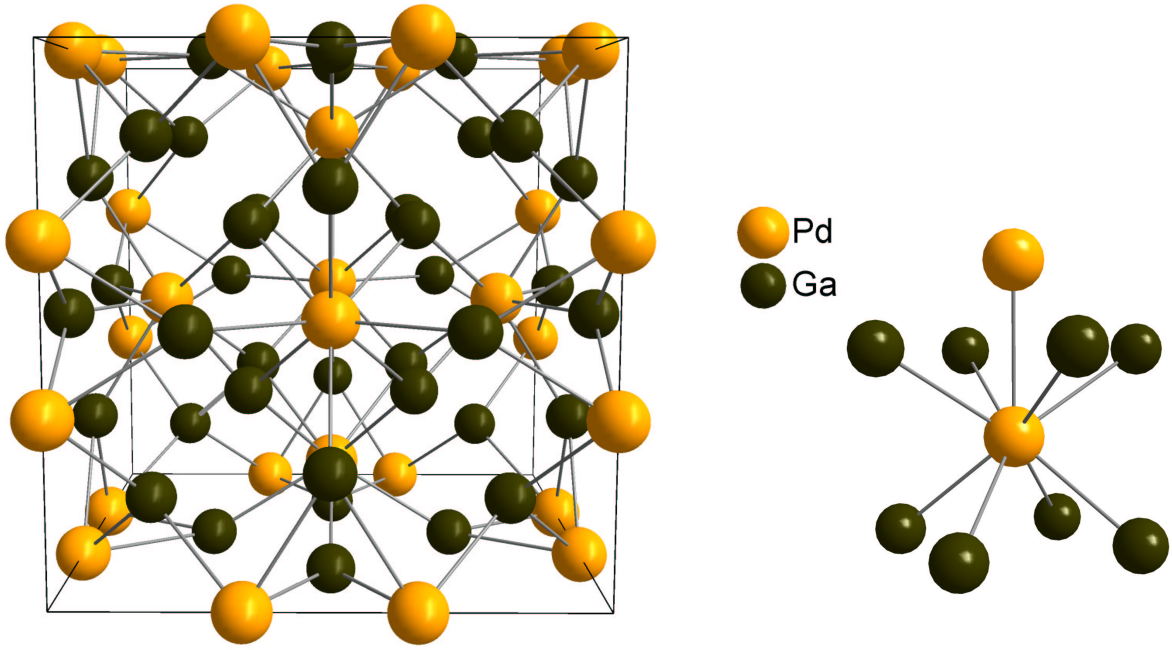

Figure 5: Unit cell of Pd_3Ga_7 and coordination sphere of Pd atoms in Pd_3Ga_7.

5.2 Ternary Pt-Pd-Ga intermetallic compounds

5.2.1 $PtPd_2Ga_3$ and $PtPd_2Ga_7$

Platinum and palladium are in group 10 of the periodic table of elements and have a similar atomic radius (Pd: 137.6 pm; Pt: 137.3 pm) [15]. PtGa and Pt_3Ga_7 crystallize in the same crystal structure like PdGa and Pd_3Ga_7 [60-62] and, therefore, a successful preparation of mixed Pt-Pd intermetallic compounds can be expected. The melting points of Pt-Ga intermetallic compounds are higher compared to the Pd-Ga analogues [58]. In particular, the melting point of Pt_3Ga_7 of 1095 K is significantly higher compared to Pd_3Ga_7 which melts at 733 K. Therefore, it can be concluded that the melting point of mixed Pd-Pt-Ga intermetallic compounds should be between the corresponding Pd-Ga and Pt-Ga intermetallic compounds.

Replacement of one third of the Pd atoms by Pt atoms in the structure of PdGa and Pd_3Ga_7 results in the compounds $PtPd_2Ga_3$ (corresponds to PdGa) and $PtPd_2Ga_7$ (corresponds to Pd_3Ga_7).

5.3 Binary Pd-Sn intermetallic compound

5.3.1 $PdSn_2$

The binary palladium-tin system includes a large number of intermetallic compounds and exhibits a high complexity [58]. On the tin-rich side there are three intermetallic compounds: $PdSn_2$, $PdSn_3$ and $PdSn_4$. $PdSn_2$ was selected to investigate the structural and catalytic properties of isolated Pd atoms in a Pd-Sn intermetallic compound. $PdSn_2$ shows the requested physical and structural properties like a high melting point (873 K) and isolated Pd atoms in the structure. $PdSn_2$ can be described as an "8-layer-type" of a distorted calcium fluoride structure (Figure 6) and the crystallographic structure was refined by Künnen et al. [65]. Every Pd atom in $PdSn_2$ is surrounded by eight Sn atoms (Figure 7) and the shortest Pd-Pd distance in the structure amounts to 2.84 Å (single Pd atom).

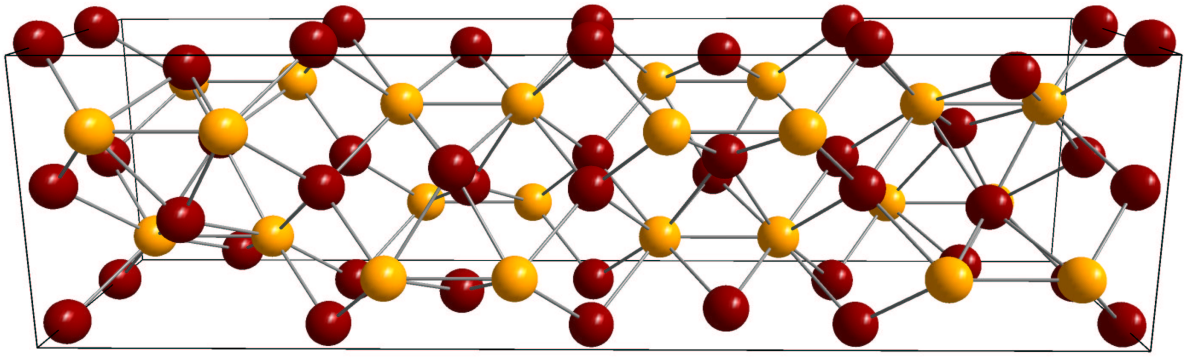

Figure 6: Unit cell of $PdSn_2$.

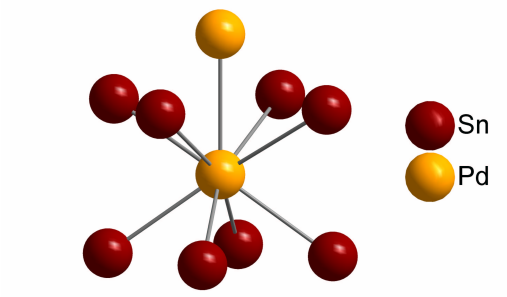

Figure 7: Coordination sphere of Pd atoms in $PdSn_2$.

Table 2: Crystallographic data of PdGa, Pd_3Ga_7 and $PdSn_2$ [60,62,64,65].

PdGa	cubic	a = 4.896 Å		$P2_13$	(198)
Atom	*Site*	*x*	*y*	*z*	*SOF*
Pd	4a	0.64220	0.64220	0.64220	1
Ga	4a	0.34270	0.34270	0.34270	1
Pd_3Ga_7	cubic	a = 8.772 Å		*Im*-3*m*	(229)
Atom	*Site*	*x*	*y*	*z*	*SOF*
Pd	12e	0.34430	0	0	1
Ga	12d	0.25	0	0.5	1
Ga	16f	0.16410	0.16410	0.16410	1
$PdSn_2$	tetragonal	a = 6.490 Å	c = 24.320 Å	$I4_1/acd$	(142)
Atom	*Site*	*x*	*y*	*z*	*SOF*
Pd	16d	0	0.25	0.31670	1
Sn	16e	0.24730	0	0.25	1
Sn	16f	0.15800	0.40800	0.12500	1

Table 3: Coordination of Pd atoms in PdGa, Pd_3Ga_7 and $PdSn_2$.

PdGa	*Element*	*CN*	*Distance [Å]*
1. Shell	Ga	1	2.540
2. Shell	Ga	3	2.570
3. Shell	Ga	3	2.707
4. Shell	Pd	6	3.008
Pd_3Ga_7	*Element*	*CN*	*Distance [Å]*
1. Shell	Ga	4	2.577
2. Shell	Ga	4	2.583
3. Shell	Pd	1	2.732
4. Shell	Ga	4	4.168
$PdSn_2$	*Element*	*CN*	*Distance [Å]*
1. Shell	Sn	2	2.800
2. Shell	Sn	2	2.821
3. Shell	Sn	4	2.827
4. Shell	Pd	1	2.837

6 Methods and experiments

6.1 Preparation

All samples were prepared by Rainer Giedigkeit and Marc Armbrüster at the Max-Planck-Institute of Chemical Physics of Solids in Dresden.

Binary palladium gallium intermetallic compounds were prepared by melting the corresponding amounts of Pd and Ga in glassy carbon crucibles under argon atmosphere in a high-frequency induction furnace [62]. 1.2083 g palladium (ChemPur 99.95 %) and 0.7917 g gallium (ChemPur 99.99 %) were used to obtain 2 g PdGa (11.354 mmol). 0.7909 g Pd (7.432 mmol) and 1.2091 g Ga (17.340 mmol) yielded 2 g Pd_3Ga_7. Pd_3Ga_7 was annealed at 673 K for 800 h in a glassy carbon crucible sealed in a silica tube filled with argon. PdGa was used without further annealing. Both samples were powdered in a swing mill (Retsch MM 200, 4 ml WC pot, 2 WC balls) for 2 x 30 min for PdGa and 2 x 10 min for Pd_3Ga_7 at 25 Hz. A more intensive ball milling procedure was used for PdGa compared to Pd_3Ga_7 whose particles seemed to agglomerate after extended ball milling.

Pt-Pd-Ga intermetallic compounds $PtPd_2Ga_3$ and $PtPd_2Ga_7$ were prepared by replacing of one third of the palladium with platinum (ChemPur 99.95%) and subsequently ballmilled and analyzed in the same way like the Pt free analogues PdGa and Pd_3Ga_7.

$PdSn_2$ was prepared by mixing of Pd (ChemPur, 99.9 %) and Sn (ChemPur 99.999 %) in a glassy carbon crucible. Commonly 0.619 g palladium and 1.381 g tin were used to prepare 2 g $PdSn_2$ (5.82 mmol). The mixture was carefully molten for five minutes in a high-frequency induction furnace under Ar atmosphere. The freshly prepared $PdSn_2$ was cooled to ambient temperature, sealed in an evacuated quartz glass tube, and additionally annealed at 873 K for one week. The sample was powdered the same way as Pd_3Ga_7.

An unsupported palladium silver alloy $Pd_{20}Ag_{80}$ was used as a benchmark catalyst for catalytic experiments. The alloy with the exact composition $Pd_{20.28}Ag_{79.72}$ was prepared by melting the weighted amounts of the elements (Ag: 99.995 % ChemPur; Pd: 99.95 % ChemPur) in an arc melter under argon. Subsequently the regulus was enclosed in an evacuated quartz glass ampoule and heated to 800 °C for six days. After the heat treatment

the regulus was powdered and X-ray powder diffraction revealed that the sample was single phase.

To confirm phase purity, X-ray diffraction patterns were collected before and after the ballmilling procedure. The experimental X-ray diffraction patterns were analyzed using the software PowderCell v2.1 [66] employing structural data from the literature [57,60,61,64,65]. Diffraction pattern of the ternary Pt-Pd-Ga intermetallic compounds were simulated using the crystallographic data of PdGa and Pd_3Ga_7 and Pd site occupancy of 0.67 and additional Pt atoms on Pd sites with an occupancy of 0.33.

The surface area of the intermetallic compounds was measured according to the BET method (Quantachrome Quantasorb Jr.). The samples (200 mg) were treated over night at 393 K in helium flow (20 ml/min) and measurements were performed by determining the total amount of nitrogen adsorbed using three different nitrogen concentrations.

6.2 Thermal analysis

Thermogravimetry (TG) and differential scanning calorimetry (DSC) are included in a group of techniques in which specific physical properties of a sample are measured as a function of temperature (so-called thermal analysis) [67-70]. TG or thermogravimetric analysis (TGA) is based on measuring weight changes as a result of thermally induced transitions. Only transitions that are associated with weight changes like decomposition, reduction, and oxidation or desorption of volatile compounds can be detected by TG. The weight is continuously recorded as a function of a temperature program. In general, the temperature program consists of a heating ramp from room temperature to the desired end-temperature may be followed by an isothermal period. In contrast to DSC, the transitions detectable by TG are mostly irreversible and, hence it is not necessary to measure weight changes from a higher to a lower temperature. To measure a thermogram, a sample is placed in a crucible which is positioned in a furnace and attached to a balance. TG can be measured in inert atmosphere, in air, or in reactive gas atmosphere. Total or partial oxidation of a sample results in an increasing mass for oxide formation and a mass loss for combustion. Reduction and decomposition is accompanied by mass loss due to desorption of water or other volatile compounds.

In contrast to TG, DSC can detect thermally induced transition without a weight change provided that they are accompanied by with heat consumption or heat formation. There are two different principles to measure heat transfer: the power-compensated DSC which detects difference in consumption of electric power to hold the sample and the reference at the same temperature, and the heat-flow DSC which detects the difference in heat flow using two thermocouples [71]. The experimental set-up for the heat-flow DSC consists of two crucibles located on two chromel wafers. The chromel wafers are supported by a thermoelectrical disk consisting of constantan to transfer the heat from the surrounding heating block to the sample and reference. A thermocouple is attached at the bottom side of each chromel wafer to measure the temperature. The difference of the voltage of both thermocouples is plotted versus temperature. A DSC signal of zero implies no difference in heat flow between sample and reference. Thermally induced transitions that consume heat result in an endothermic peak and formation of heat result in an exothermic peak.

TG and DSC measurements were performed simultaneously on a Netzsch STA 449 C TG/DSC instrument. 30 mg of sample were employed and a gas phase composition of helium, 50% hydrogen in He, or 50% oxygen in He at a total flow of 100 ml/min and a heating rate of 6 K/min up to 723 K (PdGa and $PdSn_2$) and 693 K (Pd_3Ga_7) were used. Before the measurements the instrument was evacuated two times. For the experiment in helium, the instrument was purged over night with helium to obtain the desired gas composition. An empty alumina crucible was used as a reference.

6.3 Scanning electron microscopy

Scanning electron microscopy (SEM) is an imaging method that they can provide morphology and particle size distribution of powdered solids. SEM is based on the emission of secondary electrons from atoms excited by the incident electron beam. Secondary electrons undergo elastic and inelastic scattering processes. Depending on their mean free path and the work function of the sample the secondary electrons reach the surface and can be detected to yield an image of the topography of the sample particles. Secondary electrons are also used to detect the sample composition in the near-surface region [72].

SEM was performed with a Hitachi S 4000 microscope equipped with an energy dispersive x-ray detector (EDX) for elemental analysis. The acceleration voltage was set to 5 kV.

6.4 X-ray diffraction

6.4.1 Theory of X-ray diffraction

X-ray diffraction is an important method to identify a crystalline bulk phase. The basic principle is the scattering of X-ray photons by atoms in a regular lattice. In general, there are two requirements to use XRD: monochromatic X-rays and a crystalline sample [73].

Monochromatic X-rays for XRD experiments are obtained by deceleration of fast electrons. Therefore, emitted electrons from a heated cathode are accelerated by an electrical field to a cooled anode in a so-called X-ray tube. The electrons hit the anode and are decelerated. Electrons are ejected from inner shells of the atoms of the anode material. The hole resulted is filled by electrons from higher shells accompanied by emission of sharp X-ray lines characteristic for the used anode material. Radiation induced by ejected electrons from the K-shell is denoted as K radiation and if the hole in the K shell is filled by an electron from the L shell or M shell, the radiation is called K_α or K_β radiation, respectively. Transitions rules allow filling the hole in the K shell only by electrons from p-orbitals of the higher shells. Different orientation of the angular momentum of the p-orbitals leads to the presence of $K_{\alpha1}$ and $K_{\alpha2}$ with slightly different photon energies.

Additional to sharp X-ray lines, the emission of continuous range of wavelength called bremstrahlung is induced by inelastic scattering processes of the electrons in the anode material. Linear or curved crystals are used to filter the undesired radiation to obtain monochromatic light. The most common radiation used for X-ray diffraction is Cu K_α radiation.

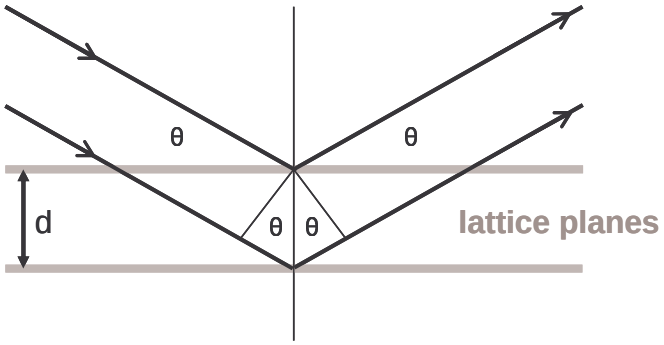

Figure 8: Bragg reflection of X-rays at lattice planes.

The smallest unit to describe a regular structure of a solid is called unit cell. Crystalline samples are compounds which exhibits a structure of periodically arranged unit cells (so-called “long-range-order”). X-ray photons from the incident beam are scattered at the atoms of the lattice. Provided that a long-range order of the sample exists, constructive interference of the scattered photons results in a peak in the X-ray diffraction pattern. The Bragg equation [74] describes the occurrence of constructive or interference:

$$2d \cdot \sin\theta = n \cdot \lambda$$

λ is the wavelength and θ is the angle of the monochromatic incident beam to the lattice planes and d the spacing between the lattice planes (Figure 8). A diffraction pattern shows the angle dependent intensity of the scattered incident beam. A carefully powdered sample shows statistic orientation of the crystallites and exhibits all possible lattice planes with so-called Millers indices *hkl* to the incident beam. Intensity of the XRD peaks depends on number and position of atoms in the unit cells, their deviation from the lattice position induced by thermal vibration and structural disordering, and the number of electrons of the scattering atoms.

XRD diffraction patterns usually show no sharp lines. This line broadening is due to the instrumental function and due to non ideal crystal structure. Wavelength dispersion and non ideal optical devices and detectors are part of the instrumental function and can be determined by measuring a reference samples with defined crystal size. Line broadening induced by non ideal crystal structure is due to microstrain (displacement of unit cells) or due to small domain size. Average domain size can be calculated with the Scherrer equation [75]

$$D = \frac{\lambda}{\beta \cdot \cos\theta}$$

where D is the average domain size, θ the Bragg angle, λ wavelength, and β the corrected integral breadth of the diffraction line. The integral breadth can be calculated with a Pseudo-Voigt profile fitting and corrected by the instrumental function. The Pseudo-Voigt profile consists of a combination of Gaussian and a Lorentzian distribution function. A large average domain size results narrow diffraction lines and the line-broadening is mainly due to the instrumental function. Therefore, no reliable data are obtained for domain size above 100 nm. In principle, average domain size is not the same as particle size because a particle may consist of a large number of crystallites. But in general, the obtained average domain size of a sample gives an indication of its particle size.

Phase analysis can be performed by simulation of a diffraction pattern of potentially present compounds and comparison with the experimental pattern.

Binary or multi-component homogeneous solutions can be investigated by XRD to determine lattice constants and compare them to the values of the single compounds. Vegard's law implies a linear correlation of the lattice constant of a mixture as a function of their relative composition with respect to the lattice constants of the single phases. Approved validity of Vegard's law implies the presence of a homogeneous composition whereas a deviation indicates a heterogeneous composition or structural changes like lattice expansion or distortion induced by additional chemical interactions between the atoms of the different components [76].

6.4.2 XRD equipment

To confirm phase purity of the prepared and the powdered samples, X-ray diffraction patterns were collected using a STOE STADI P diffractometer (CuKα1 radiation, curved Ge monochromator) in transmission geometry with a linear position sensitive detector. In situ X-ray diffraction experiments were conducted on a STOE diffractometer with Cu-Kα radiation in Bragg Brentano geometry equipped with a secondary monochromator, a scintillation counter and a Bühler HDK high temperature diffraction chamber mounted onto the goniometer (Figure 9). The sample was dispersed onto a resistively heated steel band and

the temperature was measured with type K thermocouple mounted on the bottom side of the steel band. The temperature was controlled by Eurotherm PID 818 controller and the temperature program and the XRD data collection was controlled using the STOE Win XPow (Version 1.06) software. The gases were mixed by Bronkhorst mass flow controllers and introduced in the experimental chamber with a total flow of 100 ml/min. The exhaust gas composition was continuously monitored with a Balzers quadrupole mass spectrometer (QMS 200, Pfeiffer) in channel-tron mode for multiple ion detection. For the in situ experiments usually 50 mg of the sample were used. A detailed description of the setup used can be found in reference [77].

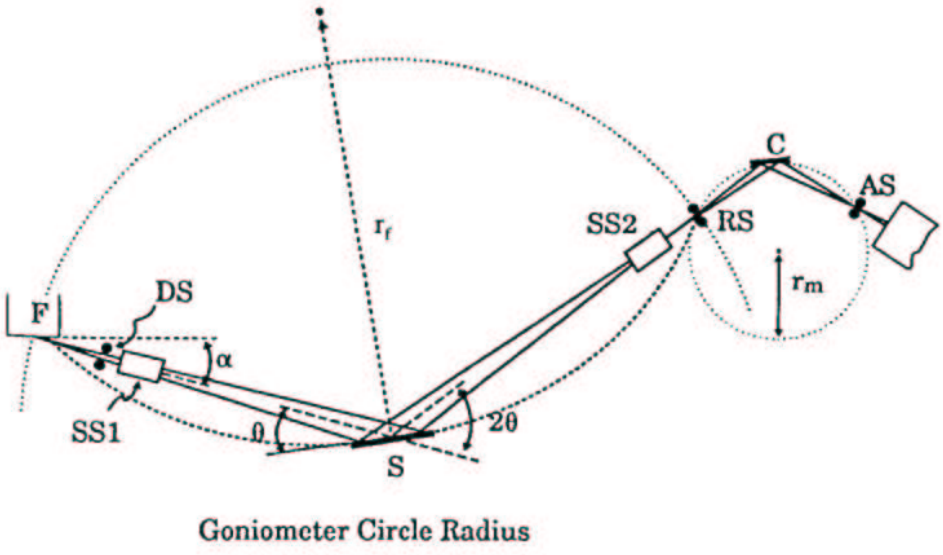

Figure 9: Geometric arrangement of the Bragg-Brentano diffractometer. X-ray beam (F) passes divergence slit (DS) and parallel plate collimator (soller slit SS1) and was scattered at the lattice of a crystalline sample (S) and passes through SS2 and a receiving slit (RS) to a monochromator (C) through a slit (AS) to the detector [73].

6.4.3 XRD measurements

The thermal stability of PdGa, Pd_3Ga_7, $PtPd_2Ga_3$, $PtPd_2Ga_7$, and $PdSn_2$ was studied in helium, 20% oxygen in He, or 50% H_2 in helium. The XRD patterns for PdGa and Pd_3Ga_7 were measured in the 2θ range from 35.5° to 48.5 and from 22.5° to 52.5°, respectively, with a step width of 0.02° and a counting time of 3 sec/step. PdGa and Pd_3Ga_7 were heated from

323 K to 723 K and from 323 K to 693 K, respectively, and XRD patterns were measured isothermally every 50 K. The effective heating rate amounted to 0.5 K/min. The XRD patterns for $PtPd_2Ga_3$, $PtPd_2Ga_7$ and $PdSn_2$ were measured in the 2θ range from 24° to 48°°, from 26° to 48°, and from 17.5° to 52.5°, respectively, with a step width of 0.02° and a counting time of 2.8 sec/step. $PtPd_2Ga_3$ was measured from 323 K to 773 K and $PtPd_2Ga_7$ and $PdSn_2$ was measured from 323 K to 723 K, and XRD patterns were measured isothermally every 50 K. The effective heating rate amounted to 0.3 K/min

Determination of the phase composition was aided by simulation of the theoretical pattern using the software PowderCell [66] and reference data from literature [57,60,61,64,65,78]. Crystallite sizes were calculated from the Scherrer equation [75] using integral breadths determined by fitting of a pseudo-Voigt profile function to selected *hkl* lines (WinXAS 3.1 [79]).

6.5 X-ray absorption spectroscopy

6.5.1 Theory of X-ray absorption

X-ray absorption spectroscopy (XAS) is a powerful method to obtain structural data of catalysts under in-situ condition. The basic principle of XAS is the absorption of X-ray photons by exciting a core level electron. If the photon energy of the incident beam exceeds the energy level of a core electron the absorption increases rapidly and results in a step in the absorption spectrum. This step is called K- or L-edge depending on the electron ejected from the K- or L-shell, respectively. The ejected electron can be scattered by neighboring atoms and the final state is the sum of the outgoing wave and of all incoming waves from the backscattering atoms (Figure 10) [72,80,81].

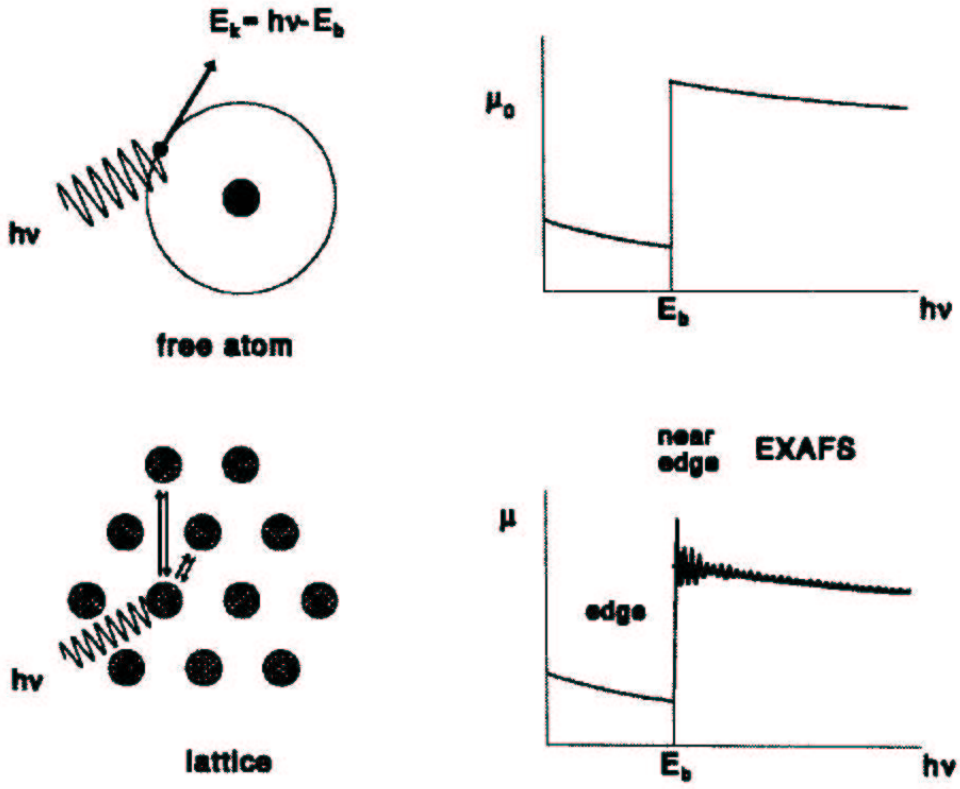

Figure 10: Absorption of X-rays as a function of photon energy by a free atom and an atom in a lattice. The fine structure is due to interference of outgoing and backscattered electron waves [80].

Dependent on the interatomic distances, the outgoing wave exhibits positive or negative interferences with the backscattered waves and results in oscillations of the absorption at energies above the edge. The oscillation frequencies of the absorption spectra are affected by the interatomic distances and their intensity provides information of the backscattering atoms like atomic number and coordination number of the neighboring atoms. Light elements have a reduced ability to backscatter the outgoing waves compared to heavier elements. Single scattering occurs by direct backscattering from an atom. In addition, there is the possibility of multiple-scattering between three or more atoms from the same or different shells. The region near the edge is called XANES (X-ray absorption near edge structure) and provides information about oxidation state of the absorbing atom. The energy region above the step containing the oscillations is called EXAFS (Extend X-ray absorption Fine Structure) and was used in the present work to obtain structural data. The fine structure $\chi(E)$ is defined as relative difference of the measured absorption $\mu(E)$ and the atomic absorption $\mu_0(E)$

$$\chi(E) = \frac{\mu(E) - \mu_0(E)}{\mu_0(E)}$$

In order to relate $\chi(E)$ to structural parameters, it is necessary to convert the energy E into the photoelectron wavevector k via

$$k = \sqrt{\frac{4m\pi}{h}(E - E_0)}$$

A theoretical $\chi(k)$ can be calculated with following equation

$$\chi(k) = \sum_j \frac{N_j S_0^2 F_j(k)}{kR_j^2} \cdot e^{\left(-2k^2\sigma_j^2\right)} \cdot e^{\left(\frac{-2R_j}{\lambda}\right)} \cdot \sin\left[2kR_j + \delta_j(k) - \frac{4}{3}\sigma'_j\, k^3\right]$$

which is used for simulation and refinement of the experimental $\chi(k)$. N is the coordination number, S_0 is the amplitude reduction factor which involves many-body effects, F is the backscattering amplitude, R the distance from absorber atom to the backscattering atom, and σ^2 is the Debye-Waller factor for thermal and structural disorder. The term including the photoelectron mean free path λ describes inelastic losses due to scattering processes, δ is the phase shift experienced by the photoelectron wave and σ' is a Debye-Waller extension so-called 3rd cumulant. The amplitude reduction factor depends only on the absorber atom whereas F is a function of the backscattering atom. The Debye-Waller factor consists of two components due to static disorder (assuming Gaussian pair distribution) and thermal

vibrations (assuming harmonic vibration). Increasing temperature of the sample leads to increasing Debye-Waller factor because of its 2nd component. Structural rearrangements like phase transition leads to maximum in the Debye-Waller factor due to the static disordering. The Debye-Waller factor can be extended by asymmetric pair distribution functions, so-called 3rd or 4th cumulant [82]. EXAFS is a method to obtain information of the local environment of the absorber atoms. This is also the reason of the reduced weight of the multiple-scattering paths due to the larger distances between three or more atoms compared to single scattering paths.

For in situ X-ray absorption measurements it is necessary to use a high flux of photons to obtain the $\chi(E)$ in a good signal-to-noise ratio with an acceptable time-resolution. High photon flux, monochromatic light in high coherence and tunable photon energy of a few keV next to the edge of the absorber atom is provided by synchrotron radiation facilities. Deceleration of high energy electrons by modulated magnetic fields in a storage ring leads to generation of synchrotron radiation. The polychromatic radiation is filtered using mirrors and crystals to obtain monochromatic light. Intensity of the X-ray beam is measured typically by ionization chambers (Hasylab Hamburg) or by CCD cameras at other synchrotron facilities (e. g. ESRF Grenoble).

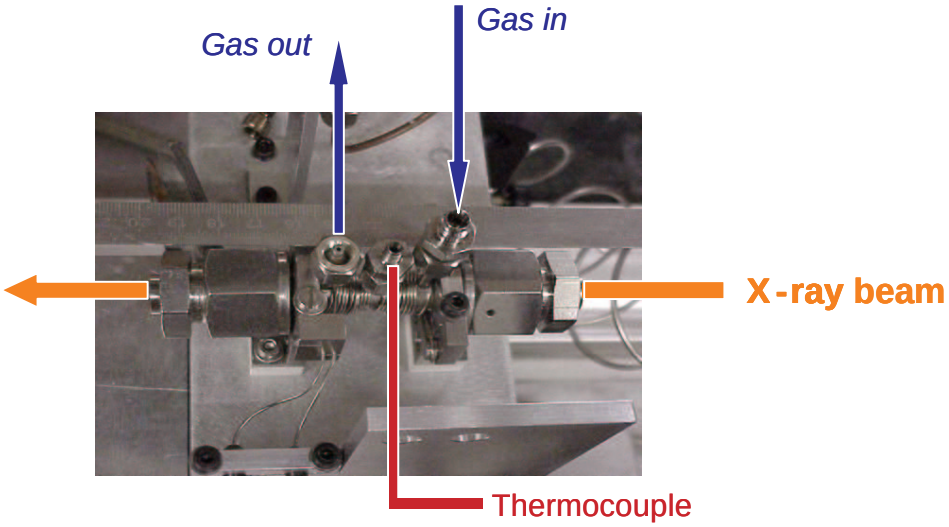

Figure 11: Transmission cell for in situ XAS measurements. The cell consists of a gas inlet from a gas mixing unit, a gas outlet to mass spectrometry to monitor product gas composition, and a thermocouple for temperature control of the cell. Inside of the cell a pressed powder pellet is mounted with a screw perpendicular to the X-ray beam.

To obtain EXAFS data under reaction condition, the application of an in-situ cell is required which allows heating the sample under desired gas atmospheres. The sample was carefully powdered, diluted with an inert support, mixed and pressed to obtain a homogeneous pellet. The diluting material has to be porous to allow contact of the sample to the gas phase and should consist of light elements for low background absorption. A sufficient signal-to-noise ratio requires a homogeneous composition of the sample and a calculated amount to obtain between 90 and 95% maximum absorption.

6.5.2 XAS measurements

In situ extended X-ray fine structure spectroscopy (EXAFS) measurements were performed at HASYLAB beamline X1 (DESY, Hamburg, Germany) at the Pd K-edge (24.350 keV). In situ EXAFS measurements were also performed at the Ga K-edge (10.367 keV). XAFS data from the Ga K-edge could not be refined because the presence of a gallium oxide on the surface (see TG, XPS and ISS data) and the presence of Ga rich areas determined with EDX. In addition, the presence of two crystallographic positions of Ga atoms in Pd_3Ga_7 increases structural complexity and resulted in no reliable data analysis. For the in situ XAS experiments a flow reactor (Figure 11) [77] at atmospheric pressure in the transmission mode was used. The in situ cell was located between the first and second ionization chamber and a palladium foil as a reference between the second and the third. Absorption of the incident beam was measured with ionization chambers filled with a mixture of nitrogen and argon (first ionization chamber) to determine I_0, I_1 (intensity after transmission of sample, filled with a mixture of argon and krypton, second chamber), and I_2 (intensity after sample and reference foil, filled with a mixture of argon and krypton, third chamber). X-ray absorption of the sample and the reference foil can be calculated from the ratio of the corresponding intensities. The gas phase composition was continuously analyzed by mass spectrometry (Pfeiffer Omnistar). The samples (10 - 15 mg) were mixed with boron nitride (30 mg) and pressed into pellets with 5 mm in diameter at a force of 15 kN. A palladium foil was measured as a reference for energy calibration. To investigate the thermal stability, PdGa, Pd_3Ga_7 and $PdSn_2$ were heated at a rate of 6 K/min in 100% helium, 50% oxygen in helium and 50% hydrogen in helium. In addition, in situ EXAFS studies in a gas mixture of 10% acetylene (2.6, Linde), 20% hydrogen and 70% helium during a thermal treatment (6

K/min) was carried out to obtain combined catalysis and structural data. Ex situ measurements at the Pd K edge were performed for all Pd-Ga, Pt-Pd-Ga and Pd-Sn intermetallic compounds at room temperature in air for structure determination with an extended measurements cycle (20 min) to increase signal-to-noise ratio.

6.5.3 Data processing

Analysis of the EXAFS spectra was performed with the software WinXAS 3.1 [79]. The spectra obtained were energy calibrated according to a palladium reference foil. The absorption spectra were background corrected and normalized using a linear pre-edge fit and a 3rd order polynomial at the post-edge. E_0 for transformation into k-space was set to the inflection point at the Pd K-edge. After transformation into the k-space, an atomic background μ_0 (k) was determined using a cubic spline function and subtracted to obtain χ(k). The radial distribution function FT(χ(k)) was obtained by Fourier transforming the k^3 – weighted experimental χ(k) function (k= 2 – 13 Å^{-1}), multiplied by a Bessel window, into the R space (Figure 12). The EXAFS refinements were performed in R space simultaneously to a k^2 and k^3 weighted χ(k) up to 5 Å. FEFF 8 was used [83,84] to calculate theoretical phases and amplitudes for Pd-Ga, Pd-Pd, Pd-Pt, and Pd-Sn scattering paths in the model structures of the Pd intermetallic compounds.

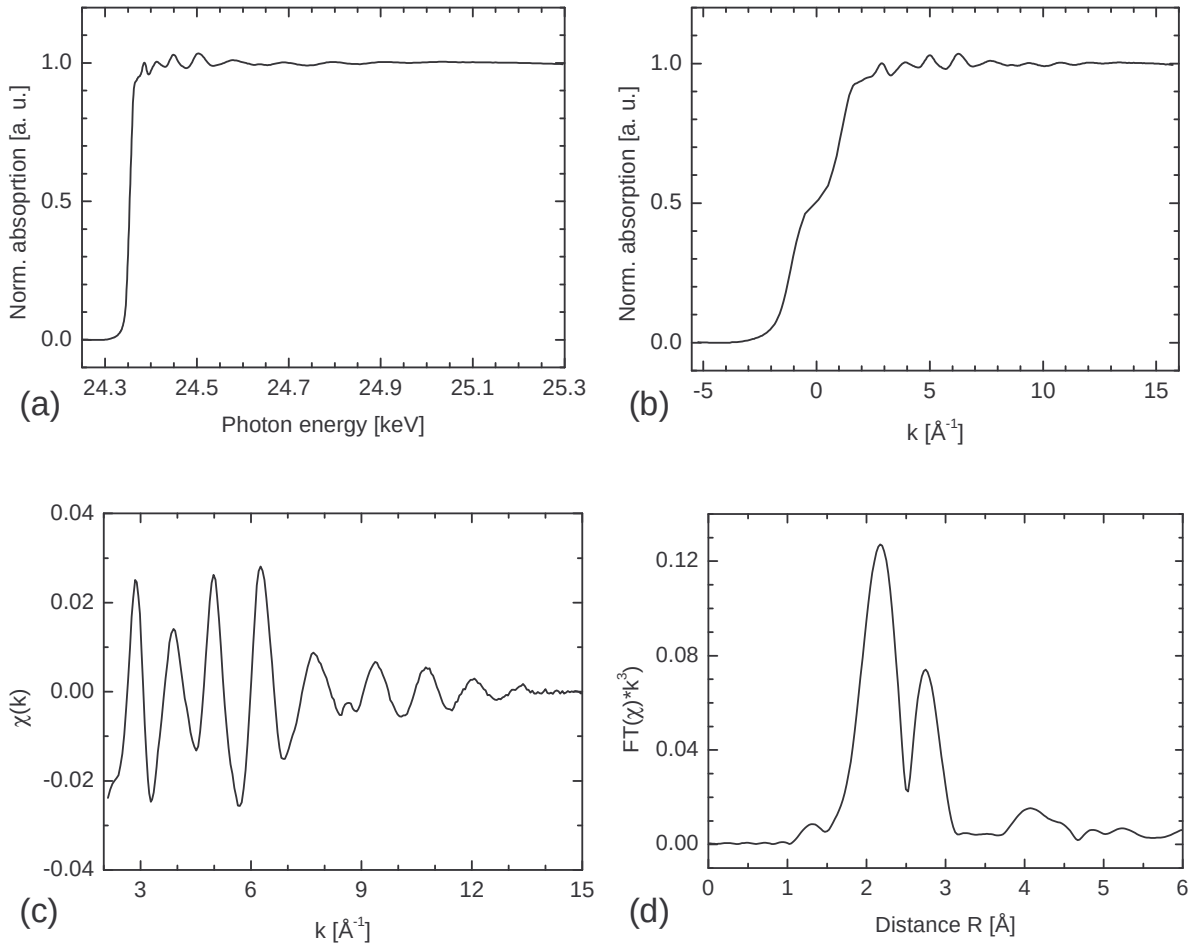

Figure 12: An example for EXAFS data processing: (a) background corrected and normalised absorption spectrum of PdGa, (b) after transformation into k-space, (c) extracted $\chi(k)$ and (d) after Fourier transformation of the $\chi(k)$.

Fitting parameters for the refinement of X-ray absorption data obtained from measurements of PdGa and Pd_3Ga_7 were (i) Debye-Waller factors for all single scattering paths, (ii) distances of single scattering paths, (iii) two E_0 shifts for Pd-Pd and Pd-Ga shells, and (iv) one 3rd cumulant for all scattering paths. Coordination numbers and S_0^2 were kept invariant. Because of the small difference in the atomic distances of the first (1 Ga atom) and second Ga shells (3 Ga atom) in PdGa (Table 3) the deviation from the crystallographic distances (R1+2) and the Debye-Waller factors (DW1+2) were correlated to be the same. All higher Ga shells (R = 4.008 Å, 4.579 Å + 4.657 Å) were correlated in the same way as well as the higher Pd shells (R = 4.402, 4.762 Å + 4.896 Å). Two multi-scattering paths (R = 4.074 Å + 4.127 Å) were included in the refinement. Accordingly, for the first and second Ga shell (4 Ga + 4 Ga atoms) in Pd_3Ga_7 (Table 3) the deviation from the crystallographic distances

(R1+2) and the Debye-Waller factors (DW1+2) were also correlated to be the same. Four higher Ga shells (R = 4.168 – 4.902 Å) and two higher Pd shells (R = 4.271 Å + 4.792 Å) were correlated in the same way. Two additional multi-scattering paths (R = 3.949 Å + 4.713 Å) were included in the refinement. First step of EXAFS refinement took place with two Debye-Waller temperatures, two E_0 shifts for Pd-Pd and Pd-Ga or Pd-Sn shells and three parameters x, y, and z for anisotropic expansion of the unit cell. For Pt sample an additional DW temperature and E_0 shift was used for the Pd-Pt shells. With every further step of the refinement, the number of free running parameter was increased. In the last refinement fitting parameters were (i) Debye-Waller factors for all single scattering paths, (ii) distances of single scattering paths, (iii) two E_0 shifts for Pd-Pd and Pd-Ga/Sn shells or respectively three for $PtPd_2Ga_3$ and $PtPd_2Ga_7$, and (iv) one 3rd cumulant for all scattering paths. Coordination numbers and S_0^2 were kept invariant. $PtPd_2Ga_3$ and $PtPd_2Ga_7$ were refined like PdGa and Pd_3Ga_7, respectively except for additional Pd-Pt shells. $PdSn_2$ was refined by correlating the first three Pd-Sn shells (2 + 2 + 4 Sn atoms) (Table 3) and two uncorrelated Pd-Pd shells (1 Pd atom at 2.837 Å + 8 Pd atoms at 4.589 Å). Higher Pd-Sn shells (4.615 – 5.020 Å) were correlated with one DW factor and the same deviation from the crystallographic distances. Two multiple-scattering paths (4.245 + 4.555 Å) were included in the refinement. A detailed XAS data reduction and data processing and is described in the literature [85]. The refined interatomic distance were plotted as deviation from crystallographic distances versus temperature and a second diagram shows the evolution of DW factors with increasing temperature.

6.6 Surface characterisation with XPS and ISS

6.6.1 X-ray photoelectron spectroscopy

X-ray photoelectron spectroscopy (XPS) is an important and common method to analyze the near-surface composition of a sample. High surface sensitivity is due to the low mean free path of electrons in bulk material. The mean free path is below 5 nm for a wide range of kinetic energies of the electrons in the majority of materials. Because of the high sensitivity due to scattering processes at gas phase molecules it is necessary to use an ultra high vacuum (UHV) chamber for XPS measurements. The basic principle of XPS is to measure the kinetic energy of electrons ejected by monochromatic X-rays from the near-surface region [72,86,87]. The binding energy (BE) can be calculated by subtracting the measured kinetic energy and the work function φ from the energy of the incident X-ray photons:

$$BE = h\nu - KE - \varphi$$

The work function φ is the energy difference between the Fermi level and the vacuum level and depends on the used spectrometer. In an X-ray photoelectron spectrum the intensity of the measured electrons is plotted versus the kinetic or binding energy. The presence of peaks at particular binding energies indicates the presence of specific elements in the sample. Hence, the elemental composition of a sample can be deduced by its XP spectra. In general, every present element results in several peaks due to presence of photoelectrons emitted from different energy levels. The elemental composition can be obtained by integration of the peak area of one peak per present element employing the corresponding sensitivity factor. There can be a shift to higher or to lower binding energies of the peaks depending on the oxidation state of the element. A positive oxidation state leads to a higher binding energy and a negative oxidation state result in a lower binding energy. Exact determination of the peak position is useful to obtain additional chemical information about the surface composition. Exact peak position determination is often difficult because of overlapping peak due to the presence of other elements or the presence of different oxidations states of the same element. In addition, samples with low electrical conductivity are difficult to analyze because of the presence of charging effects which lead to a peak shift to higher binding energies. Charging of the measured samples with low electrical conductivity occurs

by ejecting electrons from the surface without replacement from the bulk. A partial positive charge results which increases the apparent binding energy of subsequently emitted electrons. In addition to photoelectric processes, the emission of Auger electrons occurs and can overlap with the XPS peaks. In contrast to the photoelectrons, the energies of Auger electron are independent of the photon energy of the incident X-ray beam. Conventionally Al or Mg Kα radiation is used for XPS measurements.

6.6.2 Ion scattering spectroscopy

In contrast to XPS, which gives information about the composition of the near-surface region, ion scattering spectroscopy (ISS) is more surface sensitive and provides information of the topmost atom layers. The basic principle of ISS or LEIS (low energy ion spectroscopy) is the measurement of the kinetic energy of ions scattered at the surface of a sample [72,87]. An incident beam of monoenergetic ions, typically He or Ne ions in energy range from 0.5 to 3.0 keV is directed to the surface of a sample placed in an UHV system. The energy of the scattered ions is measured at a specific angle. The energy ratio of the incident beam E_0 and the scattered ions E_1 at a specific angle is described as:

$$\frac{E_1}{E_0} = \frac{1}{(1+A)^2} \cdot \left[\cos\theta_1 + \left(A^2 - \sin^2\theta_1\right)^{1/2} \right]^2 .$$

θ_1 is the angle between the incident beam and the scattered ions and A is the mass ratio M_2/M_1 of the backscattering surface atoms to the scattered ions and has to be >1 to fulfill the equation. The kinetic energy of the scattered He ions depends on the energy of the incident beam, the angle θ_1, and from the mass of scattering atoms. Scattering of light He ions on heavy metal atoms lead to He ions with kinetic energies similar to the incident beam and scattering at light elements like carbon or oxygen results in He ions with low kinetic energy. Estimation of the elemental composition of the surface region is difficult with ISS because the cross-sections of the atoms depend from their atomic weight. Therefore, heavy elements are more pronounced than light elements [72]. ISS is a destructive method because of the sputtering of the surface with helium ions. During ISS measurements the surface atom layers will be removed and information of the deeper surface regions is obtained.

6.6.3 XPS and ISS measurements

X-ray photoelectron spectroscopy (XPS) and ion scattering spectroscopy (ISS) were performed with a Leybold LHS 12 MCD UHV system. XPS data were obtained using Al Kα radiation (1486.6 eV). Shirley background correction and numeric integration of peak area were employed for XPS data reduction. Elemental composition of the near-surface region was estimated from the peak areas obtained using the corresponding sensitivity factors [88]. The palladium content was calculated from a sum of the Pd $3d^{3/2}$ and Pd $3d^{5/2}$ peaks and the carbon content was obtained from the C 1s peak. Because of the overlapping O 1s and Pd $3p^{3/2}$ peaks in the XPS spectra, the Pd $3p^{3/2}$ peak area was calculated from the Pd $3d^{3/2}$ and Pd $3d^{5/2}$ peak areas assuming a factor of 2.9 for the Pd $3p^{3/2}$ / (Pd $3d^{3/2}$ + Pd $3d^{5/2}$) ratio [88]. Subsequently, the Pd $3p^{3/2}$ peak area obtained was subtracted from the O 1s peak area to calculate the oxygen content in the near-surface region. The amounts of gallium and gallium oxide were determined by fitting the Ga $2p^{3/2}$ peak with two Gauss-Lorentz functions (30% Lorentzian). The XPS spectra were corrected for charging effects by setting the binding energy of the peak that corresponds to the Ga $2p^{3/2}$ peak of gallium oxide to a binding energy of 1117.8 eV [89].

Ion scattering spectroscopy was performed using He ions with a kinetic energy of 2 keV and an emission current of 10 mA. For ISS measurements of PdGa the first two scans were averaged and the following scans were averaged in groups of ten. For ISS measurements of Pd_3Ga_7 the first three scans were averaged and the following scans were averaged in groups of ten. As-prepared samples of PdGa and Pd_3Ga_7 were measured first by XPS followed by an ISS measurements and another XPS measurement to reveal the surface composition of the as-prepared materials and the influence of the ion scattering thereon. The influence of a hydrogen treatment on the surface composition was determined by XPS measurements before and after reduction of as-prepared PdGa in 200 mbar H_2 at 573 K for 30 min. After a second hydrogen treatment at 673 K for 30 min, XPS spectra were taken again followed by ISS and XPS measurements. Because of the reduced thermal stability of Pd_3Ga_7, XPS and ISS measurement were performed before and after a single hydrogen treatment at 573 K according to the procedure described above.

6.7 Chemisorption

Chemisorption of specific molecules on the surface of a catalyst can be used to investigate surface properties. Two possibilities exist to use chemisorption to obtain information about the catalyst surface. Both possibilities require the interaction of a probe molecule with the active sites on the catalyst surface. High selective chemisorption of the probe molecule on all active site of the surface permits to determine the total number of active sites of the catalyst by measuring the total amount of chemisorbed probe molecules. The information about the amount of active sites on a catalyst surface is more important than the total surface area obtained by nitrogen BET. The active surface area can significantly differ from the total surface area if a part of the surface is inactive in catalysis. The second possibility is to investigate the probe molecule adsorbed on the active sites with spectroscopic methods. Interaction of the probe molecule with the catalyst surface can change the configuration and bonding of the adsorbed probe molecule compared to the gas phase molecule. Infrared spectroscopy (IR) is a common method to obtain bonding properties of the chemisorbed molecule which maybe modified by the interaction with the active site on the catalyst surface.

6.7.1 Active surface determination by volumetric measurement of CO chemisorption

Carbon monoxide chemisorbs strongly on Pd metal surface [90]. CO chemisorption is a common method to obtain the metal surface area of supported Pd catalysts. Chemisorption equipments allow measuring the total amount of chemisorbed CO on a Pd sample, and consequently, the calculation of the number of Pd atoms present on the sample surface. Measuring the total amount of the adsorbed CO has to take the chemisorbed and physisorbed part of the adsorbed CO into account. Chemisorption is defined as adsorption with chemical interaction of the adsorbat molecule with the surface whereas physisorption is defined as weakly van-der-Waals interaction. Physisorption occurs preferentially at temperatures near the boiling point of the adsorbat and often leads to multi-layer adsorption on the surface.

Simultaneous occurrence of chemisorption and physisorption makes it mandatory to be able to distinguish between both kinds of adsorption.

Carbon monoxide chemisorption measurements were carried out in an Autosorb 1C (Quantachrome Instruments). The samples (PdGa: 1.5 g, Pd_3Ga_7: 1 g, Pd/Al_2O_3: 180 mg) were pretreated in situ in the sample cell by heating to 673 K (Pd_3Ga_7), 773 K (PdGa), or 473 K (Pd/Al_2O_3) in helium flow (20 ml/min), followed by an isothermal hydrogen treatment for 30 min (20 ml/min of 100% H_2 flow) and evacuation (180 min) at the pretreatment temperature. The samples were cooled down to 300 K under vacuum and evacuated for additional 180 min. Subsequently, the CO chemisorption measurements (CO 4.7, Westfalen Gas, Germany) were performed at 300 K.

The active Pd surface area was determined by stepwise measuring the amount of chemisorbed and physisorbed CO. An initial CO pressure of 10.7 kPa was employed, followed by nine equidistant steps up to a final pressure of 106.7 kPa. The pressure drop in the sample cell can be used to calculate the amount of CO adsorbed [91-93].

The integrated amounts of adsorbed CO were plotted versus the pressure and resulted in a so-called combined isothermal curve refers to the chemisorbed and physisorbed CO. The physisorbed CO was removed by evacuating the sample cell and the adsorption procedure was carried out again and results in a second so-called weak isothermal curve. The active Pd surface area was calculated by two methods. The first method is based on the assumption that after occupation of all chemisorption sites on the surface a further increase of CO partial pressure leads to physisorption of CO. The chemisorbed part can be distinguished from physisorbed part by linear extrapolation of the combined isothermal. The chemisorbed part of adsorbed CO can be obtained from the intercept of the linear correlation at the y-axis. The second possibility is the calculation of chemisorbed CO by using the Dual isotherm method. The weak isotherm curve was measured after the combined isothermal curve and contains only the physisorbed part of the CO because all adsorption sites for the chemisorbed CO are still occupied. The difference of combined and weak isothermal curve results in the chemisorbed amount of the CO. The resulting values of the chemisorbed CO should be similar for every pressure step after occupation of all chemisorption sites on the surface of the Pd-Ga intermetallic compounds.

6.7.2 Infrared absorption spectroscopy

Vibrations in molecules or a solid lattice can be excited with energies typical for infrared radiation. A change in the dipole moment is a prerequisite for the excitation of vibrational modes of molecules by IR radiation. Information about the bonding in molecules can be obtained by IR absorption data. IR spectroscopy in catalysis is a useful method to obtain data from adsorbed species on catalyst surfaces.

Infrared absorption of chemisorbed probe molecules

Carbon monoxide is a typical probe molecule which adsorbs strongly on Pd metal surfaces. The CO molecule has a gas phase absorption band at ~2180 cm^{-1} [90]. Differences in IR absorption spectra between gas phase and chemisorbed molecules provide information about the adsorption strength and configuration. Chemisorbed CO molecules show a shift to lower wavenumbers of vibrational frequencies because the interaction of the Pd surface and the CO molecule leads to a weakening of the C-O bond. The interaction between the CO molecule and the Pd surface is due to electron density donation from the 5σ-orbital of the CO and electron density backdonation from the Pd to the unoccupied anti-bonding 2π*-orbital of the CO molecule [90]. In particular the backdonation to the antibonding orbital of the CO molecule decreases the bond strength of the CO molecule. The extent of weakening of the C-O bond correlates with the strength of the interaction between surface and CO molecule. CO molecules can be adsorbed on top of a single Pd atom, in a bridging mode between two Pd atoms, and in a three hollow mode. All three adsorption configurations can occur on palladium depending on CO partial pressure and Pd surface facets. The increasing number of involved Pd atoms leads to increasing interaction between the surface and the CO molecule and, therefore, a stronger shift in the wavenumber depending on the on-top, bridging, or three-hollow chemisorption mode results. Typical wavenumbers for on-top adsorbed CO molecules are ~2080 cm^{-1} and ~1960 cm^{-1} or 1850 - 1920 cm^{-1} for the bridge or three-fold adsorption mode, respectively [94]. The ratio between three-hollow, bridging or on-top mode of chemisorbed CO provides also geometric information. Preferred chemisorption to three or two Pd atoms indicates the presence of ensembles of Pd atoms on the surface. Active site isolated catalysts provide only isolated Pd atoms on the surface. Consequently, only on-top bonded CO molecules are detectable. Therefore, IR absorption spectroscopy allows verifying the isolation of Pd atoms on the surface of the Pd-Ga intermetallic compounds [33]. In

addition, modification of palladium by alloying changes the electronic structure of the Pd surface and influences the chemisorption of carbon monoxide. Reduction of the d-band density of states by alloying of the Pd leads to weaker interaction of the metal with the CO molecule and, thus, results in a higher wavenumber of the chemisorbed CO in the IR spectrum [95].

IR measurement with carbon monoxide as a probe molecule provides two different information: First, determination of CO chemisorption on Pd catalyst is possible. IR measurements are more sensitive to adsorbed CO molecule compared to the volumetric measurement of the amount of CO adsorbed. Second, measurements of the vibrational modes of chemisorbed CO molecules indicate the presence or absence of Pd ensembles on the surfaces and give information about the electronic structure of a Pd based alloy or Pd intermetallic compound compared to Pd metal.

Diffuse reflectance infrared Fourier transform spectroscopy

DRIFTS is a spectroscopic method to measure infrared absorption of chemisorbed species on surfaces. Multiple diffuse reflectances at the surface of a powdered sample allow detecting a monolayer of adsorbat by multiple absorption of the chemisorbed molecule or atom. Absorption of infrared radiation occurs by excitation of an IR active vibrational mode of the surface lattice or a chemisorbed species.

A Bruker IFS 66 was used with 150 mg of chemical etched PdGa and Pd_3Ga_7 and 50 mg of 1:4 mixture of Pd/A_2O_3 (commercial from ALDRICH, 5 wt% Pd) and boron nitride as reference. The DRIFTS cell was carefully purged with helium (He 5.0, Westfalen Gas, Germany, equipped with an additional gas purification system). For adsorption measurements 1% CO (4.7, Messer Griesheim, Germany) in helium was used with a total flow of 100 ml/min at atmospheric pressure.

6.8 Catalytic studies

6.8.1 Gas chromatography

Chromatographic techniques using a gas as mobile phase and a solid as stationary phase are referred to gas chromatography. Gas chromatography is the technique of choice for the separation of thermally stable and volatile compounds using an inert carrier gas as mobile phase and a solid as stationary phase [70,71]. Separation of light hydrocarbons or inorganic gases is performed by adsorption and desorption of the components on the stationary phase. In general, the basic principle of chromatography is the equilibrium of the distribution of the gaseous sample in the mobile and the stationary phase and the ratio of the two concentrations is called thermodynamic partition coefficient

$$K = \frac{c_{stationary}}{c_{mobile}} .$$

Interaction of the gaseous sample with the stationary phase leads to retention of the gaseous sample compared to the mobile phase. The retention time t_R refers to the time between injection of the sample onto the column and the detection at the end of the column. Multiplication of the retention time t_R by the volumetric flowrate F_c is defined as the retention volume V_R. The transit time of a nonretained component is called dead time t_M and together with t_R can be used to calculate the partition ratio (or capacity ratio) k'

$$k' = \frac{t_R - t_M}{t_M}$$

which is the most important quantity since it relates the equilibrium distribution of a sample to the thermodynamic properties of the column. Two different samples A and B interact differently with the stationary phase and lead to different retention times t_R and retention volumes V_R and consequential different partition ratios k'_A and k'_B. The relative retention (or selectivity factor) α describes the extend of separation of compound A and B (compound A elutes before compound B) with

$$\alpha = \frac{k'_A}{k'_B}$$

on a column under the same measuring condition. A high value for α leads to effective and fast separation and a value next to 1 may leads to no sufficient separation of the peaks in the chromatogram. The separation of two or more components can be increased by varying the composition of the stationary phase, the column length, the column temperature and the pressure of the carrier gas to obtain a high value for the relative retention α. The columns in gas chromatography are packed with interactive solids like molecular sieves or porous polymers. Different adsorption behavior is reached by varying the pore size of the molecular sieves or the composition of the polymers to modulate the polarity of the porous polymers. A multicolumn system is required for separation of complex gas mixtures. Backflushing on a pre-column is necessary to prevent poisoning of the column for separation of light alkanes and alkenes or light inorganic gases with less volatile compounds. Modern gas chromatography devices like MicroGCs consist of micro capillaries etched in a silicon waver and operate isothermal instead of temperature-programmed which is common for standard GC equipments. A pressure program with increasing pressure can be applied to reduce measurement time to a few minutes per cycle. A detector located at the end of the separation column detects the presence of the individual components as they leave the column. Several kinds of detectors are used like thermal conductivity detectors (TCD), flame ionization detectors (FID), and thermionic emission detector (TED), and electron capture detector (ECD). Thermal conductivity detectors use a heated filament placed in the gas stream at the end of the column and measure the amount of heat loss from conductivity of the gas stream. Changes in gas composition increases or decreases thermal conductivity and result in an increased or decreased filament temperature. A change in the filament temperature influences the electrical resistivity and can be detected. The thermal conductivity of most inorganic gases and volatile organic compounds is relatively low compared to helium or hydrogen. Hence, both gases are used as mobile phase. Low amount of organic material leads to relatively large decrease in thermal conductivity and a high signal of the TC-detector if helium or hydrogen is used as mobile phase.

6.8.2 Experimental equipment

Catalytic investigations were performed in a plug flow reactor consisting of a quartz tube with a length of 300 mm, an inside diameter of 7 mm and equipped with a sintered glass frit to support the catalyst bed. For temperature control, a thermocouple was located next to the heating wire wound around the reactor (Figure 13). A second thermocouple was placed inside the reactor to measure the temperature of the catalyst bed. The reactant gases were mixed with Bronkhorst mass flow controllers (total flow 30 ml/min). A Varian CP 4900 Micro gas chromatography (GC) and a Pfeiffer omnistar quadropol mass spectrometer (MS) were used for effluent gas analysis. The Varian MicroGC contains three modules, each with an individual column and a thermal conductivity detector. Hydrogen and helium of the feed gas, and possible oxygen and nitrogen impurities because of leaks in the set-up were separated on a molsieve column. Acetylene, ethylene, and ethane were separated on an alumina column. The total concentration of C4 hydrocarbons (1-butene, 1,3-butadiene, n-butane, trans and cis-2-butene) was determined using a siloxane (dimethylpolysiloxane) column. Higher hydrocarbons were also separated on the siloxane column but not further quantified because of the presence of many different C6 and C8 hydrocarbons and their low total concentration (less than 0.1% of absolute product stream concentration). Argon (6.0) and helium (6.0) were used as carrier gases for the molsieve column and for the other columns, respectively. A measurement cycle including stabilization, sampling, injection, and separation took between 4 and 5 minutes.

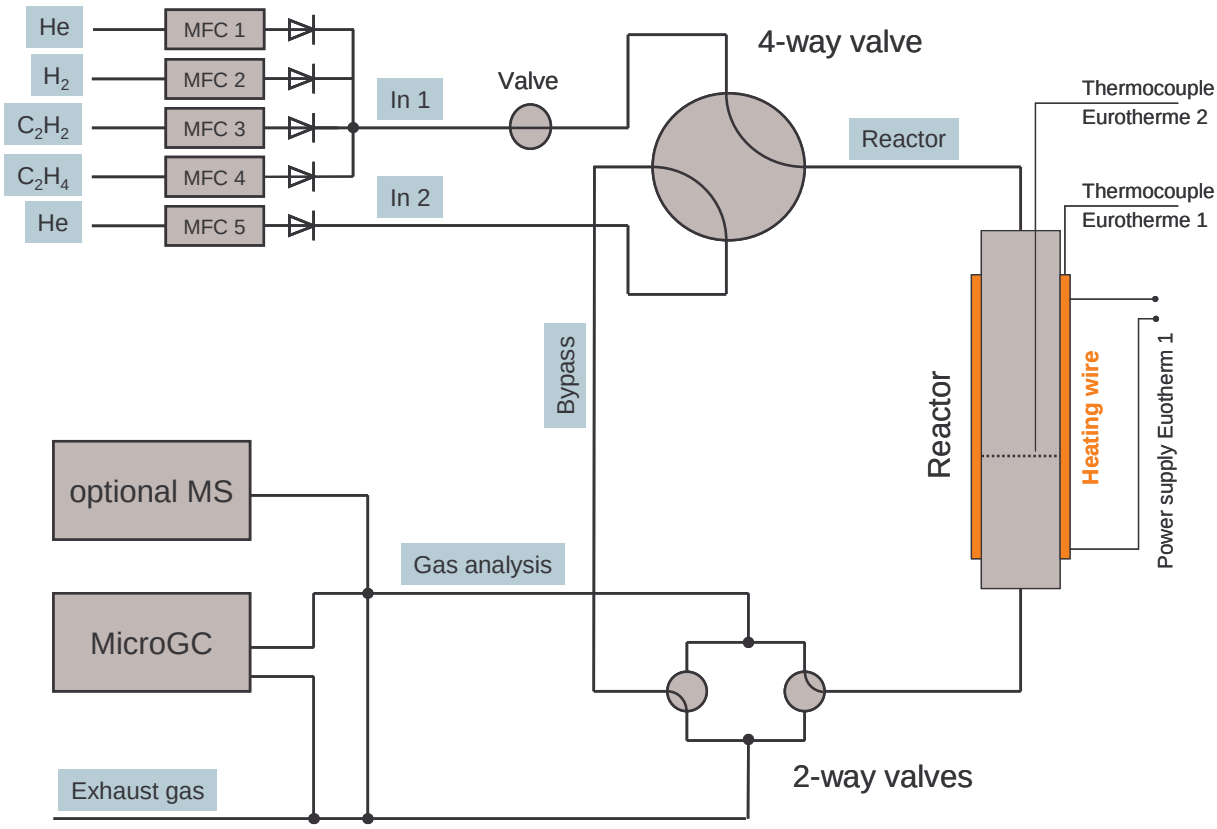

Figure 13: Scheme of the experimental catalysis set-up. The gases were mixed by mass flow controllers (mfc) and a 4-way-valve allowed to introduce the acetylene feed or the helium bypass into the reactor. Temperature of the reactor was controlled by two thermocouples. Inside thermocouple measured the catalyst bed temperature and outside thermocouple was used to control the heating power. Two 2-ways-valves downside of the reactor allowed switching the product gas either to the gas analysis equipment or directly to the exhaust gas.

Acetylene hydrogenation experiments were carried out under two different conditions: (condition A) 2% acetylene and 4% hydrogen in helium and (condition B) 0.5% acetylene, 5% hydrogen, and 50% ethylene in helium. Solvent free acetylene (2.6), hydrogen (5.0), and helium (5.0) were used for studies under conditions A, while a mixture of 2% acetylene in helium (C_2H_2: 2.6, He: 4.6), hydrogen (5.0), ethylene (3.5), and helium (5.0) were used for studies under conditions B. The solvent free acetylene was obtained from Linde (Germany). All other gases were obtained from Westfalen Gas (Germany). The samples were diluted with 30 mg (condition A) or 50 mg (condition B) boron nitride (hexagonal, 99.5%, 325 mesh, Aldrich). A commercial Pd on alumina catalyst (5 wt% Pd, Aldrich) was used as a reference under conditions A and B.

6.8.3 Catalytic measurements and data processing

Activity and selectivity of the materials in the hydrogenation of acetylene were measured by temperature-programmed and by isothermal experiments. In the temperature programmed mode, the composition of the product gas stream was measured every 15 K in the range from 298 K to 613 K (condition A). In the isothermal mode, the experiments were performed at 393 K (condition A) and 473 K (condition B). The conversion rate was calculated using the following equation:

$$Conv = \frac{(C_{bypass} - C_x)}{C_{bypass}}$$

where C_x is the acetylene concentration in the product stream and C_{bypass} is the acetylene concentration in the feed before the reaction. Under reaction condition A, the selectivity is calculated using the following equation:

$$Sel_A = \frac{C_{ethylene}}{C_{ethylene} + C_{ethane} + 2 \cdot C_{C4Hx}}$$

where C_{C4Hx} is the sum of the C4 hydrocarbons. The changing ethylene concentration $\Delta C_{ethylene}$ cannot be accurately measured in an excess of ethylene under condition B and, hence, cannot be used for calculating the selectivity. Therefore, the selectivity under condition B was calculated from the following equation, with c_{bypass} the acetylene concentration before the reactor and C_x the acetylene concentration after the reactor:

$$Sel_B = \frac{C_{bypass} - C_x}{C_{bypass} - C_x + C_{ethane} + 2 \cdot C_{C4Hx}}$$

Calculation of the selectivity under condition B assumes that acetylene is only hydrogenated to ethylene, which may be further hydrogenated to ethane. The amount of C4 hydrocarbons and carbon deposits formed was supposed to be negligible. In addition to hydrogenation of acetylene to ethane, ethylene from feed may be hydrogenated to ethane, which is included in the selectivity equation. In order to measure selectivity in acetylene hydrogenation at the same conversion, different amounts of catalysts were used according to their specific activity determined in a previous experiment.

Activity of the samples was calculated using following equation:

$$Act = \frac{Conv \cdot C_{feed} \cdot C_{\exp}}{m_{cat}}$$

where *Conv* is the calculated acetylene conversion, C_{feed} the concentration of acetylene in feed (condition A: 2%, condition B: 0.5%), m_{cat} the amount of used catalyst in g and the constant C_{exp} = 1.904 g_{C2H2}/h contains experimental flow parameters like total gas flow (30 ml/min), temperature (300 K) and pressure (1013 mbar) and is based on the perfect gas model.

6.9 Chemical etching

Catalytic activity of catalysts is often proportional to the active surface area. Hence, increasing the surface area can lead to higher activity. An increased active surface area can be obtained by increasing the total surface area by special preparation techniques like precipitation on supports or by ballmilling to obtain smaller particles. Another possibility is to increase the ratio of active surface area to the total surface area. If the surface of a catalyst is partly covered with an inactive compound it might be possible to remove the inactive materials. Inactive material can consist of poisoned or oxidized catalyst surface and may be removed by treatment like reduction or chemical etching.

6.9.1 Chemical etching of PdGa and Pd_3Ga_7

In order to increase the active catalyst surface of PdGa and Pd_3Ga_7, chemical etching was performed by ammonia solution at various pH. Commercial ammonia solution (Merck, 25% p. a.) was diluted with water to the required pH value. pH-measurements were performed with a Knick pH-Meter 761 Calimatic and a Mettler-Toledo Inlab 422 electrode calibrated with buffer solutions (Merck centiPUR pH = 7 and pH = 9). 50 mg PdGa or Pd_3Ga_7 were added to 75 ml of the diluted ammonia solution and stirred for 10 minutes at 300 K. The solution was filtrated under Argon flow and washed with additional 50 ml of the diluted ammonia solution. The etched sample was dried by evacuation for 120 min in a desiccator and stored under Ar in a glove box.

6.9.2 Chemical etching of $PdSn_2$

The Pd-Sn intermetallic compound was chemical etched with an aqueous solution of sodium hydroxide and ethylene-diamine-tetraacetic-acid (EDTA). The etching solution was prepared by dissolving 5 mg NaOH p. a. (Aldrich, Germany) and 500 mg EDTA (99.5%, Aldrich Germany) in 300 ml water. 150 mg $PdSn_2$ were stirred for ten minutes in 250 ml etching

solution followed by filtration under Ar atmosphere and additional washing with 150 ml diluted etching solution (remaining 50 ml + 100 ml water). The sample was evacuated for 1 hour in a desiccator and directly used for catalysis experiments. Additional etching solutions were investigated containing ammonia (Merck, 25% p. a.) and hydrogen peroxide (Merck, 30% p. a.).

7 Pd-Ga intermetallic compounds

7.1 Results

7.1.1 Preparation and characterization of PdGa and Pd_3Ga_7

As-prepared PdGa and Pd_3Ga_7 were ground by hand and phase purity was confirmed by ex situ X-ray diffraction. The experimental XRD pattern showed no deviation from the calculated pattern of PdGa [60-62] (Figure 14) and Pd_3Ga_7 [57,62,64] (Figure 15). In order to increase the surface area, the materials were treated in a ball-mill. XRD patterns of the ball-milled samples showed no change in the phase composition but an increase in the FWHM of the peaks which indicates a smaller crystallite size (17.5 nm for PdGa and 34.0 nm for Pd_3Ga_7) and a higher surface area (Figure 14 + Figure 15). Nitrogen adsorption measurements resulted in a BET surface area of about 1 m^2/g for both samples after the ball milling procedure.

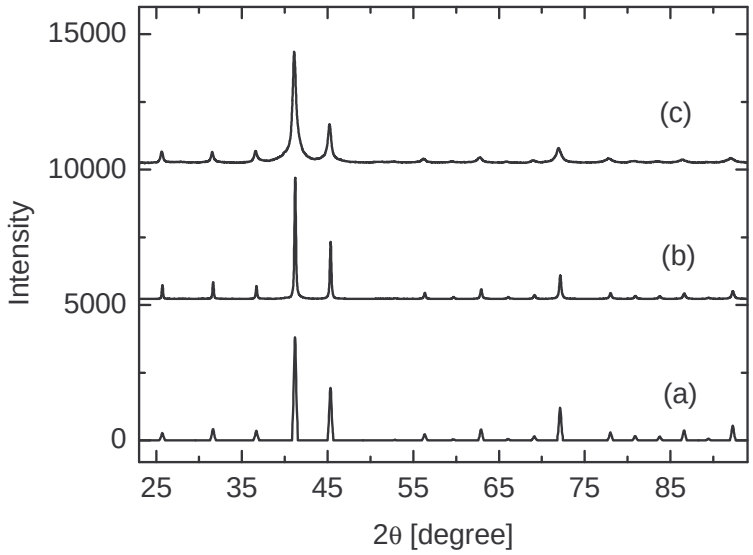

Figure 14: Experimental X-ray diffraction patterns of PdGa (b) after grinding in a mortar and (c) after ball milling, together with a simulated pattern of PdGa (a) [62].

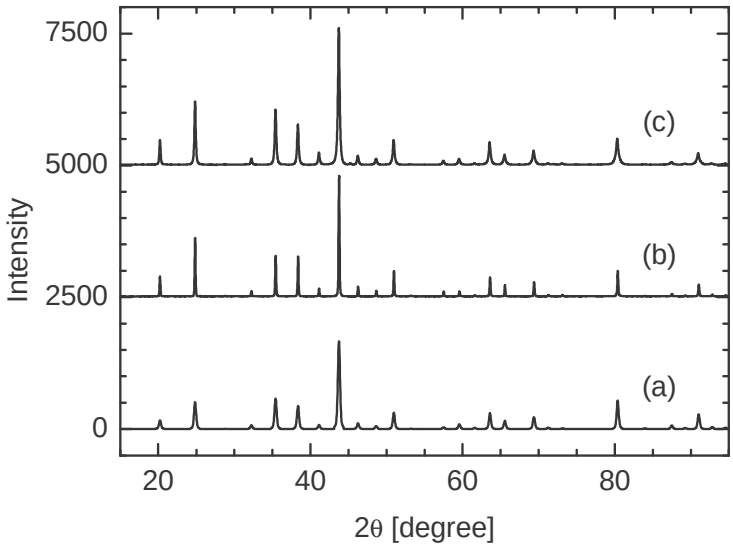

Figure 15: Experimental X-ray diffraction patterns of Pd_3Ga_7 (b) after grinding in a mortar and (c) after ball milling, together with a simulated pattern of Pd_3Ga_7 (a) [62].

Figure 16 shows the experimental FT(χ(k)*k^3) of PdGa ex-situ at 300 K together with a theoretical FT(χ(k)*k^3) obtained by the refinement procedure described above. The FT(χ(k)*k^3) shows two main maxima at 2.2 Å and 2.8 Å. The first maximum can be assigned to the three Ga shells and the second maximum to the first Pd-Pd shell. A good agreement between the experimental and theoretical FT(χ(k)*k^3) can be seen and the interatomic distances obtained (Table 4) show only minor deviations from the crystallographic data. The low Debye-Waller factors indicate a highly ordered structure of PdGa.

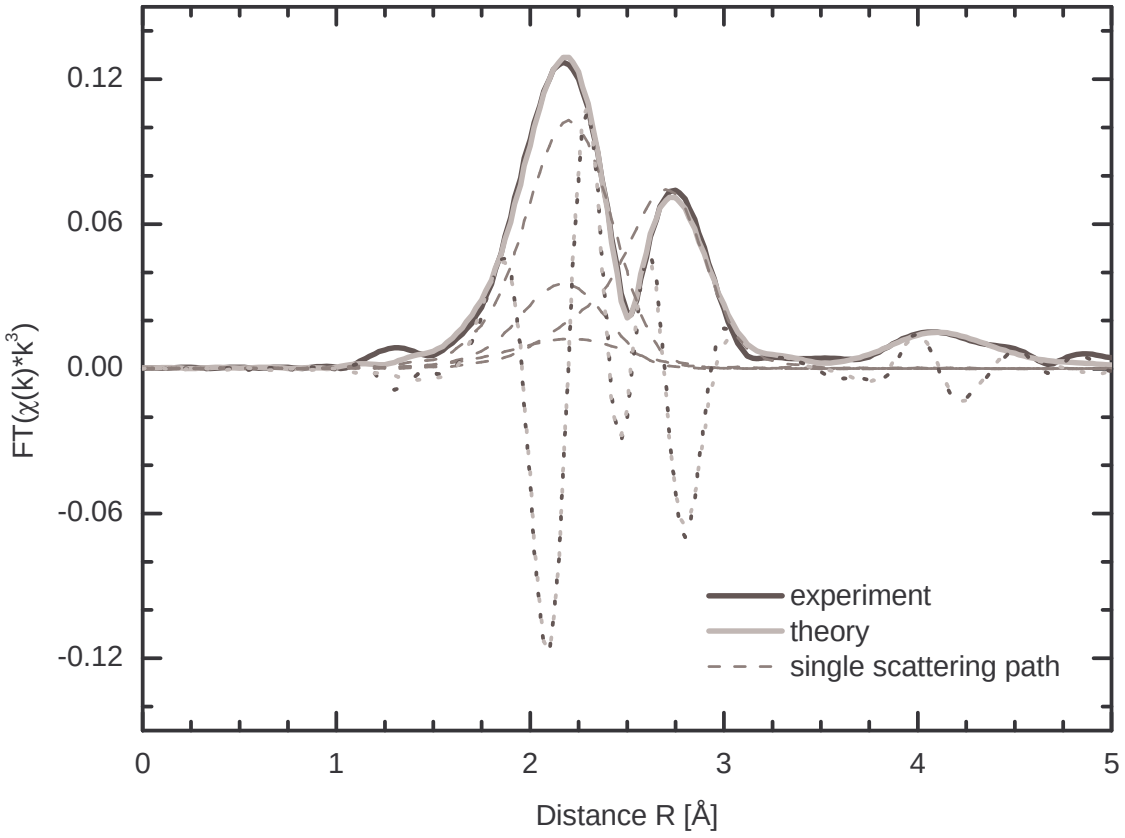

Figure 16: Experimental and theoretical Pd K edge FT(χ(k)*k^3) of PdGa at 300 K.

The experimental and theoretical FT(χ(k)*k^3) of Pd_3Ga_7 at RT showed only one maximum (Figure 17). This maximum can be assigned to the three Ga shells consisting of 8 Ga atoms and the first single Pd atom. Destructive interference and attenuation of the single and multiple scattering paths at higher distances resulted in a low total amplitude of the RDF above 3 Å. The refined interatomic distances of Pd_3Ga_7 showed only minor deviations compared to the distances from crystallographic structure and the low Debye-Waller factors indicate a highly ordered structure (Table 4).

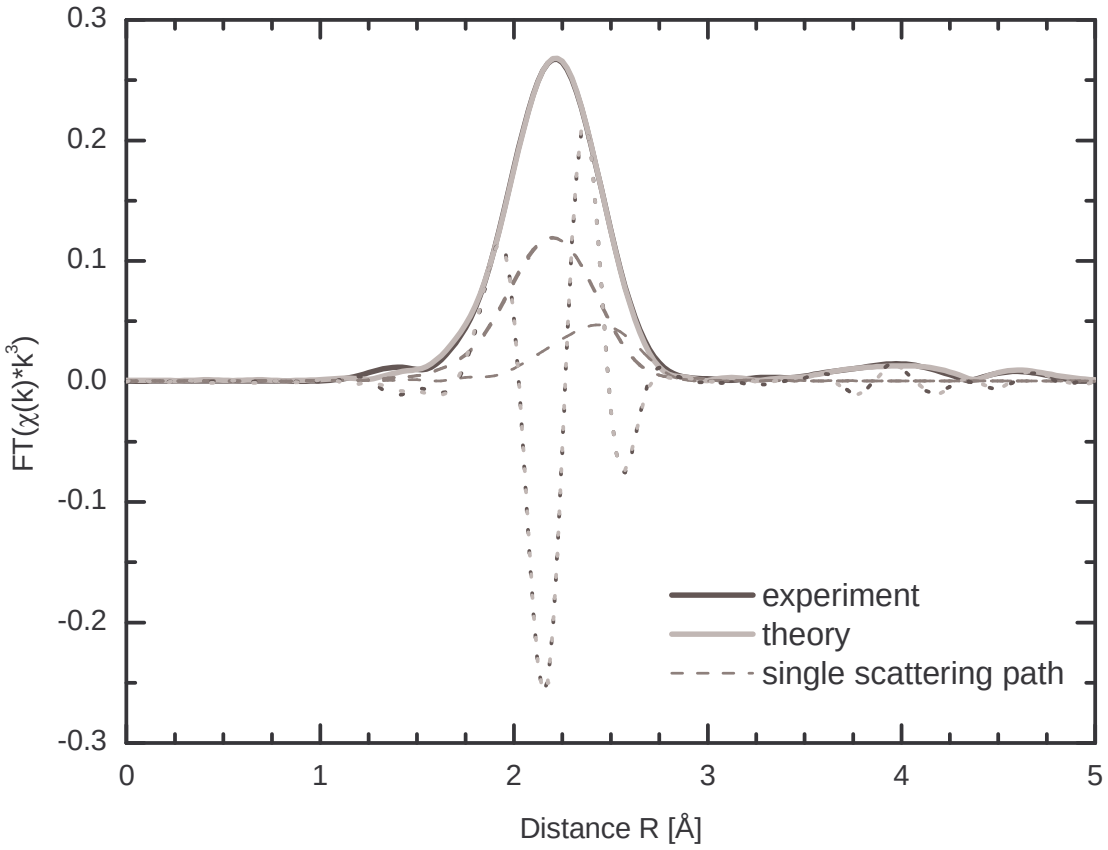

Figure 17: Experimental and theoretical Pd K edge FT(χ(k)*k^3) of Pd_3Ga_7 at 300 K.

Table 4: Result of EXAFS refinement of PdGa and Pd_3Ga_7 ex-situ at the Pd K-edge. ΔR_c refers to the deviation of the refined interatomic distance to the crystallographic data.

PdGa	**CN**	**R [Å]**	**ΔR_c [Å]**	**σ^2 [Å^2]**	**E_0 [eV]**
Ga	1	2.52	-0.02	0.008	-2.58
Ga	3	2.55	-0.02	0.008	-2.58
Ga	3	2.68	-0.02	0.007	-2.58
Pd	6	2.98	-0.03	0.011	-3.12
Pd_3Ga_7	**CN**	**R [Å]**	**ΔR_c [Å]**	**σ^2 [Å^2]**	**E_0 [eV]**
Ga	4	2.57	-0.01	0.007	-0.65
Ga	4	2.58	-0.01	0.007	-0.65
Pd	1	2.73	0.00	0.005	1.03

7.1.2 Structural and thermal investigations

Thermal analysis

Thermal gravimetric analysis of PdGa and Pd_3Ga_7 yielded a considerable stability of the materials up to 600 K and 550 K in reducing (H_2) and oxidizing (O_2) atmospheres, respectively. During treatment in 50% hydrogen in He, PdGa showed a small mass loss in the range from 300 K to 600 K possibly because of the desorption of water or CO_2, or slight reduction of a surface oxide (Figure 18). A more pronounced mass loss at ~ 600 K indicates the onset of a significant surface oxide reduction. Pd_3Ga_7 showed an even smaller mass loss in the range from 300 K to 620 K indicating only slight contribution of oxide reduction in the temperature range employed (Figure 19). During treatment in 50% oxygen in He, PdGa showed a mass gain with an onset of temperature at 500 K indicating proceeding oxidation of the material (Figure 18). Pd_3Ga_7 showed a similar behavior during treatment in oxygen. Thermal treatment of PdGa and Pd_3Ga_7 in pure helium resulted in slight mass loss (< 0.05%)

due to desorption of water and an additional mass gain to 100% at the final temperature may contribute to surface oxidation by traces of oxygen in the helium feed (Figure 19). The DSC traces measured of the two materials under reducing and oxidizing atmospheres exhibited a small exothermic peak at about 420 K for Pd_3Ga_7 and 460 K for PdGa.

Thermal gravimetric analysis of PdGa and Pd_3Ga_7 yielded a considerable stability of the materials up to 600 K and 550 K in reducing (H_2) and oxidizing (O_2) atmospheres, respectively. During treatment in 50% hydrogen in He, PdGa showed a small mass loss in the range from 300 K to 600 K possibly because of the desorption of water or CO_2, or slight reduction of a surface oxide (Figure 18). A more pronounced mass loss at ~ 600 K indicates the onset of a significant surface oxide reduction. Pd_3Ga_7 showed an even smaller mass loss in the range from 300 K to 620 K indicating only slight contribution of oxide reduction in the temperature range employed (Figure 19). During treatment in 50% oxygen in He, PdGa showed a mass gain with an onset of temperature at 500 K indicating proceeding oxidation of the material (Figure 18). Pd_3Ga_7 showed a similar behavior during treatment in oxygen (Figure 19). Thermal treatment of PdGa and Pd_3Ga_7 in pure helium results in slight mass loss (< 0.05%) due to desorption of water and an additional mass gain to 100% at the final temperature may contribute to surface oxidation by traces of oxygen in the helium feed (Figure 19). The DSC traces measured of the two materials under reducing, oxidizing and in inert atmospheres exhibited a small exothermic peak at about 420 K for Pd_3Ga_7 and 460 K for PdGa.

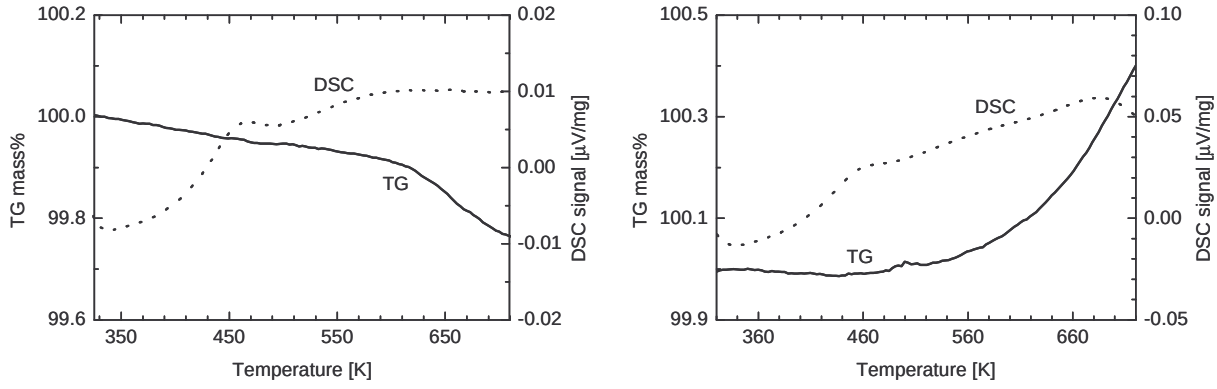

Figure 18: Relative mass (TG) (solid) and DSC signal (dotted) during thermal treatment (300 K – 723 K at 6 K/min) of PdGa in 50% hydrogen in helium (left) and in 50% oxygen in helium (right).

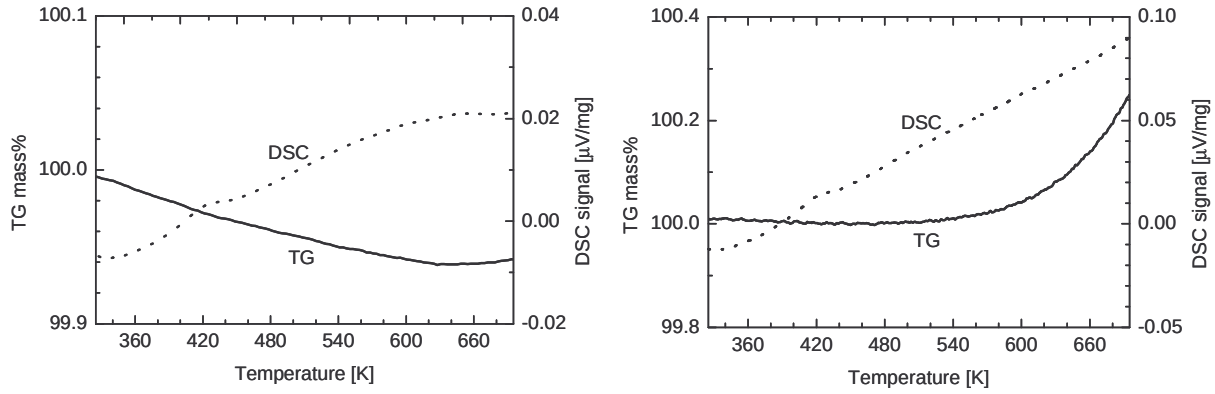

Figure 19: Relative mass (TG) (solid) and DSC signal (dotted) during thermal treatment (300 K – 693 K at 6 K/min) of Pd_3Ga_7 in 50% hydrogen in He (left) and in 50% oxygen in He (right).

Scanning electron microscopy

Scanning electron microscopy images of PdGa after ball milling and after subsequent treatment in 50% hydrogen in helium treatment for 30 minutes are depicted in Figure 20. Pd_3Ga_7 showed a similar morphology and behavior. The ball milled sample exhibited particles sizes at crystalline agglomerates in the range from 2 µm to 20 µm (Figure 21) with Pd_3Ga_7 having a slightly larger average particle size than PdGa. Both Pd-Ga intermetallic compounds exhibited surfaces with a homogeneous Pd-Ga ratio while regions with a higher concentration of gallium were also detected. After treatment in hydrogen at 573 K the particles appeared to be slightly more coalesced and exhibited smoother surfaces (Figure 4b). Regions that show a higher Ga content persisted.

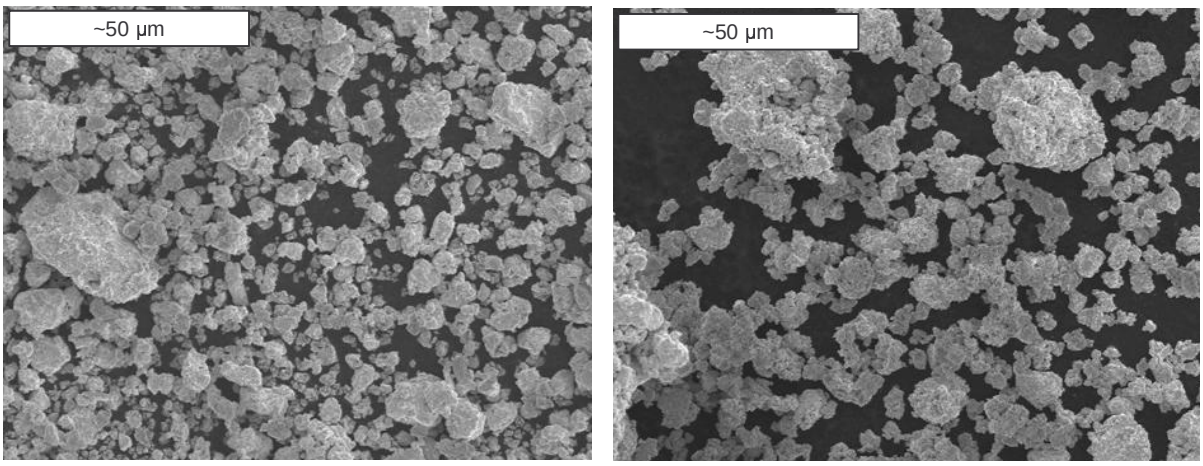

Figure 20: Scanning electron microscopy images of ball-milled PdGa before (left) and after (right) heating in 50% hydrogen in helium to 573 K.

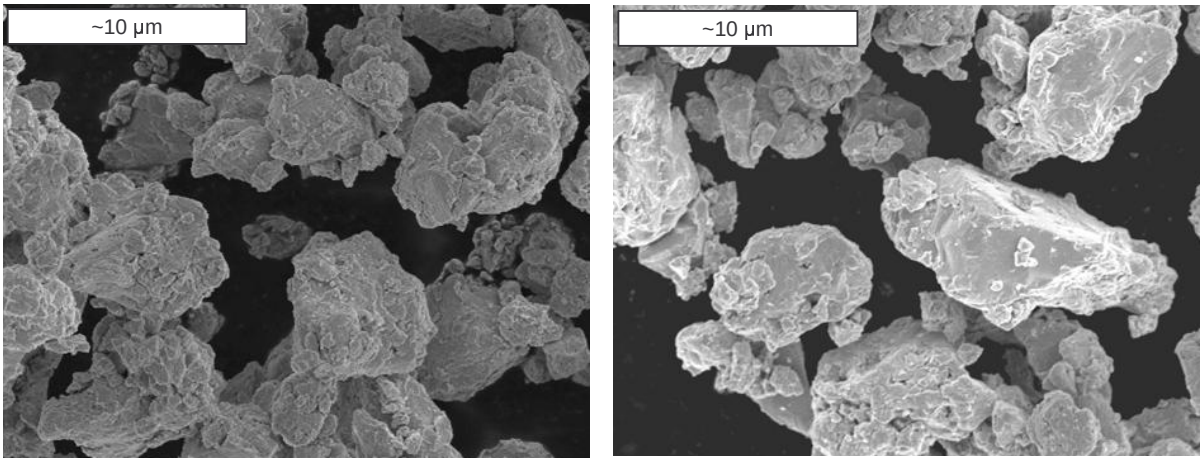

Figure 21: Scanning electron microscopy images of ball-milled Pd_3Ga_7 before (left) and after (right) heating in 50% hydrogen in helium to 573 K.

In situ X-ray diffraction

In situ XRD patterns measured during thermal treatment of PdGa in 50% hydrogen in He and in 20% oxygen in He are shown in (Figure 22 + Figure 23), respectively. No additional diffraction lines corresponding to Pd metal, PdO, or Ga_2O_3 were detected in the temperature range employed for the hydrogen containing atmosphere. In 20% oxygen the formation of a peak at 2θ = 39.7 ° at 673 K indicates the presence of small amounts of Pd metal. An additional peak at 2θ = 44.5 ° formed at 673 K could not be identified. A significant narrowing of the diffraction lines with temperature can be observed indicative of crystallite growth and sintering of the ball milled material. A linear shift of 0.2° in 2θ of the (201) diffraction line with increasing temperature in helium, oxygen, and hydrogen is attributed to a thermal expansion of the PdGa lattice. Incorporation of hydrogen or oxygen atoms in the bulk structure is not detected.

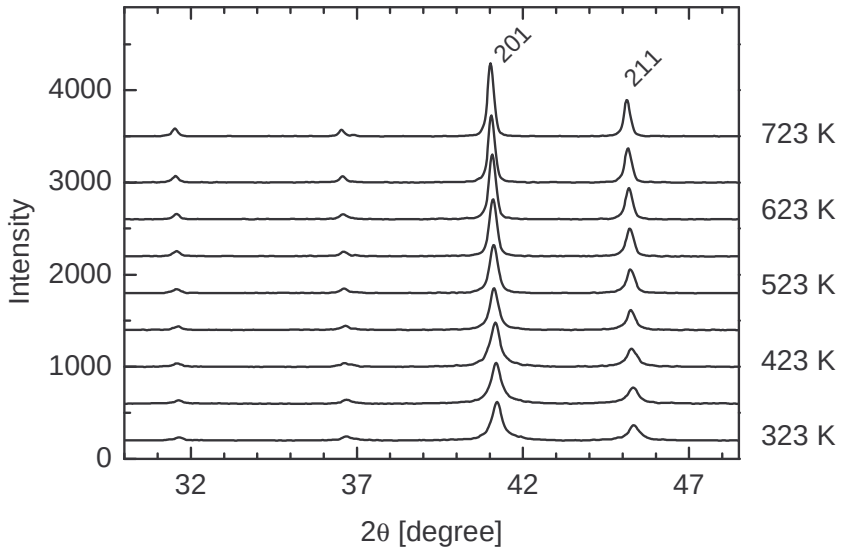

Figure 22: Evolution of in situ X-ray diffraction patterns measured during thermal treatment of PdGa in 50% hydrogen in helium from 323 K to 723 K.

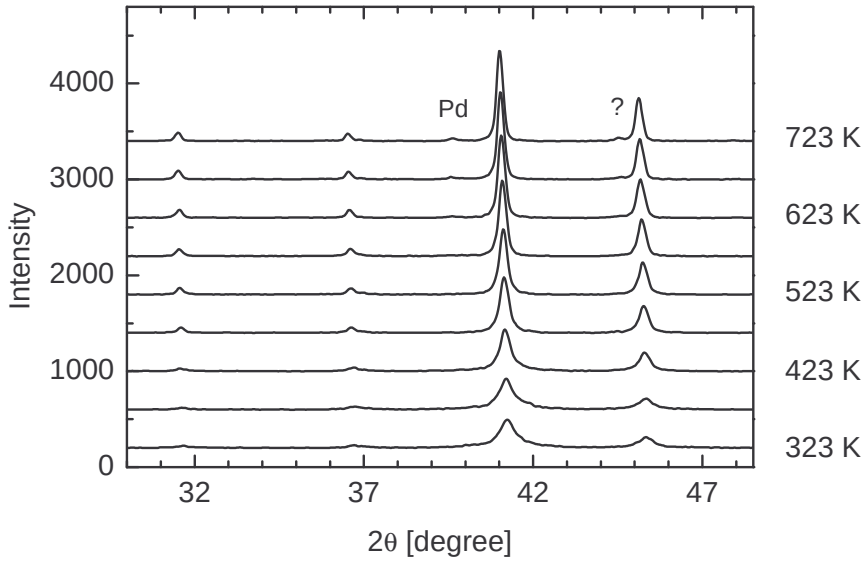

Figure 23: Evolution of in situ X-ray diffraction patterns measured during thermal treatment of PdGa in 20% oxygen in helium from 323 K to 723 K. Additional peaks at 674 K are due to the formation of Pd metal and an unidentified phase.

In situ XRD patterns measured during thermal treatment of Pd_3Ga_7 in 50% hydrogen in He are shown in Figure 24. Small additional peaks at $2\theta = 36.7°$ and $2\theta = 45.3°$ appear at 523 K in helium (Figure 25) and oxygen atmospheres, and at 573 K in hydrogen atmosphere indicative of PdGa formed during thermal treatment. A small amount of PdGa may form by disproportion of Pd_3Ga_7 to PdGa [58] and a gallium rich compound or liquid Ga metal. Refinement of the experimental pattern at 693 K with simulated diffraction pattern of Pd_3Ga_7 and PdGa yields an amount of 5 wt% of PdGa with no additional phases detectable. Refinement of the powder pattern after cooling down to room temperature results in a composition of 91% (hydrogen) and 88% (oxygen and helium) Pd_3Ga_7 together with PdGa. An additional phase with two small peaks at 22.2° and 39.1° in the diffraction pattern could not be identified. A linear shift of 0.2° in 2θ of the (330) diffraction line of Pd_3Ga_7 with temperature in helium, oxygen, and hydrogen is again attributed to thermal expansion of the Pd_3Ga_7 lattice with no incorporation of hydrogen or oxygen atoms detectable.

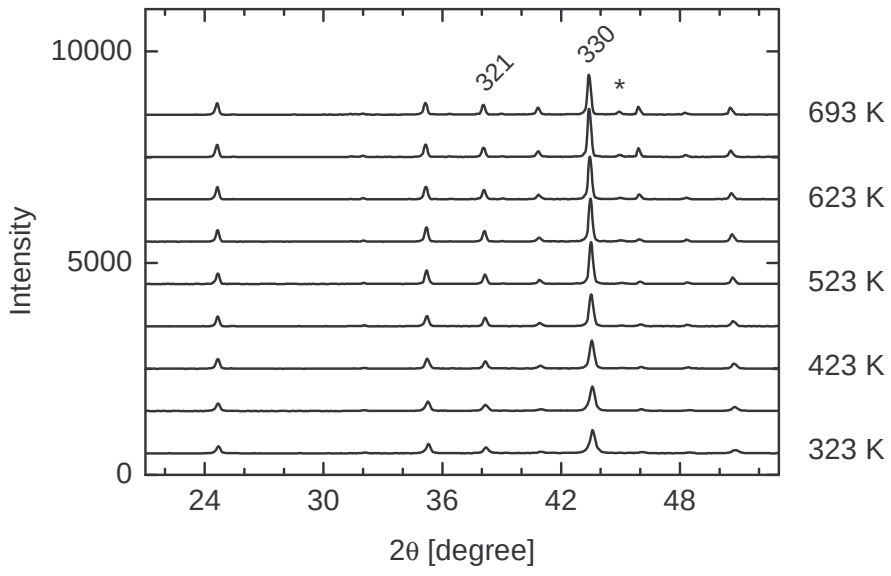

Figure 24: Evolution of in situ X-ray diffraction patterns measured during thermal treatment of Pd_3Ga_7 in 50% hydrogen in helium from 323 K to 693 K. Formation of PdGa at higher temperature is observable (*).

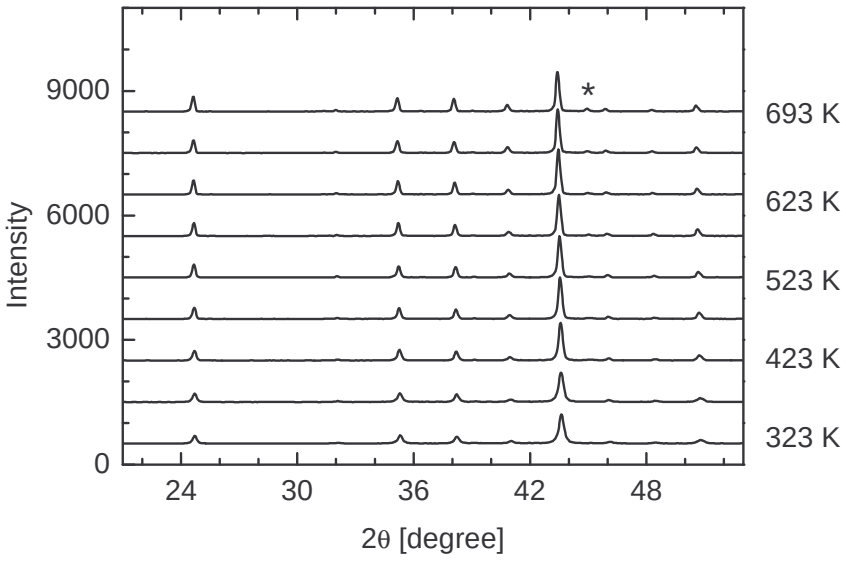

Figure 25: Evolution of in situ X-ray diffraction patterns measured during thermal treatment of Pd_3Ga_7 in 100% helium from 323 K to 693 K. Formation of PdGa at higher temperature is observable (*).

Profile fitting of the PdGa (201) and (211) diffraction lines resulted in an average crystallite size of 18 nm for ball-milled PdGa while the average crystallite size increases to 70 nm at 723 K during thermal treatment. Profile fitting of the (321) diffraction line of Pd_3Ga_7 yielded a crystallite size of about 34 nm for ball-milled Pd_3Ga_7 and of about 100 nm for Pd_3Ga_7 at 693 K (Figure 26).

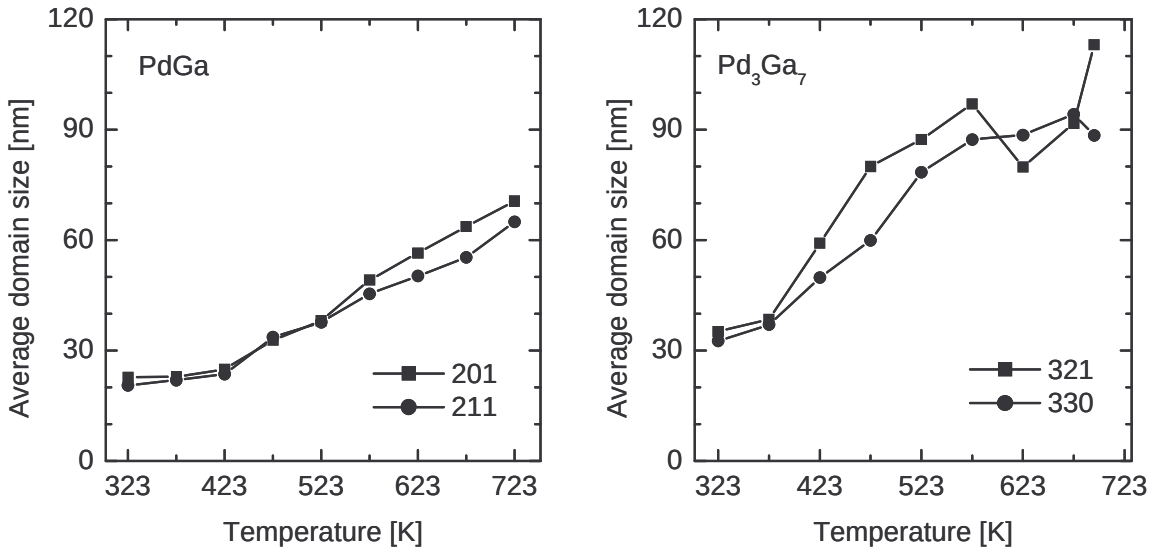

Figure 26: Evolution of average domain size of PdGa (left) and Pd_3Ga_7 (right) during thermal treatment in 50% hydrogen in helium obtained from by profile analysis of diffraction lines.

In situ X-ray absorption spectroscopy

In situ EXAFS studies on PdGa and Pd_3Ga_7 were performed during thermal treatment in helium, 50% hydrogen in He, or a mixture of 10% acetylene and 20% hydrogen. The evolution of the FT(χ(k)*k^3) of PdGa during treatment in 50% hydrogen in helium from 300 K to 723 K is depicted in Figure 27. The overall decrease in amplitude of the FT(χ(k)*k^3) is caused by an increasing thermal disorder during heating.

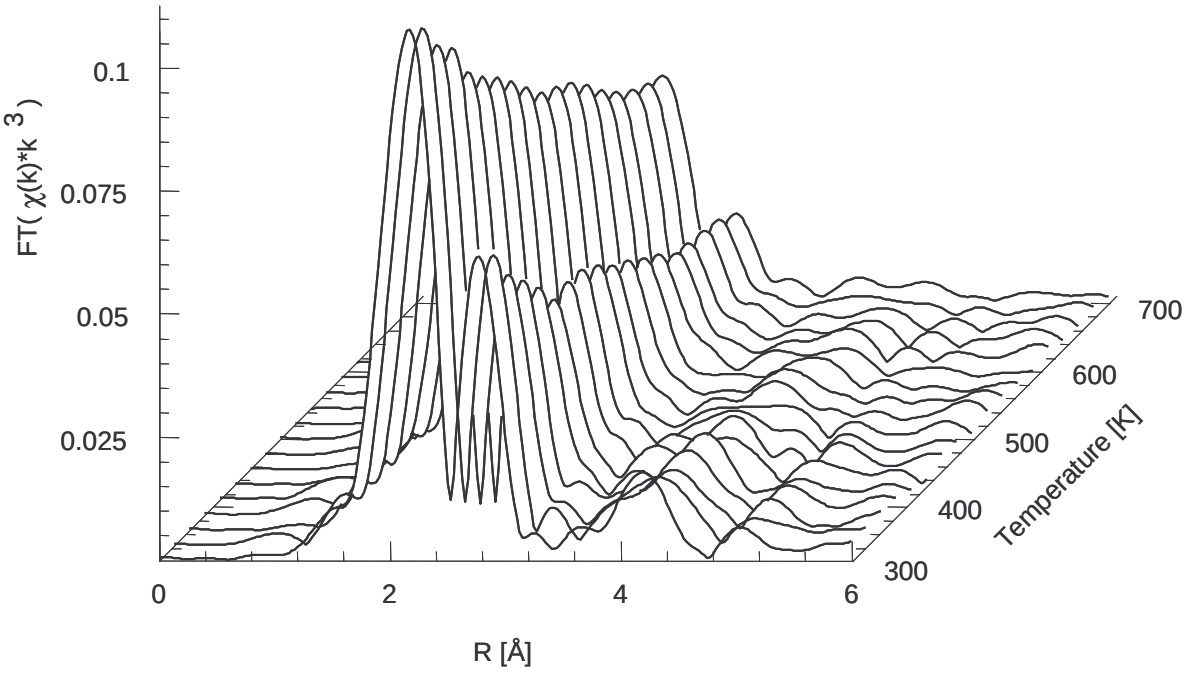

Figure 27: Evolution of RDF of PdGa during thermal treatment from 300 K to 723 K in 50% H_2 + 50% He.

The characteristic distances of PdGa heated in hydrogen, helium, oxygen and in reaction feed containing acetylene and hydrogen obtained from the EXAFS analysis remain nearly constant over the temperature range employed. The Debye-Waller factors of three selected shells exhibit an expected nearly linear increase with temperature (Figure 28 + Figure 29). Less changes in the trend of distances and more linear behavior of Debye-Waller factors for Pd_3Ga_7 compared to PdGa is observed during treatment in hydrogen, helium, and oxygen (Figure 30 + Figure 31). Structural changes that can be attributed to phase transitions or formation of hydrides (incorporation of hydrogen) during thermal treatment in the various atmospheres employed were not detected. In the acetylene hydrogenation feed, PdGa and Pd_3Ga_7 showed a similar behavior compared to the treatment of the materials in hydrogen. The onset of catalytic activity on both materials did not correlate with changes in the long-range (XRD) or short-range order structure (EXAFS).

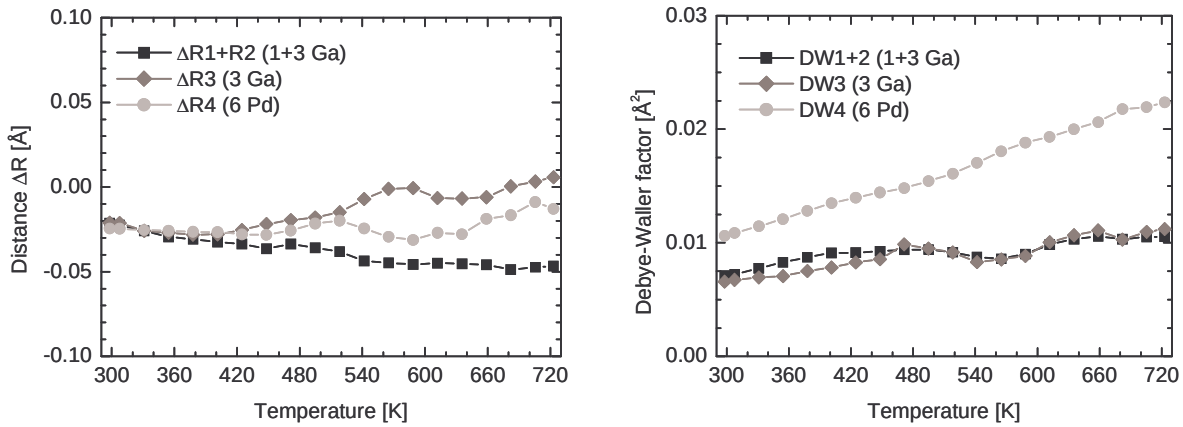

Figure 28: Evolution of selected relative Pd-Ga and Pd-Pd distances (left) and Debye-Waller factors (right) of selected scattering paths of PdGa during thermal treatment of PdGa in helium from 323 K to 723 K obtained from analysis of the corresponding EXAFS spectra.

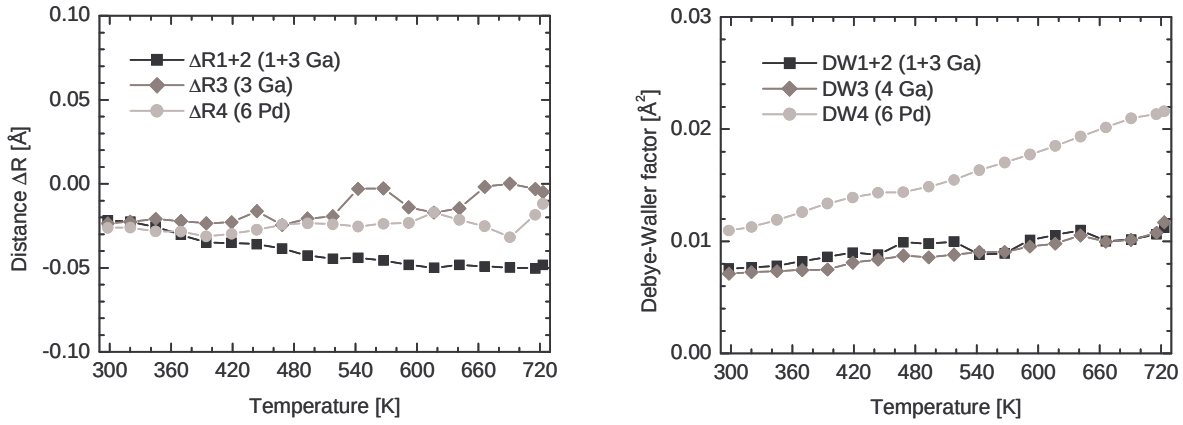

Figure 29: Evolution of selected relative Pd-Ga and Pd-Pd distances and Debye-Waller factors (right) of selected scattering paths of PdGa during thermal treatment of PdGa in 50% hydrogen in helium from 323 K to 723 K obtained from analysis of the corresponding EXAFS spectra.

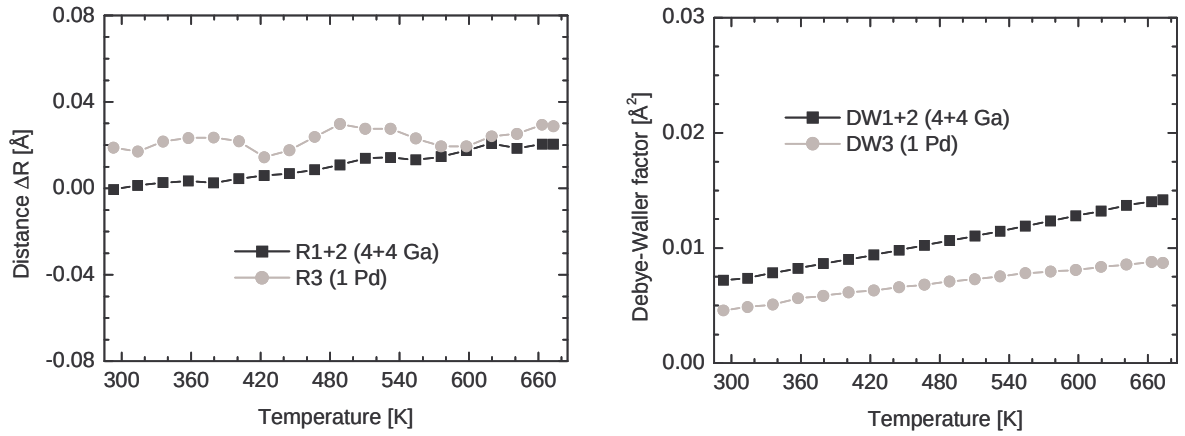

Figure 30: Evolution of selected relative Pd-Ga and Pd-Pd distances and Debye-Waller factors (right) of selected scattering paths of PdGa during thermal treatment of Pd_3Ga_7 in 50% hydrogen in helium from 323 K to 693 K obtained from analysis of the corresponding EXAFS spectra.

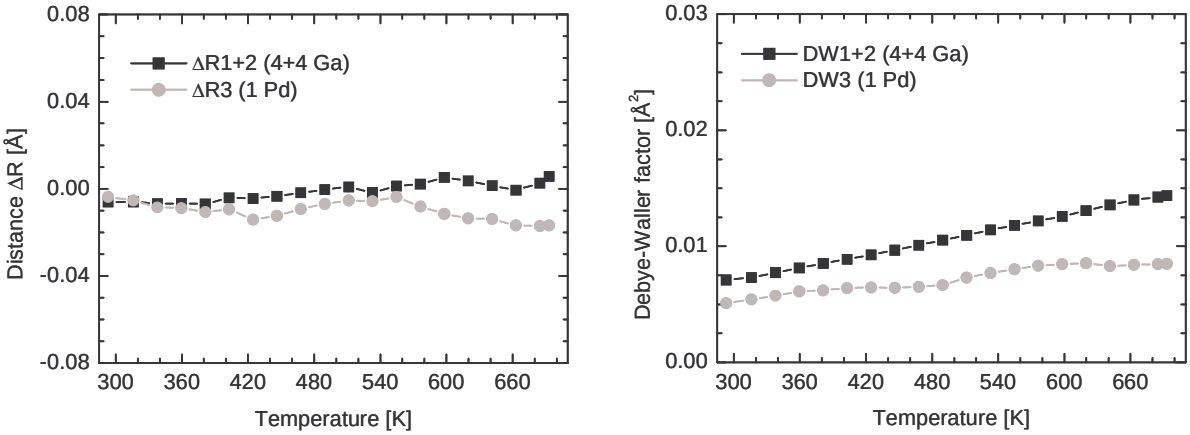

Figure 31: Evolution of selected relative Pd-Ga and Pd-Pd distances and Debye-Waller factors (right) of selected scattering paths of PdGa during thermal treatment of Pd_3Ga_7 in 10% acetylene in 20% hydrogen in helium from 323 K to 693 K obtained from analysis of the corresponding EXAFS spectra.

7.1.3 Surface characterization

X-ray photoelectron spectroscopy

XPS data of PdGa showed that the surface of untreated as-prepared material mainly consists of oxygen and gallium (Table 5). The surface concentration of palladium amounted to only 6%. After hydrogen treatment at 573 K and 673 K for 30 minutes, the oxygen content decreased to 49% and 47%, respectively. The palladium concentration at the surface increased to 10% after hydrogen treatment at 673 K and reached 17% after sputtering with He ions. The XPS data of untreated PdGa exhibits only a single Ga $2p^{3/2}$ peak indicating that only gallium oxide is present on the surface which was only partly reduced after hydrogen treatment. The gallium metal of the as-prepared PdGa intermetallic compound seems to be not detectable by XPS under the conditions employed. After hydrogen treatment at 573 K and 673 K, a shoulder of the Ga $2p^{3/2}$ peak at lower binding energy was observed indicative of the formation of a reduced gallium species (Figure 32). After ion sputtering during the ISS measurements, a very broad Ga $2p^{3/2}$ peak appeared indicative of a mixture of metallic and oxidized gallium. Curve fitting of the Ga $2p^{3/2}$ peak resulted in an increasing metallic gallium content, however, 74% of gallium remains in an oxide state after hydrogen treatment at 673 K (Table 6). The Ga $2p^{3/2}$ peak measured after hydrogen treatment at 673 K exhibited a binding energy of 1116.5 eV in good agreement with that of metallic gallium [89]. The Pd $3d^{5/2}$ peak of PdGa after hydrogen treatment at 673 K was located at a binding energy of 334.9 eV similar to that of metallic Pd (335.1 eV) [96].

Table 5: Surface composition as calculated from XPS data (in atom-%) of untreated PdGa, after hydrogen treatment at 573 K and 673 K, and after ISS.

PdGa	*Gallium* *Ga 2p$^{3/2}$*	*Oxygen* *O 1s*	*Carbon* *C 1s*	*Palladium* *Pd 3d*
untreated	32	57	5	6
H_2 treatment at 573 K	39	49	7	7
H_2 treatment at 673 K	37	47	6	10
after ISS	40	41	2	17
Pd_3Ga_7	*Gallium* *Ga 2p$^{3/2}$*	*Oxygen* *O 1s*	*Carbon* *C 1s*	*Palladium* *Pd 3d*
untreated	37	57	4	2
H_2 treatment at 573 K	38	55	5	2
after ISS	51	36	2	11

Table 6: Amount of oxidized and metallic Ga at the surface of untreated PdGa and Pd_3Ga_7, and after H_2 treatment as calculated from a Ga 2p$^{3/2}$ XPS peak refinement (in atom-%).

Ga 2p$^{3/2}$	**PdGa**		**Pd_3Ga_7**	
treatment	oxidized	metallic	oxidized	metallic
untreated	94	6	96	4
H_2 treatment at 573 K	84	16	97	3
H_2 treatment at 673 K	74	26	-	-

XPS data of untreated as-prepared Pd_3Ga_7 showed a similar oxygen content of the near-surface region like PdGa (Table 5). In contrast to PdGa, the amount of oxygen was not significantly reduced after thermal treatment in hydrogen. The palladium content of the surface was very low and remained at 2% after hydrogen treatment at 573 K. Only after He ion sputtering during ISS measurements, the oxygen content was reduced to 36% and the gallium and palladium content increased to 51% and 11%, respectively. XPS data of untreated Pd_3Ga_7 exhibited a single Ga 2p$^{3/2}$ peak indicating that only gallium oxide was

detectable at the surface. While the width of the Ga $2p^{3/2}$ peak decreased after hydrogen treatment at 573 K, no additional shoulder was observed (Figure 32, Table 6). Only after He ion sputtering, two Ga $2p^{3/2}$ peaks were obtained indicative of a mixture of gallium metal and gallium oxide on the surface.

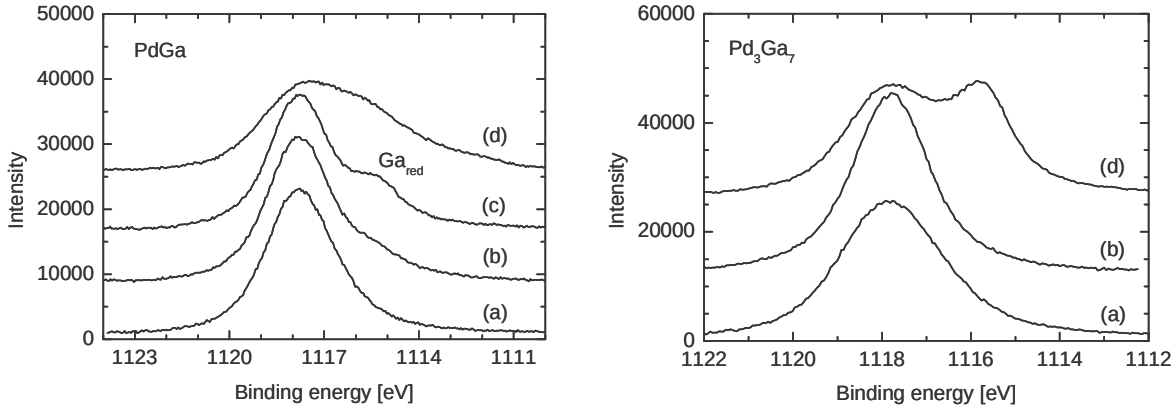

Figure 32: XPS data of the Ga $2p^{3/2}$ peak of PdGa (left) and Pd_3Ga_7 (right): (a) untreated, (b) after H_2 treatment at 573 K, (c) after H_2 treatment at 673 K, and (d) after ISS. A shoulder at lower binding energy that corresponds to reduced Ga species is indicated.

Ion scattering spectroscopy

ISS spectra (first 2 scans) of untreated PdGa and of PdGa after hydrogen treatment at 673 K are depicted in Figure 33. The kinetic energy of the scattered He ions depends on the energy of the incident beam, the incident angle, and the mass of the scattering atoms on the surface of the material studied [72]. Because scattering at heavier elements results in He ions with higher kinetic energy, the peak in the ISS spectra at the highest kinetic energy can be assigned to Pd atoms on the surface. An ISS peak at a kinetic energy of 1650 eV corresponds to Ga atoms, while light elements like carbon and oxygen scatter He ions with kinetic energy in the range from 800 to 1000 eV.

The amplitude of the Ga ISS peak and the Pd ISS peak increased after hydrogen treatment at 673 K and the Ga/Pd peak ratio decreased from 1.7 to 1.3 (Figure 33). Because the cross-section of the various elements in ISS is unknown, the elemental composition of the surface region cannot be accurately quantified from the ISS data taken. Assuming a stoichiometric composition (1 : 1) of both the surface and the bulk of PdGa, the amplitude of the Pd peak

should be higher than the Ga peak. Conversely, the ISS spectra measured indicate an excess of gallium oxide on the surface in agreement with the XPS data. While the amplitude of the oxygen ISS peak was reduced after the hydrogen treatment of PdGa, a high concentration of oxygen persists on the surface.

In contrast to XPS which reveals the composition of the near-surface region within a few nanometers, ISS is more surface sensitive and yields the composition of the top most surface layer. During ISS measurements the surface layer will be removed by the He ions. Hence, a series of ISS measurements results in a depth profiling of the material studied. A series of ISS scans of untreated PdGa resulted in different spectra compared to those of hydrogen treated PdGa. After eight series of ISS scans, the Pd peak was higher than the Ga peak and the amount of oxygen on the surface was significantly reduced.

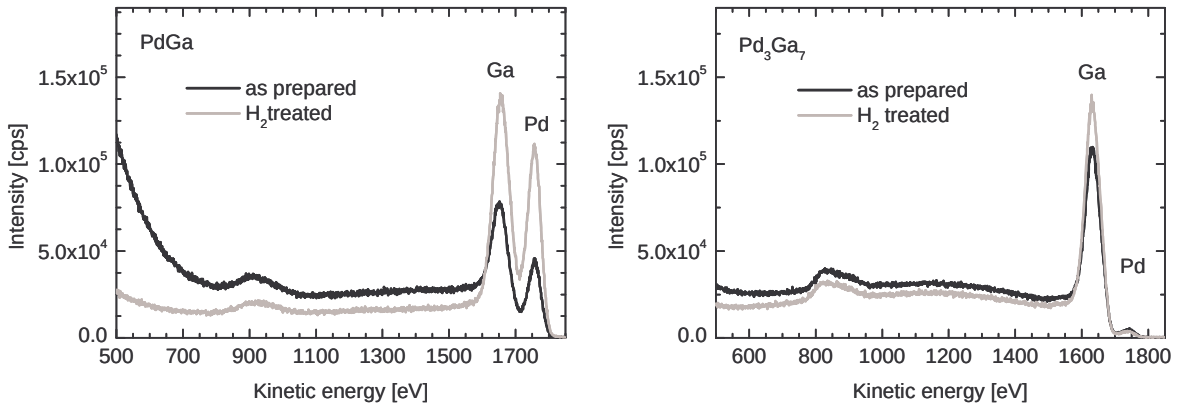

Figure 33: ISS data of untreated PdGa (first 2 scans) and Pd_3Ga_7 (first 3 scans) and after H_2 treatment at 673 K. Peaks at 1750 eV (Pd) and 1650 eV (Ga) are indicated.

ISS measurement of Pd_3Ga_7 revealed similar results compared to PdGa. Hydrogen treatment at 573 K resulted in a slightly decreased oxygen peak and an increased Ga peak (Figure 33). No change in the Pd peak was observed. A series of ISS measurements resulted in an increased amount of Ga and Pd on the surface while the amount of oxygen decreased. However, the estimated amount of Pd on the surface remained low compared to the expected composition of Pd_3Ga_7. In contrast to PdGa, no increased amplitude of the Pd peak was observed after hydrogen treatment of Pd_3Ga_7.

CO chemisorption

Prior to the chemisorption measurements, PdGa (m = 1.5 g) and Pd_3Ga_7 (m = 1.0 g) were reduced in hydrogen in the temperature range from 323 K to 773 K or 673 K, respectively. Carbon monoxide adsorption experiments at 300 K showed no chemisorption of CO on the surface of reduced PdGa and Pd_3Ga_7. CO chemisorption on Pd/Al_2O_3 was measured after hydrogen treatment at 473 K and showed chemisorption and physisorption.

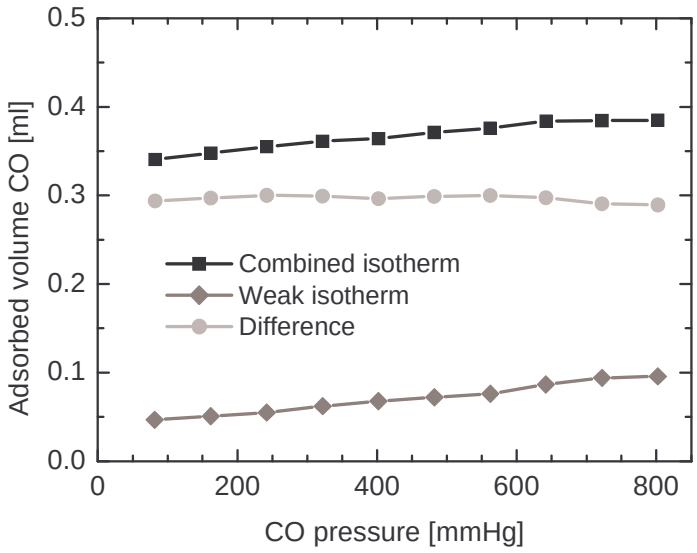

Figure 34: CO chemisorption on Pd/Al_2O_3 (5%wt) after hydrogen pre-treatment at 473 K. First adsorption isotherm (combined) contains the chemisorbed and physisorbed part of CO on Pd/Al_2O_3. Second isotherm was measured after evacuation and resulted in the weak isotherm (only physisorbed CO). The difference of combined and weak isotherm can be used for calculation of the chemisorbed part of the CO on Pd/Al_2O_3.

Calculation of the chemisorbed CO part referring to the Dual isotherm method resulted in an active metal surface area of 5.3 m^2/g and a metal dispersion of 24%. Another possibility to calculate the Pd surface area refers to the extrapolation of the combined isotherm and resulted in an active metal area of 6.0 m^2/g and a metal dispersion of 27%. Assuming the presence of on-top and bridged bond CO molecules on the Pd surface, a stoichiometric factor of 1.5 was used to calculate the Pd surface area [91,97,98]. A BET measurement of Pd/Al_2O_3 resulted in a total surface area of 114 m^2/g. A detection limit of 0.02 m^2 Pd metal surface area was estimated for the sorption equipment used which should be sufficient to detect CO adsorption on the low surface area of the intermetallic compounds studied.

Diffuse reflectance infrared spectroscopy

DRIFTS measurements were performed on Pd-Ga intermetallic compounds with CO as probe molecule. In contrast to CO chemisorption measurements performed by sorption equipment using untreated samples, for DRIFTS measurements chemically etched PdGa and Pd_3Ga_7 were used. Pd_3Ga_7 was chemically etched using an ammonia solution at pH = 9.0 as an example for slight etching conditions and PdGa was chemically etched at pH = 9.8 as an example for strong etching condition. On both samples DRIFTS measurements were performed with 1% CO in He (total flow 100 ml/min) direct after the etching and drying procedure and after thermal treatment in hydrogen for 15 min at 423 K. Neither PdGa nor Pd_3Ga_7 showed IR absorption indicative for chemisorbed CO on the surface of the Pd-Ga intermetallic compounds direct after the etching procedure and after the hydrogen treatment.

7.1.4 Investigation of the catalytic performance of PdGa and Pd_3Ga_7

Acetylene hydrogenation

PdGa showed high activity in acetylene hydrogenation under condition A (2% acetylene and 4% hydrogen) in the range of 370 to 570 K with a maximum at 430 K and an activity of 0.639 $g_{C2H2}/g_{cat}\cdot h$. Pd_3Ga_7 also showed high activity in the temperature range from 390 K to 570 K with a maximum at 490 K (0.313 $g_{C2H2}/g_{cat}\cdot h$) (Figure 35 + Figure 36). Under these conditions more C4 hydrocarbons than ethane were obtained as by-product. In contrast, acetylene hydrogenation on Pd/Al_2O_3 (activity at 450 K: 64.07 $g_{C2H2}/g_{cat}\cdot h$) resulted in more ethane than C4 hydrocarbon formation (Figure 35). Figure 36 shows the acetylene conversion of 50 mg PdGa, 100 mg Pd_3Ga_7, and 0.5 mg Pd/Al_2O_3. The conversion rapidly increased with increasing temperature in the sequence PdGa, Pd/Al_2O_3, and Pd_3Ga_7 and all three catalysts reached a conversion level of 80%. Above 500 K, however, the activity of Pd/Al_2O_3 decreased faster than that of the intermetallic compounds. Moreover, Figure 36 depicts a significantly higher selectivity to ethylene in the temperature range from 330 K to 470 K for the Pd-Ga intermetallic compounds compared to Pd/Al_2O_3. At temperatures above

470 K the selectivity of Pd_3Ga_7 is similar to that of Pd/Al_2O_3 and higher compared to that of PdGa.

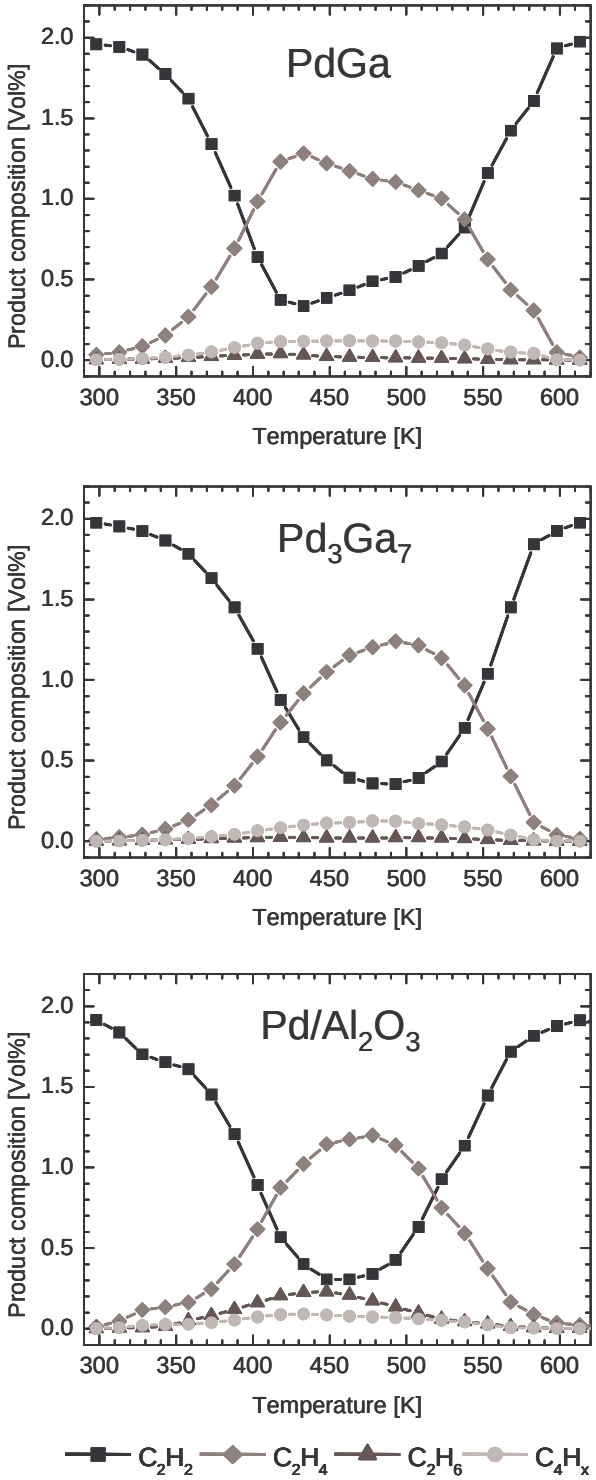

Figure 35: Product composition measured during hydrogenation of acetylene on PdGa (50 mg), Pd_3Ga_7 (100 mg), and Pd/Al_2O_3 (0.5 mg) (2% C_2H_2 + 4% H_2, condition A).

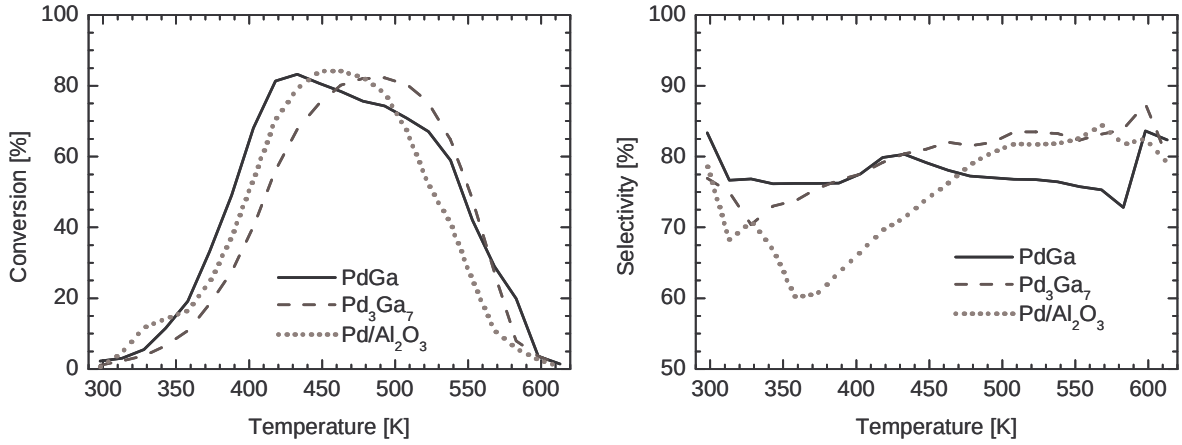

Figure 36: Conversion (left) and selectivity (right) measured during acetylene hydrogenation on PdGa (50 mg), Pd_3Ga_7 (100 mg), and Pd/Al_2O_3 (0.5 mg) (condition A).

Acetylene hydrogenation on PdGa and Pd/Al_2O_3 under reaction conditions A was measured isothermal at 393 K in acetylene feed for at least 17 hours (Figure 37) to investigate the deactivation behavior of PdGa and Pd/Al_2O_3. In the first two hours, PdGa showed a deactivation from 55% to 45% acetylene conversion followed by a slow increase to about 50% acetylene conversion an activity of 0.378 g_{C2H2}/g_{cat}·h. The selectivity of PdGa of 80 % remained constant during the entire 17 hours experiment. Conversely, Pd/Al_2O_3 exhibited a pronounced deactivation behavior during the first two hours from about 95% to 30% conversion (Figure 37). Further deactivation resulted in only 15% acetylene conversion and an activity of 10.81 g_{C2H2}/g_{cat}·h after 17 hours time on stream. The selectivity of Pd/Al_2O_3 in acetylene hydrogenation to ethylene exhibited a maximum of 70% after two hours and slowly decreased to 55% after 24 hours time on stream.

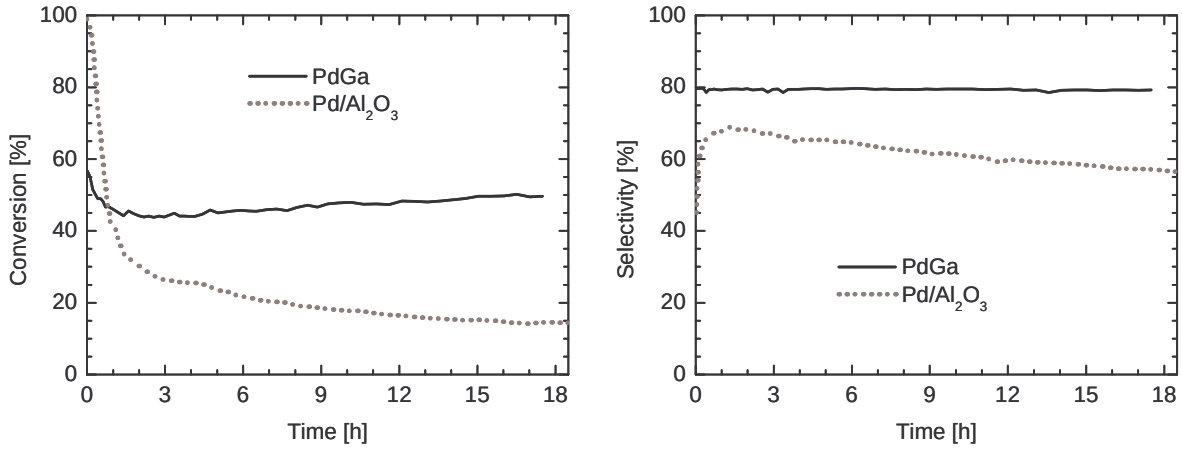

Figure 37: Conversion and selectivity of PdGa (50 mg) and of Pd/Al_2O_3 (0.5 mg) in acetylene hydrogenation (isothermal at 393 K under condition A).

Chemical etching of Pd-Ga intermetallic compounds

Chemical etching of Pd-Ga intermetallic compounds was performed to remove gallium oxide from the catalyst surface and, thus, increase the active Pd surface area. Chemical etching of PdGa by using an ammonia solution at pH = 9.8 resulted in a ten times higher activity (6.860 $g_{C2H2}/g_{cat}\cdot h$ at 450 K) in acetylene hydrogenation while maintaining a high selectivity (Figure 38). Acetylene conversion and selectivity of PdGa depended strongly on the etching conditions used. At a pH of 9.5, a significantly reduced activity compared to a sample etched at a pH of 9.8 was obtained. Increasing the pH to 10 or higher resulted in a further increase in activity accompanied, however, by a strong loss in selectivity.

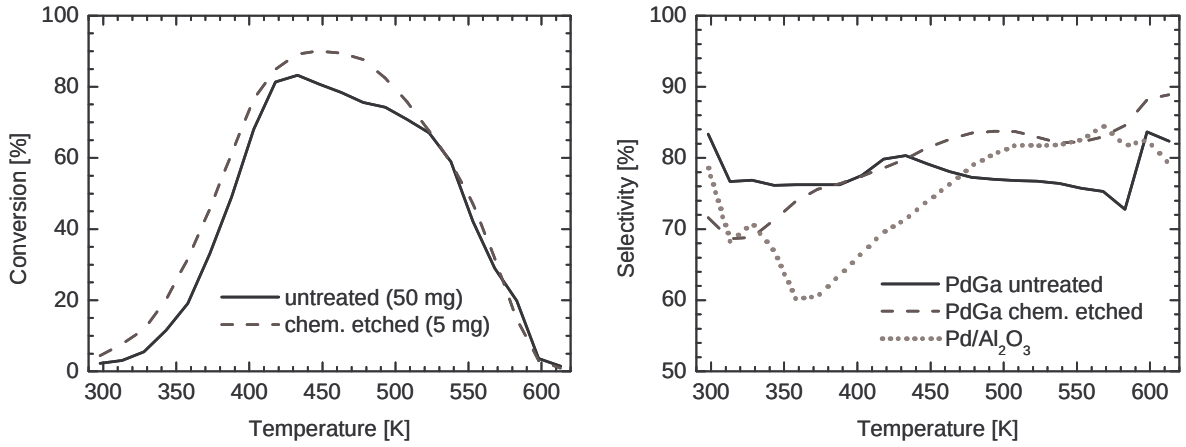

Figure 38: Conversion and selectivity (together with the selectivity of Pd/Al_2O_3) of untreated (50 mg) and chemically etched (5 mg, pH= 9.8) PdGa in acetylene hydrogenation (condition A).

Conversely, catalytic performance of Pd_3Ga_7 in acetylene hydrogenation was less dependent on varying the pH of the ammonia solution. The highest activity and selectivity of Pd_3Ga_7 was obtained at a pH of 10.5 (Figure 40). The maximum in acetylene conversion as a function of temperature was shifted by 40 K to lower temperatures and only 15 mg of chemically etched Pd_3Ga_7 sufficed to reach 80% conversion of acetylene and resulted in ~seven times higher activity (2.092 g_{C2H2}/g_{cat}·h) compared to untreated Pd_3Ga_7. The chemically etched Pd_3Ga_7 sample maintained a similar high selectivity like untreated Pd_3Ga_7.

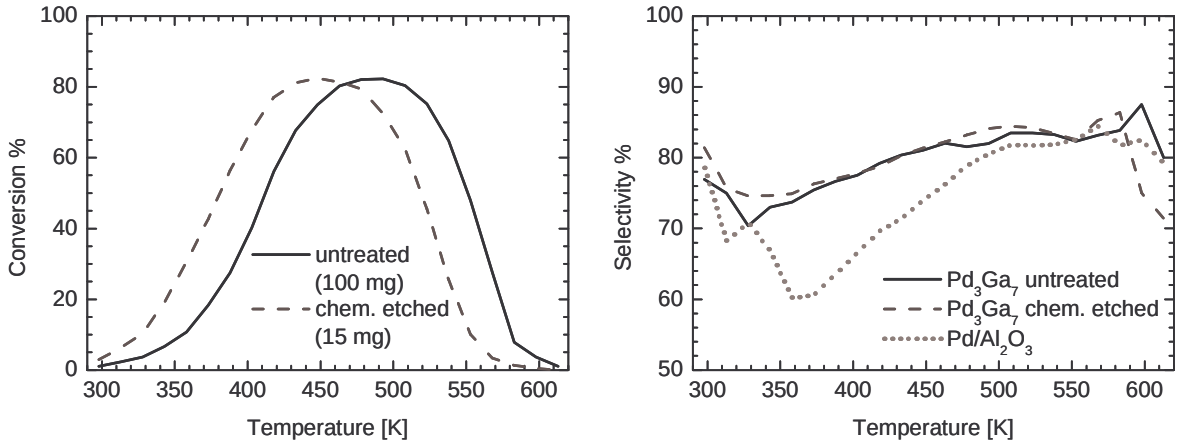

Figure 39: Conversion and selectivity (together with the selectivity of Pd/Al_2O_3) of untreated (50 mg) and chemically etched (15 mg, pH= 10.5) Pd_3Ga_7 in acetylene hydrogenation (condition A).

Acetylene hydrogenation in ethylene feed

Activity, selectivity, and long-term stability of untreated and chemically etched Pd-Ga intermetallic compounds in acetylene hydrogenation were determined in an excess of ethylene under reaction conditions B (0.5% C_2H_2 + 5% H_2 + 50% C_2H_4) and compared to the catalytic performance of Pd/Al_2O_3 and a $Pd_{20}Ag_{80}$ alloy. First, isothermal catalysis experiments were performed by heating the untreated intermetallic compounds and the reference materials (PdGa: 40 mg, Pd_3Ga_7: 100 mg, Pd/Al_2O_3: 0.15 mg, and $Pd_{20}Ag_{80}$: 200 mg) in helium to a reaction temperature of 473 K followed by switching to the ethylene-rich feed (conditions B). The acetylene conversion and the corresponding selectivity obtained are plotted in Figure 40. During 20 hours time on stream Pd_3Ga_7 showed a constant acetylene conversion of 99%. PdGa reached a constant acetylene conversion of about 90% after two hours time on stream. $Pd_{20}Ag_{80}$ showed a nearly constant conversion level at 85%, whereas Pd/Al_2O_3 exhibited a strong deactivation from 100% to 40% conversion during 20 hours time on stream (Figure 40). In addition to a high conversion of acetylene, the untreated intermetallic compounds PdGa and Pd_3Ga_7 possessed a high long-time stable selectivity of about 70% compared to 50% selectivity of $Pd_{20}Ag_{80}$, and only 20 % selectivity of Pd/Al_2O_3 (Table 7).

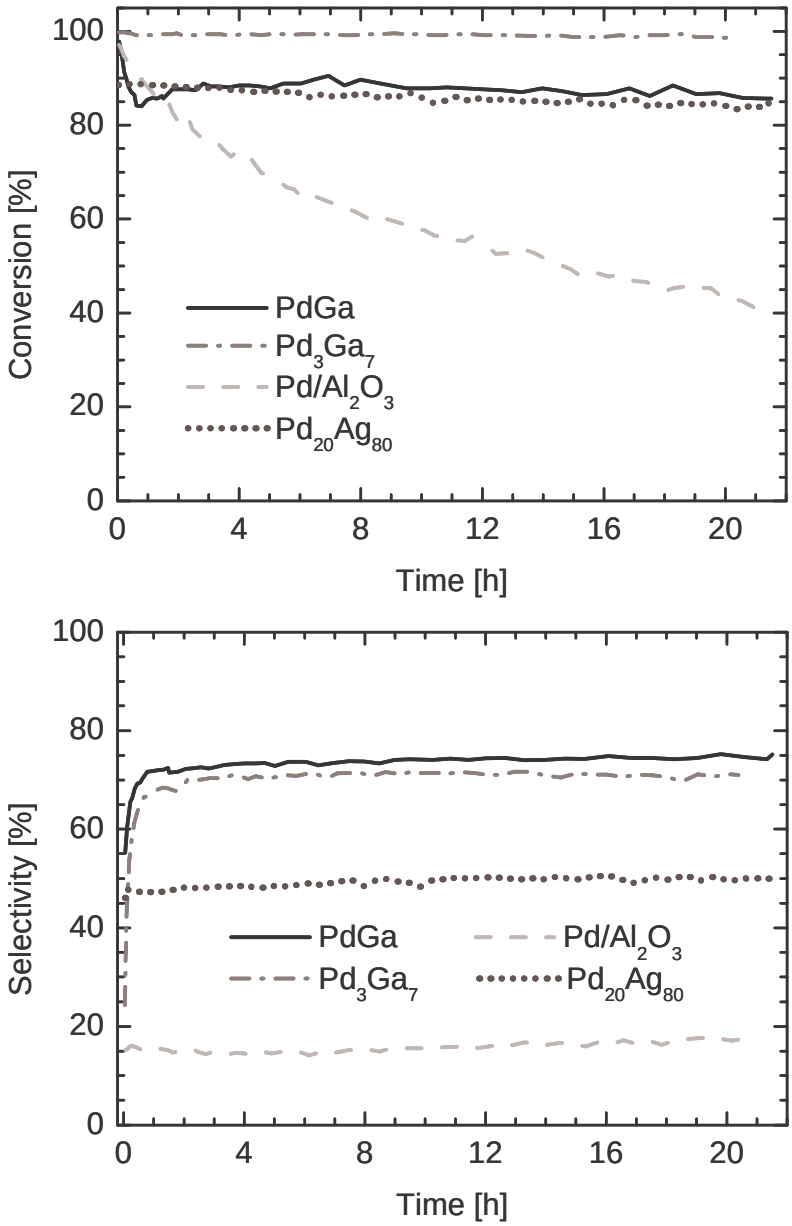

Figure 40: Acetylene conversion and selectivity of PdGa (40 mg), Pd_3Ga_7 (100 mg), Pd/Al_2O_3 (0.15 mg) and $Pd_{20}Ag_{80}$ (200 mg) isothermal at 473 K (condition B).

Isothermal catalysis experiments were performed by heating the chemically etched intermetallic compounds in helium to a reaction temperature of 473 K followed by switching to the ethylene-rich feed (conditions B). Figure 41 shows acetylene conversion and selectivity, respectively, of untreated PdGa and chemically etched PdGa samples. Chemically etching of PdGa at a pH of 9.8 resulted in a pronounced increase in activity by more than 25 times compared to untreated PdGa while the selectivity was decreased to about

40%. The selectivity slowly increased to 56% with time on stream without reaching a constant value after 20 hours. PdGa chemically etched at a pH of 9.8 (m = 1.5 mg) still exhibits a higher selectivity compared to $Pd_{20}Ag_{80}$ and Pd/Al_2O_3. Chemical etching of PdGa at a pH of 9.0 (m = 5 mg) resulted in 93% acetylene conversion and 64% selectivity after 20 hours time on stream (Figure 41 + Table 7). This corresponds to an eight times higher activity compared to untreated PdGa (m = 40 mg). Furthermore, under reaction conditions B, a "softer" chemical etching (pH = 9.0) seems to be required compared to conditions A (pH = 9.8) in order to obtain both an increased catalytic activity and a high selectivity.

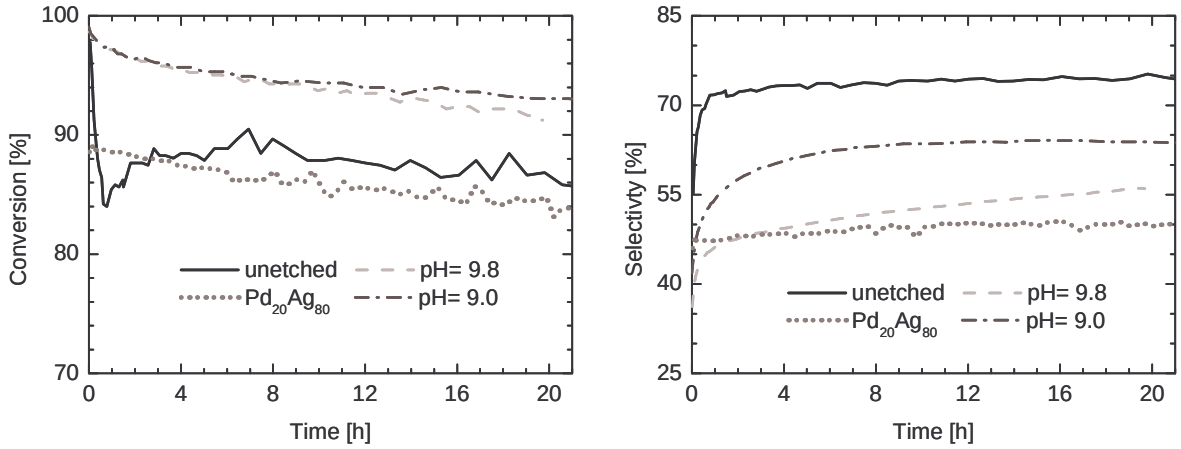

Figure 41: Conversion (left) and selectivity (right) of untreated PdGa (40 mg), PdGa chemically etched at pH= 9.8 (1.5 mg) and pH= 9.0 (5 mg), and $Pd_{20}Ag_{80}$ (200 mg) in acetylene hydrogenation (isothermal at 473 under condition B).

Chemically etched Pd_3Ga_7 also exhibited an increased activity in acetylene hydrogenation under reaction condition B (Figure 42). 7 mg of Pd_3Ga_7 etched at a pH of 10.5 were sufficient to reach a similar acetylene conversion like 100 mg untreated Pd_3Ga_7. However, the more active etched Pd_3Ga_7 exhibited a strongly reduced selectivity. Compared to $Pd_{20}Ag_{80}$ at a conversion of 83% and a selectivity of 50%, etched Pd_3Ga_7 showed a selectivity of 50% at a conversion of 98%, with a slowly increasing selectivity with time on stream (Figure 42). Lowering the pH of the etching solution resulted only in a decreased activity without an increasing selectivity. Etching of Pd_3Ga_7 at a pH of 9.0, for instance, yielded an acetylene conversion of 97% (m = 13 mg) and a corresponding selectivity of 53% after 20 hours time on stream (Table 7).

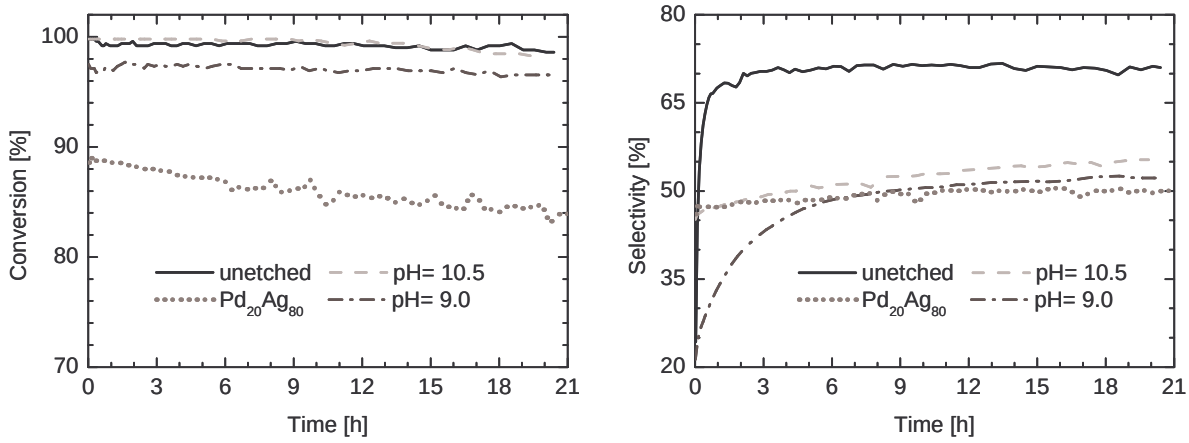

Figure 42: Conversion (left) and selectivity (right) of untreated Pd_3Ga_7 (100 mg), chemically etched Pd_3Ga_7 (pH= 10.5, 7 mg), chemically etched Pd_3Ga_7 (pH= 9.0, 13 mg) and $Pd_{20}Ag_{80}$ (200 mg) in acetylene hydrogenation (isothermal at 473 under condition B).

Table 7: Acetylene conversion and corresponding selectivity of untreated and chemically etched PdGa, Pd_3Ga_7, Pd/Al_2O_3 and $Pd_{20}Ag_{80}$ after 20 h at 473 K under condition B.

Sample	pH of etching solution	sample mass [mg]	acetylene conversion [%]	selectivity [%]	activity [g_{C2H2}/g_{cat}·h]
PdGa	-	40.0	86	75	0.205
PdGa	9.0	5.00	93	64	1.771
PdGa	9.8	1.50	91	56	5.775
Pd_3Ga_7	-	100	99	71	0.094
Pd_3Ga_7	9.0	13.0	97	52	0.710
Pd_3Ga_7	10.5	7.00	98	55	1.333
Pd/Al_2O_3	-	0.15	43	17	27.29
$Pd_{20}Ag_{80}$	-	200	83	49	0.040

7.2 Discussion

7.2.1 Structural characteristics of PdGa and Pd_3Ga_7

In the palladium gallium intermetallic compounds investigated here Pd atoms are only coordinated by Ga atoms and, hence, are effectively isolated from each other. PdGa [60,61,61] crystallizes in a FeSi type structure [63] (space group: *P* 2_13) with each Pd atom coordinated by 7 Ga atoms at distances between 2.5 and 2.7 Å (Figure 4)[57,64]. The first Pd shell with a coordination number of 6 and a distance of 3.01 Å is significantly different from Pd metal with 12 Pd atoms a distance of 2.75 Å in the first shell (Table 3). In the gallium-rich Pd_3Ga_7 [78] (Figure 5) [57,64] (space group: *I* m-3m) each Pd atom is coordinated by 8 Ga atoms with an average distance of ~ 2.58 Å. PdGa and Pd_3Ga_7 possess a high melting points of 1318 K and 733 K, respectively [58].

PdGa was prepared by the standard preparation method of melting the metal powders with an atomic ratio of 1:1 under Ar atmosphere [62]. Pd_3Ga_7 required an additional annealing procedure at 673 K for 800 h to obtain Pd_3Ga_7 which would not directly crystallize by cooling down the melted mixture to room temperature [58]. The very low surface area of the as-prepared PdGa and Pd_3Ga_7 materials could be increased by ballmilling without significant structural degradation (Figure 14 - Figure 17). During both mechanical and thermal treatment, PdGa exhibited a higher stability compared to Pd_3Ga_7. Hence, to prevent structural transformations, Pd_3Ga_7 had to be ball-milled for a shorted period of time which resulted in a larger average crystallite size compared to PdGa. Apparently, with the bulk intermetallic compounds employed, small crystallite sizes and high surface areas may be difficult to achieve because of sintering effects and undesired structural changes during extended mechanical treatment (Figure 26). In order to further increase catalyst surface area, alternative preparation methods like precipitation, sol-gel chemistry, or use of an inert support will be pursued in the future.

7.2.2 Structural investigations during thermal treatment

Thermal stability of Pd-Ga intermetallic compounds

The preparation procedures employed here resulted in intermetallic compounds PdGa and Pd_3Ga_7 with a high degree of structural ordering in both the long-range (Figure 14 + Figure 15) and the short-range (Figure 16 + Figure 17, Table 4) and no additional phases detectable. Hence, they constitute suitable model systems to investigate the beneficiary effect of isolating Pd sites in hydrogenation catalysis and are promising candidates for more selective hydrogenation catalysts. From the concept of "active site isolation" it may be expected, that isolated Pd atoms exhibit an increase selectivity and long-term stability under hydrogenation conditions. The structural motive of isolated Pd atoms is inherent in the palladium gallium intermetallic compounds investigated. However, in addition to possess the desired structure in the as-prepared material, the long-range and short-range order structure (i.e. Pd site isolation) need to be stable at elevated temperature and under reactive gas atmospheres. Industrial selective hydrogenation is commonly performed in the temperature range from room temperature to 500 K [13], thus, defines a stability interval required for intermetallic compounds to be used as hydrogenation catalysts.

Thermal analysis (TG / DSC) measurements of PdGa and Pd_3Ga_7 showed a considerable stability of the intermetallic compounds under various atmospheres. Heating the samples in hydrogen, helium, or oxygen (Figure 18) did not result in significant decomposition or phases transition up to temperatures of about 600 K. Small changes in sample mass during treatment in hydrogen below 600 K can be attributed to surface reduction processes. More pronounced changes in sample mass for PdGa during treatment in hydrogen or oxygen (Figure 18 + Figure 19) at temperatures above 600 K may be caused by accelerated reduction of surface oxides or onset of bulk oxidation, respectively. Compared to the behavior of PdGa, Pd_3Ga_7 exhibited smaller changes in sample mass upon heating in reducing or oxidizing atmospheres (Figure 19). Given the overall lower stability of Pd_3Ga_7 compared to PdGa, this effect may be caused by the smaller surface area of Pd_3Ga_7 as a result of the less intensive ball milling employed. The small exothermic DSC signal detected at ~ 460 K during treatment of PdGa in hydrogen and oxygen (Figure 18), and at ~ 420 K during treatment of Pd_3Ga_7 in hydrogen (Figure 19) may indicate sintering and annealing of the ball-milled intermetallic compounds. This is in good agreement with the onset of

crystallite growth of PdGa at ~ 460 K during treatment in hydrogen as determined by in situ XRD (Figure 26) and can be also observed in the trend of the Debye-Waller factors (Figure 28 - Figure 31). SEM measurements of PdGa confirm the overall stability of the morphology during treatment in hydrogen (Figure 20 + Figure 21) with only small increases in the coalescence of the particles and a smoother surface detectable. SEM images of Pd_3Ga_7 show a similar behavior. EDX measurements also resulted in a homogeneous composition of the particles before and after heating in hydrogen except for a few regions with higher Ga content.

In addition to thermal analysis measurements, which give rather unspecific structural information, the complementary structural techniques in situ XAFS and XRD were used to investigate the evolution of short-range and long-range order structure of palladium gallium intermetallic compounds under various reaction atmospheres. The evolution of the long-range order structure as determined by in situ X-ray diffraction measurements of PdGa in 50% hydrogen showed no formation of additional phases in the temperature range from 300 K to 700 K (Figure 14). The ball-milled material exhibited a pronounced increase in crystallite size at temperatures above 460 K (Figure 26) partially annihilating the intended surface-increasing effect of the mechanical treatment procedure employed. Therefore, with respect to using PdGa as a hydrogenation catalyst, it appears advisable to keep the reaction temperature below 450 K to avoid sintering and loss of active catalyst surface. The same holds for potential regeneration procedures of the catalyst under oxidative conditions, which will not result in bulk oxidation or phase transitions of the material, in contrast to Pd metal.

In situ XRD measurements of Pd_3Ga_7 under reactive atmospheres confirm the thermal stability of the material up to 600 (Figure 24). The sintering of the ball-milled material is less pronounced compared to PdGa, most likely because of the reduced period of mechanical treatment, which resulted in larger and less defective crystallites (Figure 26). The reduced stability of Pd_3Ga_7 compared to PdGa is caused by a possible disproportion at higher temperature to yield PdGa. In addition to surface oxide reduction or oxidation of PdGa at temperatures above 600 K may accounting for the mass changes of PdGa detected by TG/DSC measurements (Figure 18). Hence, similar to PdGa, reaction temperatures during acetylene hydrogenation on Pd_3Ga_7 should remain below 500 K to avoid structural degradation of changes in phase composition.

In good agreement with the in situ XRD results, the short-range order of the palladium gallium intermetallic compounds studied exhibited only slight changes during thermal treatment in the various gas atmospheres (Figure 27 - Figure 31). The local distances and Debye Waller factors as determined from an analysis of the in situ EXAFS data showed the expected behavior as a function of temperature with no significant structural changes correlating with the onset of catalytic activity. Only an additional step between 400 K and 500 K in the Debye-Waller factors indicates an increased structural ordering in PdGa and corresponds to the exothermic peaks observed by DSC (Figure 18) and the onset of sintering obtained by profile fitting of XRD peaks (Figure 26). This indicates a sufficient thermal stability under acetylene and hydrogen containing conditions for the materials to be used as a selective hydrogenation catalyst. Moreover, it confirms our previous assumption that the isolation of the Pd atoms in the crystallographic structure of PdGa and Pd_3Ga_7 will still be present under reaction conditions. This shall permit to investigate the beneficiary effect of "active site isolation" in Pd hydrogenation catalysts.

Incorporation of hydrogen in palladium hydrogenation catalysts

In addition to being effected by the presence of neighboring Pd sites on the catalyst surface, the limited selectivity and long-time stability of palladium in acetylene hydrogenation may also be caused by the formation of palladium hydrides under reaction conditions. It has been reported that the formation of β-hydride may decrease the selectivity to ethylene by enhancing complete hydrogenation of acetylene [39]. This effect has been ascribed to a higher concentration of surface hydrogen in β-hydride [40]. Doyle et al have shown that hydrogenation of alkenes requires the formation of weakly bond subsurface hydrogen [41]. Apparently, materials that do not exhibit formation of hydrides should possess a limited availability of hydrogen from the bulk, which should result in an improved selectivity. In combination with the absence of hydrogen in the catalyst bulk, isolating Pd atoms on the catalyst surface will reduce the number of adsorption and dissociation sites for hydrogen and thereby further diminish the hydrogen supply for unwanted ethylene hydrogenation [42-45,94]. In addition to the formation of hydrides under hydrogenation reaction conditions, palladium metal may also dissolve carbon in the bulk resulting in a ternary phase of palladium, hydrogen, and carbon. Although difficult to analyze, this ternary system has been shown to influences activity, stability, and selectivity of palladium catalysts [8,99,100].

Palladium intermetallic compounds should exhibit a small tendency towards incorporation of hydrogen or carbon in the bulk and, hence, should allow for a reduced surface concentration of hydrogen under reaction conditions and an increased selectivity [42-45,94]. The incorporation of hydrogen in palladium metal and the formation hydrides results in a lattice expansion [14] and increased interatomic distances. Both effects should be detectable by in situ XRD and in situ EXAFS [101-103]. In situ XRD patterns of PdGa and Pd_3Ga_7 measured under reaction conditions showed a small and linear peak shift towards lower diffraction angles (i.e. larger distances) (Figure 22 + Figure 24). Both lattice expansion due to hydride formation and thermal lattice expansion will result in a shift of the diffraction peaks to lower angles. However, while thermal expansion will lead to a linear peak shift with temperature independent of the gas atmosphere, formation and decomposition of hydrides with increasing temperature will be discernible from a nonlinear shift of the diffraction peaks to lower and higher angles, respectively. From the linear increase in distances with temperature observed in the in situ XRD and EXAFS data (Figure 22 - Figure 31) under all atmospheres, it can be concluded that the intermetallic compounds form no detectable amount of hydrides under reaction conditions. Similar to the incorporation of hydrogen in the lattice of the intermetallic compounds, no formation of additional carbon containing phases under acetylene reaction conditions was detected.

7.2.3 Surface characterization

XPS, ISS and CO chemisorption

Isolated Pd atoms are present in the bulk structure of Pd-Ga intermetallic compounds which exhibits a pronounced stability under hydrogenation reaction condition as determined by TG/DSC, in situ XRD, and in situ EXAFS investigations. However, the composition and the structure of the surface of these materials may differ from those of the bulk. Therefore, as-prepared and pre-treated Pd-Ga intermetallic compounds were further investigated by various surface sensitive techniques. From the stoichiometric composition of PdGa and Pd_3Ga_7, a surface composition of 50% gallium and 50% palladium, and 70% gallium and 30% palladium, respectively, is expected. XPS studies on as-prepared PdGa and Pd_3Ga_7 resulted in a high oxygen concentration on the surface accompanied by mainly oxidized Ga

and a low Pd content. Hydrogen treatment resulted in the formation of a reduced Ga species in the near-surface region (Figure 32 + Table 6) and a slightly increased Ga and Pd concentration (Table 5). Compared to PdGa, hydrogen treatment of Pd_3Ga_7 caused even smaller changes to the surface composition and also did not yield the expected concentration of reduced Ga and Pd. For Pd_3Ga_7 a very low content of reduced Ga species was observed before and after hydrogen treatment (Table 5). Even with taking the reduced treatment temperature (573 K) of Pd_3Ga_7 into account, the oxide layer on Pd_3Ga_7 appears to be more stable or thicker compared to that of PdGa. The gallium oxide layer observed indicates a segregation of gallium to the surface of PdGa and Pd_3Ga_7 followed by oxidation to gallium oxide. After reductive treatment at elevated temperature, no segregation of Pd atoms to the surface of the Pd-Ga intermetallic compounds and formation of Pd clusters or overlayers was detected. Hence, the structural stability as determined by in situ XRD and EXAFS does also hold for the near-surface region of the intermetallic compounds used. The temperature employed for the hydrogen treatment of PdGa and Pd_3Ga_7 was higher than the temperature used for isothermal catalytic investigation under reaction condition B. Hence, the surface composition of reduced PdGa and Pd_3Ga_7 should also be stable under the hydrogenation reaction conditions employed.

ISS measurements yielded a small amount of Pd at the surface of both untreated and reduced intermetallic compounds (Figure 33). The fact that Pd is detectable by ISS excludes a total coverage of the surface of PdGa and Pd_3Ga_7 by a gallium oxide layer. Segregation of Pd and formation of Pd clusters or Pd overlayers was not detected in agreement with the XPS data. XPS and ISS experiments showed that sputtering with He atoms removes the gallium oxide layer more efficiently than reduction with hydrogen. However, the gallium oxide that covers the surface of the as-prepared Pd-Ga intermetallic compounds will mostly remain under hydrogenation condition while only a small fraction of the surface will correspond to the bulk structure of PdGa or Pd_3Ga_7. In total, activation of PdGa and Pd_3Ga_7 in hydrogen is clearly inferior to chemical etching in increasing the active Pd surface area.

CO chemisorption measurements neither using sorption equipment nor DRIFTS investigation showed no detectable adsorption of CO on PdGa and Pd_3Ga_7 at 300 K. Because CO chemisorbs strongly on Pd metal surfaces [90], the presence of regular metallic Pd at the surface of the untreated Pd-Ga intermetallic compounds can be excluded. Reduction in hydrogen did not yield in a detectable CO chemisorption, which additionally excludes the formation of Pd clusters also under strong reducing atmosphere and elevated temperature in

good agreement with the XPS and ISS measurements. In addition, the absence of CO chemisorption on chemically etched Pd-Ga intermetallic compounds determined by IR investigation showed the reduced interaction of CO molecules with the surface of Pd-Ga intermetallic compounds and is further discussed as “electronic effect” in the catalysis section.

7.2.4 Acetylene hydrogenation on Pd-Ga intermetallic compounds

Chemical etching increases activity of Pd-Ga intermetallic compounds

Chemical etching with ammonia solution was employed to effectively remove the gallium oxide layer from the surface of the intermetallic compounds. Ammonia solutions are well-known for chemical etching of semi-conductors like GaAs [104-106]. Untreated Pd-Ga intermetallic compounds showed a low activity ratio of 1 : 100 : 200 for Pd/Al_2O_3 : PdGa : Pd_3Ga_7 (Figure 38 + Figure 39) under condition A (2% acetylene and 4% hydrogen). After chemical etching (pH = 9.8 for PdGa, pH = 10.5 for Pd_3Ga_7) the activity ratio was improved to 1 : 10 : 30. Under reaction conditions B (excess of ethylene) the activity ratio was improved from 1 : 133 : 300 for the untreated samples to 1 : 15 : 20 for the chemically etched catalysts (Figure 40 + Figure 41 + Figure 42, Table 7). Prolonged chemical etching, however, may result in the formation of neighboring Pd atoms and, thus, Pd clusters or Pd overlayers, by dissolution of Ga from the bulk structure of the Pd-Ga intermetallic compounds. The latter will cause a significant loss in selectivity of the corresponding catalyst under acetylene hydrogenation conditions, and, thus, an increased formation of ethane. Therefore, maintaining selectivity while increasing hydrogenation activity of an etched material is indicative of an optimized etching procedure.

PdGa and Pd_3Ga_7 could be successfully chemically etched to obtain a higher activity at nearly the originally high selectivity under reaction condition A (Figure 38 + Figure 39). Using a higher pH for the etching solution resulted in a further increased activity but a decreased selectivity and enhanced ethane formation. Similarly, an etching solution with an even lower pH of 9.0 had to be employed to maintain high selectivity of the etched catalysts under reaction condition B. Apparently, even a minor amount of neighboring Pd sites not

detectable under condition A may cause a pronounced loss in selectivity in an excess of ethylene. The slightly reduced selectivity of etched PdGa below 370 K under conditions A compared to untreated PdGa may also indicate the formation of neighboring Pd sites (more active, less selective) during chemical etching already at a pH of 9.8. Restructuring of the PdGa surface or preferred poisoning of the neighboring Pd sites may account for the similar selectivity of chemically etched and untreated PdGa observed above 370 K. The lower pH value required for a successful etching of PdGa (9.8) compared to Pd_3Ga_7 (10.5) indicates a facilitated dissolution of the gallium oxide layer from the surface of PdGa. This may be caused by a reduced interaction at the interface between gallium oxide and PdGa or a more amorphous structure of the gallium oxide on PdGa.

The varying influence of the pH of the ammonia solution used on the selectivity of the chemically etched Pd-Ga intermetallic compounds indicates that ammonia solution is not the most suitable agent to selectively remove the gallium oxide layer without structural degradation of the underlying intermetallic compound. Hence, further investigations will have to focus on more selective chemical etching procedures that permit to fully explore the superior catalytic properties of Pd-Ga intermetallic compounds. However, given the low BET surface area of PdGa and Pd_3Ga_7 of ~1 m^2/g and a partial coverage of the surface by gallium oxide even after an optimized chemical etching, it appears that the activity per Pd site of, for instance, etched PdGa is at least similar to that of Pd/Al_2O_3 (Pd surface area of 5.2 m^2/g, activity ratio of Pd/Al_2O_3 : PdGa of 1 : 10).

Selective acetylene hydrogenation on Pd-Ga intermetallic compounds

Untreated (Figure 36) and chemically etched (Figure 38 + Figure 39) Pd-Ga intermetallic compounds showed a high selectivity to ethylene in hydrogenation of acetylene under condition A accompanied by a reduced formation of ethane and an increased formation of C4 hydrocarbons compared to Pd/Al_2O_3 (Figure 35). Only traces of ethane were detected in the product stream under reaction condition A. Hence, after hydrogenation of acetylene, the ethylene formed rapidly desorbs from the surface of the intermetallic compounds before further hydrogenation to ethane can occur.

In an excess of ethylene (condition B) ethane may be formed by a total hydrogenation of adsorbed acetylene or by adsorption and hydrogenation of ethylene from the gas phase. A direct hydrogenation reaction path from acetylene to ethane [5,107-109], and a Horiuti–

Polyani mechanism with consecutive addition of hydrogen [110,111] have been proposed in the literature. Because of the very low formation of ethane under reaction condition A, a direct hydrogenation path from acetylene to ethane appears to play a minor role on the surface of PdGa and Pd_3Ga_7 (Figure 35 + Figure 36). Instead, the low ethane concentration and the formation of C4 hydrocarbons indicate a preferred Horiuti–Polyani mechanism with consecutive addition of hydrogen. Stepwise addition of hydrogen leads to free radicals as intermediates which can readily oligomerize to higher olefins.

Reducing ethylene hydrogenation is most important to obtain high selectivity in acetylene hydrogenation in an excess of ethylene under reaction condition B. Oligomerisation of acetylene to higher hydrocarbons (equation 3) plays only a minor role under these conditions. PdGa and Pd_3Ga_7 produce significantly less ethane under condition B compared to Pd/Al_2O_3 or $Pd_{20}Ag_{80}$ (Figure 40, Table 7) in good agreement with the assumption of weakly adsorbing ethylene and acetylene and rapidly desorbing ethylene from the surface of the intermetallic compounds. Weak bonding of acetylene and ethylene to the Pd-Ga surfaces can be explained by a “geometric effect” (i.e. active-site isolation) and an “electronic effect” (i.e. modified average valences of palladium and gallium). Moreover, a “kinetic effect” due to the absence of hydride formation and, thus, a decreased hydrogen concentration on the catalyst surface, will increase selectivity in acetylene hydrogenation. Conversely, formation of hydrides and, hence, high availability of hydrogen at the surface results in a preferred total hydrogenation of acetylene to ethane and a decreased [39-45,94]. In contrast to Pd/Al_2O_3, no incorporation of hydrogen of the Pd-Ga intermetallic compounds was detectable by in situ XRD and in situ EXAFS investigations in the temperature range from 300 to 700 K (Figure 22 + Figure 24)

Increased selectivity due to a “geometric effect“

The π-bond system of unsaturated hydrocarbon molecules has several possibilities to interact with a palladium surface. Interaction of acetylene or ethylene with a single Pd atom of the surface results in so-called weakly π-bonded acetylene or ethylene, respectively. Interaction with two neighboring Pd atoms on the surface leads to more strongly di- σ -bond acetylene and ethylene, with a partial hybridisation from sp to sp^2 for acetylene or sp^2 to sp^3 for ethylene, respectively [21-23]. Moreover, co-adsorption with hydrogen results in vinylidene ($=C=CH_2$) and ethylidyne ($\equiv C\text{-}CH_3$) species on the surface which require two or three neighboring Pd atoms [112-117]. Di-σ-bonded alkenes have been recently proposed to be the

precursor in the alkane formation [24]. Shaikhutdinov and co-workers [25] showed that π-bonded ethylene desorbs already at 200 K under UHV conditions. Only di-σ-bonded ethylene on a palladium surface appears to be stable at elevated temperatures and, hence, may be hydrogenated to ethane or may decompose and form carbon deposits [28].

Isolation of active Pd sites on the surface of hydrogenation catalysts (so-called "geometric effect") results in increased Pd-Pd distances and the absence of neighboring Pd sites. This may suppress the formation of di-σ-bonded alkene and alkyne species and lead to preferentially weakly π-bonded acetylene molecules on the catalyst surface. Under hydrogenation reaction conditions above 300 K, the weakly π-bonded acetylene molecules will be hydrogenated to ethylene and rapidly desorbs from the surface before further hydrogenation to ethane can occur. Structurally well-defined Pd-Ga intermetallic compounds possess isolated Pd atoms that permit only π-bonded acetylene molecules and are ideally suited to selectively hydrogenate these molecules to ethylene without further hydrogenation to ethane. Hence, the high selectivity of PdGa and Pd_3Ga_7 in acetylene hydrogenation appears to corroborate the concept of active-site isolation to obtain more selective hydrogenation catalysts.

Increased selectivity due to an "electronic effect"

In addition to geometric effects by active-site isolation and kinetic effects by reduced hydride formation, changes of adsorption and desorption properties of reactant molecules may be induced by modification of the electronic structure of the palladium phase ("electronic effect"). Acetylene possesses a higher adsorption energy on palladium metal than ethylene which results in a replacement of the ethylene formed on the catalyst surface by gaseous acetylene [6,118,119]. Hence, an increased selectivity may be obtained by an overall shift to lower adsorption energies or by increasing the difference in the adsorption energies of acetylene and ethylene on the catalyst surface [36]. Modification of the electronic structure of palladium by alloying with another metal can influence the adsorption properties of the corresponding catalyst and, thus, increase the selectivity in acetylene hydrogenation [7,19]. Various palladium alloys with Ag [37], Sn [120], Au [121], or Ni [122] have been described to improve the catalytic performance of Pd catalysts in hydrogenation reactions. In addition to a modified electronic structure, alloying of palladium may also cause a reduced activity ("kinetic effect") and, hence, an increased selectivity by blocking of active site as suggested for Pb additives used in Lindlar catalysts [51,52].

The electronic state of Pd surfaces can be assessed by chemisorption experiments [95,123]. CO chemisorption, for instance, can be used to determine the active surface area by measuring the amount of CO adsorbed or to investigate the electronic properties of the catalyst surface by determining the chemisorption strength (temperature programmed desorption, TPD) [124-126], by infrared (IR) spectroscopy [90] or C-13 NMR [127]. Chemisorption of CO on Pd surfaces takes path by electron density donation from the 5σ-orbital of the CO molecule located next to the carbon atom and electron density backdonation to the unoccupied anti-bonding 2π*-orbital of the CO molecule [90]. Reducing the d-band density of states of Pd by alloying with another metal results in a weaker interaction of the resulting Pd catalyst with CO [95] and, hence, a detectable adsorption of CO only at lower temperatures compared to palladium metal.

The π-orbital (HOMO) and the π*-orbital (LUMO) of adsorbed unsaturated hydrocarbons are located below and next to the Fermi edge of the Pd metal, respectively, and both orbitals are coupled with the electronic bands at the surface. Similar to the interaction of Pd with CO [90], electron density is donated from the HOMO of the adsorbed molecule to the s-band of the metal surface accompanied by electron density backdonation from the metal d-band to the LUMO of the adsorbed reactant [16,17]. Hence, the strength of adsorption of CO on various Pd surfaces should exhibit a similar tendency like to strength of adsorption of acetylene or ethylene.

The absence of detectable CO chemisorption on as-prepared and chemically etched PdGa and Pd_3Ga_7 at room temperature indicates different adsorption properties of the Pd-Ga intermetallic compounds compared to Pd/Al_2O_3. Apparently, the formation of Pd-Ga intermetallic compounds results in a modified electronic structure at the surface palladium sites compared to those of palladium metal. Quantum chemical calculations of the electronic structure (ab initio band structure calculation) and chemical bonding (electron localization function) of PdGa and Pd_3Ga_7 showed a significant contribution of covalent bonding [128] and results in a modified local electronic structure of the Pd atoms compared to palladium metal. Contributions to covalent bonding may suppress the electron density backdonation from the catalyst surface to the CO molecules and which may account for the reduced adsorption energy of CO on the Pd sites of the intermetallic compounds. Further IR absorption measurements of chemisorbed CO at low temperature are necessary to investigate the electronic interaction between Pd-Ga intermetallic surfaces and CO molecules. Similar to the adsorption properties of CO on PdGa and Pd_3Ga_7, the active Pd sites on the surface of the

intermetallic compounds will exhibit a reduced interaction with ethylene and, thus, an increased selectivity in the hydrogenation of acetylene. Palczewska et al. reported increased selectivity in the hydrogenation of unsaturated hydrocarbons on a Pd-Pb intermetallic compound compared to conventional Lindlar catalysts [32] which may be caused by the modified local electronic structure of Pd atoms in intermetallic compounds compared to Pd atoms in a Pd based alloy. A high-selective chemical etching procedure has to be developed to obtain a clean and oxide free Pd-Ga intermetallic surface which allows the investigation of the electronic structure using ultraviolet photoelectron spectroscopy (UPS).

Long-term stability of Pd-Ga intermetallic compounds in acetylene hydrogenation

Conventional supported palladium catalysts exhibit rapid deactivation under acetylene hydrogenation conditions. Deactivation is mainly caused by carbon deposits [6-8] formed by oligomerisation reactions (green oil) and decomposition of hydrocarbons [26-28,129]. Oligomerisation mainly occurs on the Pd catalyst surface [129] but minor parts of green oil can also be formed on acidic sites on the catalyst support [130]. Pd/Al_2O_3 exhibited rapid deactivation during isothermal acetylene hydrogenation at 473 K in an excess of ethylene (condition B). Conversely, PdGa and Pd_3Ga_7 showed a nearly constant acetylene conversion while maintaining a high selectivity under condition B (Figure 37 + Figure 40, Table 7). Because the reaction temperature of 473 K diminishes deposition of volatile green oil on the catalyst surface, oligomerisation and green oil formation played only a minor role in catalyst deactivation observed. Instead, Pd/Al_2O_3 was mainly deactivated by decomposition of hydrocarbons by C-C bond scission leading to carbonaceous deposits. Di-σ-bonded acetylene and ethylene, and vinylidene and ethylidyne species have been proposed as precursors for acetylene decomposition resulting in deactivation of the Pd catalysts [25,28,131-133]. However, formation of these species requires the presence of neighboring Pd sites on the surface. Therefore, Pd/Al_2O_3 showed a much stronger deactivation behavior than the intermetallic compounds. Because the isolated Pd sites on the latter permit only weakly π-bonded hydrocarbons, PdGa and Pd_3Ga_7 suppress hydrocarbon decomposition and, hence, possess a strongly increased long-term stability in the hydrogenation of acetylene [26,27,35].

Industrially used catalysts like palladium-silver alloys with a silver content of more than 50 at% contain an increased number of isolated Pd atoms at the surface and, hence, should also exhibit a reduced deactivation by hydrocarbon decomposition [134]. The $Pd_{20}Ag_{80}$ alloy

employed here possesses an improved long-term stability and a higher selectivity in acetylene hydrogenation than Pd/Al_2O_3. However, the selectivity of $Pd_{20}Ag_{80}$ remained below that of the Pd-Ga intermetallic compounds (Figure 40, Table 7). Besides the "random" isolation of Pd sites in $Pd_{20}Ag_{80}$, segregation of palladium and formation of ensembles of Pd atoms on the catalyst surface [48,49,135] will decrease selectivity in acetylene hydrogenation and facilitate the deactivation by carbon deposits. Conversely, Pd site isolation constitutes a distinct structural feature of Pd-Ga intermetallic compounds. Owing to the high structural stability (Figure 22 - Figure 25, Figure 28 -Figure 31) of these compounds, isolation of Pd atoms and, hence, superior selectivity and deactivation behavior are maintained under long-term reaction conditions.

Comparison of the catalytic behaviour of PdGa and Pd_3Ga_7

PdGa exhibited a higher activity-per-mass ratio in acetylene hydrogenation than Pd_3Ga_7. The higher activity per mass of PdGa can be predominantly assigned to the facilitated removal of the gallium oxide layer compared to Pd_3Ga_7. Additionally, the higher Pd content of PdGa (60.4 wt-%, Pd_3Ga_7 39.5 wt-%) and the slightly larger surface area obtained by a prolonged ballmilling procedure may contribute to the higher activity of PdGa compared to Pd_3Ga_7. Under the reaction conditions employed, untreated PdGa and Pd_3Ga_7 showed a similar selectivity in acetylene hydrogenation. Conversely, chemical etching of Pd_3Ga_7 resulted in a more pronounced loss of selectivity compared to chemically etched PdGa. The decreased selectivity of chemically etched Pd_3Ga_7 may be caused by dissolution of Ga atoms from the bulk and preferred formation of ensembles of Pd atoms on the surface. Alternatively, the inferior selectivity of etched Pd_3Ga_7 may indicate a structure-selectivity correlation that ranges from completely isolated Pd atoms in PdGa (Pd-Pd distance of 3.01 Å), through isolated Pd-Pd pairs in Pd_3Ga_7 (Pd-Pd distance of 2.73 Å and diluted Pd in $Pd_{20}Ag_{80}$, to 12 next nearest Pd neighbors in palladium metal (Pd-Pd distance of 2.76 Å).

Both PdGa and Pd_3Ga_7 exhibit isolated active Pd sites in their crystallographic structure ("geometric effect"), contribution of covalent Pd-Ga bonding resulting in a modified electronic structure at the Pd site ("electronic effect"), and an inhibited formation of hydrides ("kinetic effect"). All effects have been proposed to yield an improved selectivity in acetylene hydrogenation. On the one hand, it remains difficult to estimate the relative importance of these effects for the superior selectivity of palladium containing intermetallic compounds. Further investigations, employed other non-gallium containing palladium

intermetallic compounds will help to elucidate the effects of site-isolation, electronic structure, and hydride formation on the selectivity in acetylene hydrogenation. On the other hand, it is the combination of all three effects in Pd-Ga intermetallic compounds that makes them ideally suited selective and long-term stable hydrogenation catalysts.

8 Pt-Pd-Ga intermetallic compounds

8.1 Results

8.1.1 Preparation and characterization of $PtPd_2Ga_3$ and $PtPd_2Ga_7$

Similar as PdGa and Pd_3Ga_7, the Pt-Pd-Ga intermetallic compounds prepared were investigated with X-ray diffraction and X-ray absorption spectroscopy to confirm structure and phase purity. XRD measurements of $PtPd_2Ga_3$ and $PtPd_2Ga_7$ were performed after the ballmilling procedure and before and after ballmilling, respectively. Both samples showed no difference between the experimental and simulated diffraction pattern (Figure 43 + Figure 44). Ballmilling of $PtPd_2Ga_7$ resulted in an increased FWHM indicating a reduced average domain size. For $PtPd_2Ga_3$ and for $PtPd_2Ga_7$, average domain sizes of 14 nm and 35 nm, respectively, were obtained by P-Voigt profile fitting of selected diffraction peaks. Both compounds were ball-milled in the same way as the Pt free samples and the ballmilling of the gallium-rich samples resulted in similar average domain sizes, whereas ballmilling of $PtPd_2Ga_3$ resulted in a significantly smaller average domain size compared to PdGa. BET measurements yielded a total surface area of around 1 m^2/g for both Pt samples.

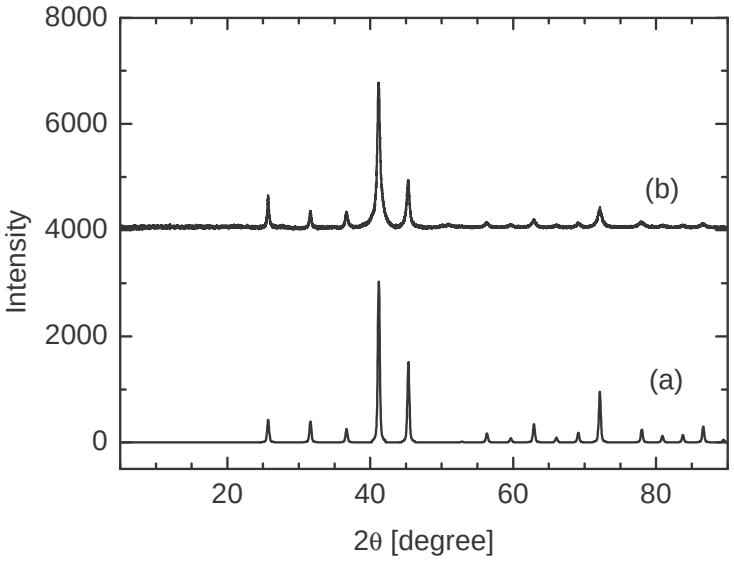

Figure 43: Experimental XRD pattern of $PtPd_2Ga_3$: simulated pattern (a) and after ballmilling (b).

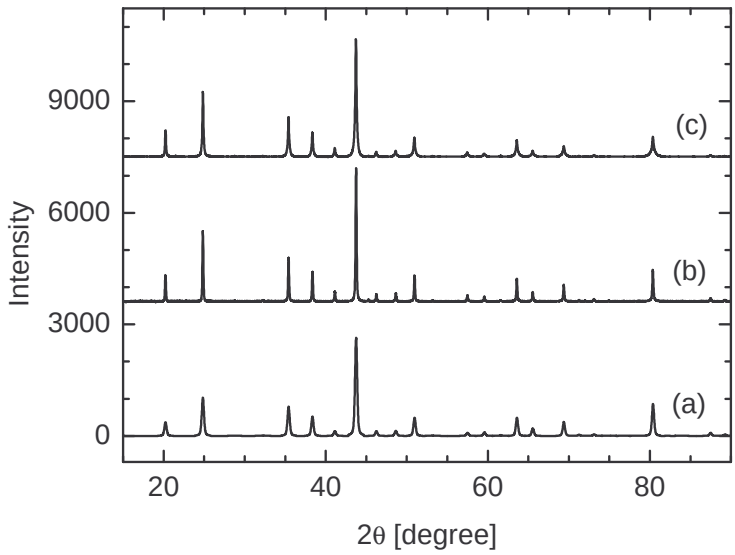

Figure 44: XRD pattern of $PtPd_2Ga_7$: Simulated pattern (a), experimental pattern after grinding in a mortar (b) and after ballmilling (c).

The theoretical lattice constant of $PtPd_2Ga_3$ and $PtPd_2Ga_7$ were calculated from literature data of Pd-Ga and Pt-Ga intermetallic compounds assuming the validity of Vegard's law.

$PtPd_2Ga_3$ showed a deviation of 0.0038 Å of the experimental to the calculated value (Table 8). $PtPd_2Ga_7$ also showed a very small difference of 0.0004 Å to the calculated value.

Table 8: Crystallographic lattice constants of PdGa [61], Pd_3Ga_7 [62], PtGa [61] and Pt_3Ga_7 [136] from literature and obtained by refinement of experimental XRD pattern in Å. Lattice constants of the ternary Pt-Pd-Ga intermetallic compounds were calculated by assuming of the validity of Vegard's law.

Experimental	Reference	Experimental	Calculated	Reference
PdGa	**PdGa**	**$PtPd_2Ga_3$**	**$PtPd_2Ga_3$**	**PtGa**
4.8908	4.890	4.8968	4.893	4.90
Pd_3Ga_7	**Pd_3Ga_7**	**$PtPd_2Ga_7$**	**$PtPd_2Ga_7$**	**Pt_3Ga_7**
8.7730	8.7716	8.7743	8.7747	8.781

Ex-situ EXAFS studies of $PtPd_2Ga_3$ and $PtPd_2Ga_7$ were performed at the Pd K-edge and the interatomic distances and Debye-Waller factors obtained are similar to that of PdGa and Pd_3Ga_7. The simulated RDF showed good agreement to the experimental RDF (Figure 45). The refined interatomic distances of the third Ga shell of $PtPd_2Ga_3$ showed only minor deviation to the theoretical value from structural data and a slightly increased Debye-Waller factor (Table 9). Similar results were obtained for $PtPd_2Ga_7$. Only the first Pt shell showed a deviation of 0.004 Å to the theoretical interatomic distance. All Debye-Waller factors obtained by refinement of $PtPd_2Ga_7$ were below 0.01 $Å^2$ (Table 9).

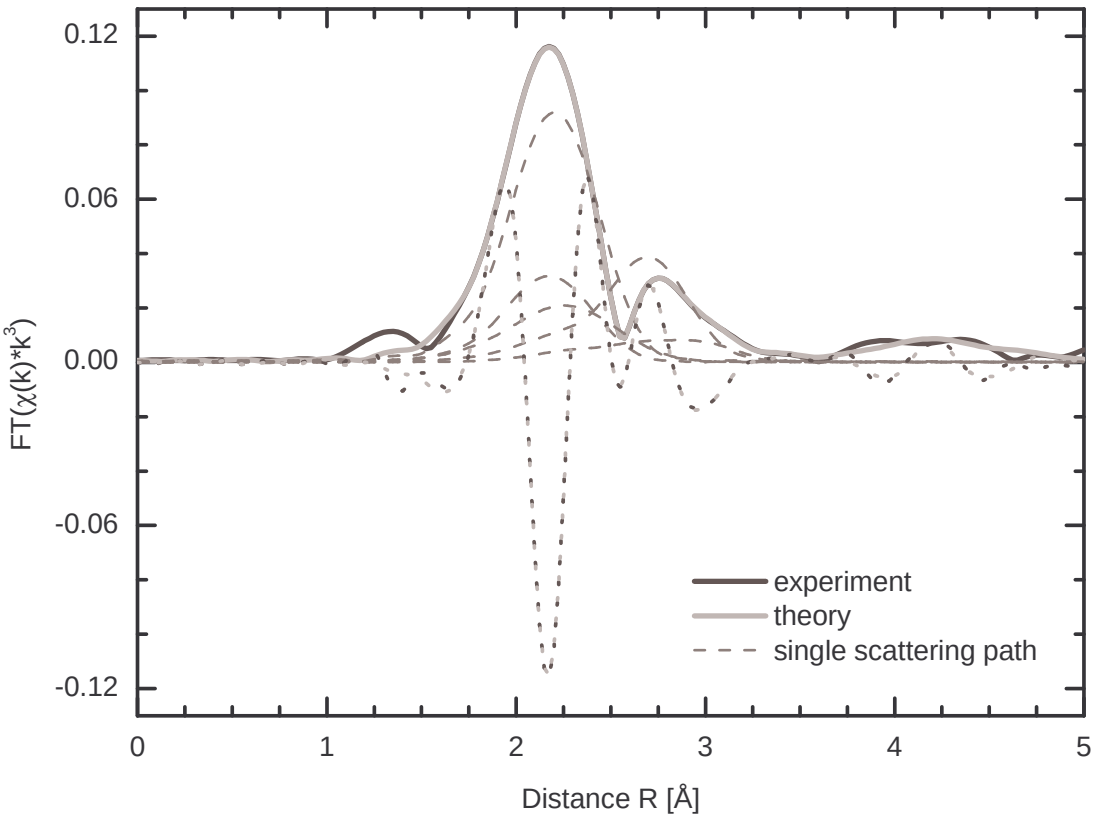

Figure 45: Experimental and theoretical FT(χ(k)*k^3) of $PtPd_2Ga_3$. Dotted lines refer to imaginary part and dashed lines to first five single-scattering paths (3x Ga, 1x Pd and 1x Pt).

Table 9: Results of EXAFS refinement of $PtPd_2Ga_3$ and $PtPd_2Ga_7$. ΔR_c refers to the deviation of refined interatomic distances to crystallographic data of PdGa and Pd_3Ga_7.

$PtPd_2Ga_3$	**CN**	**R [Å]**	**ΔR_c [Å]**	**σ^2 [Å^2]**	**E_0 [eV]**
Ga	1	2.55	0.01	0.006	-3.08
Ga	3	2.58	0.01	0.006	-3.08
Ga	3	2.67	-0.04	0.016	-3.08
Pt	2	3.01	0.00	0.012	0.23
Pd	4	2.97	-0.03	0.011	-5.29
$PtPd_2Ga_7$	**CN**	**R [Å]**	**ΔR_c [Å]**	**σ^2 [Å^2]**	**E_0 [eV]**
Ga	4	2.57	-0.01	0.007	-0.65
Ga	4	2.58	-0.01	0.007	-0.65
Pt	0.33	2.77	0.04	0.005	5.18
Pd	0.67	2.71	-0.02	0.004	4.07

8.1.2 Structural investigations during thermal treatment

In situ X-ray diffraction

Investigation of the structural stability of the Pt-Pd-Ga intermetallic compounds during thermal treatment in 50% hydrogen + 50% helium, 20% oxygen + 80% helium and in pure helium were performed by in situ XRD similar to the Pd-Ga intermetallic compounds. X-ray diffraction pattern of $PtPd_2Ga_3$ and $PtPd_2Ga_7$ were collected from 323 K to 773 K and 723 K, respectively. Both Pt-Pd-Ga intermetallic compounds showed a high stability during thermal treatment in hydrogen. $PtPd_2Ga_3$ showed no additional peaks indicating the presence of an additional phase and $PtPd_2Ga_3$ showed at 773 K in pure helium and in 20% oxygen in helium additional peaks due to the formation of Pd or Pt which were more pronounced in oxygen compared to helium collected XRD pattern. At 773 K in 20% oxygen an additional

peak appeared at 48° indicating the formation of gallium oxide. In situ XRD measurements of $PtPd_2Ga_7$ in 50% hydrogen in helium indicated the presence of $PtPd_2Ga_3$ by a small peak formed at $2\theta = 45°$ at 623 K but similar to $PtPd_2Ga_3$, no indication of a hydride formation was found. At 723 K in pure helium $PtPd_2Ga_7$ showed small and in 20% oxygen and 80% helium more pronounced peaks in the diffraction pattern indicative of the presence of traces of $PtPd_2Ga_3$ compared to the corresponding experiment in 50% hydrogen.

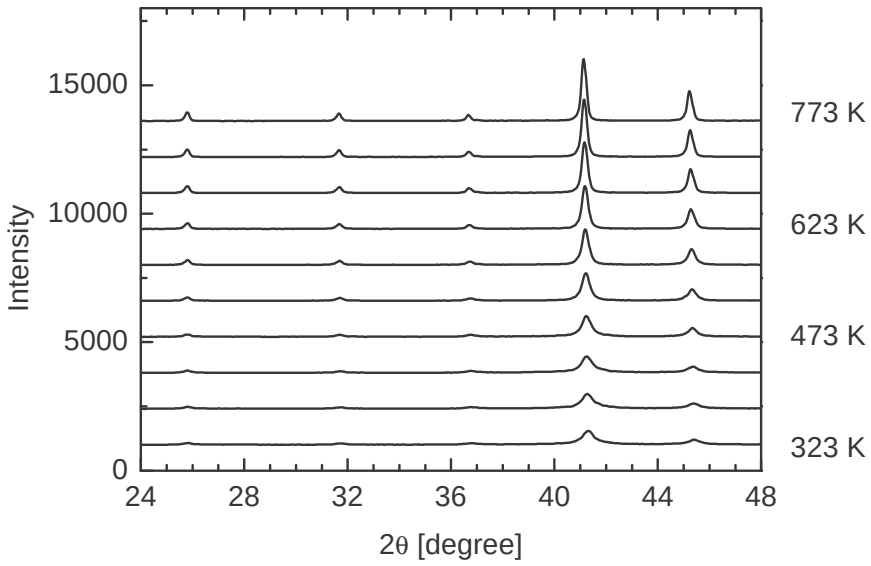

Figure 46: Evolution of in situ X-ray diffraction patterns of $PtPd_2Ga_3$ during thermal treatment from 323 K to 773 K in 50% H_2 + 50% He.

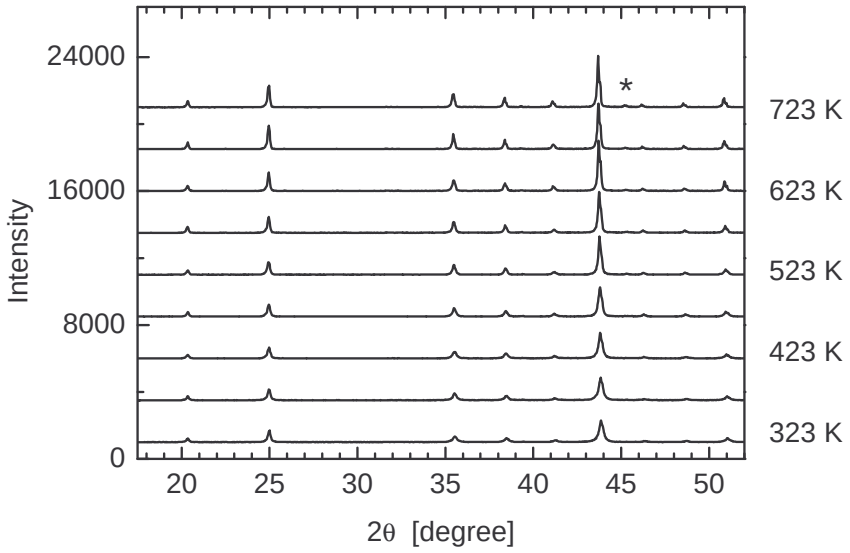

Figure 47: Evolution of in situ X-ray diffraction patterns of $PtPd_2Ga_7$ during thermal treatment from 323 K to 723 K in 50% H_2 + 50% He. Formation of $PtPd_2Ga_3$ at higher temperature is observable (*).

Comparison of the average domain size by P-Voigt profile fitting of selected *hkl* peaks of $PtPd_2Ga_3$ and $PtPd_2Ga_7$ with their corresponding Pt free intermetallic compounds resulted in fewer tendencies to sinter of the Pt containing samples. The ballmilling procedure of $PtPd_2Ga_3$ resulted in a smaller domain size compared to PdGa. During thermal treatment in hydrogen the average domain size of the Pt sample was significantly lower over the entire experiment compared to the Pt free sample (Figure 48). In contrast, the replacement of Pd by Pt for Pd_3Ga_7 did not lead to a decreased average domain size after ballmilling. Thermal treatment of both samples in hydrogen led to a decreased sintering effect above 373 K of $PtPd_2Ga_7$ compared to Pd_3Ga_7 (Figure 48).

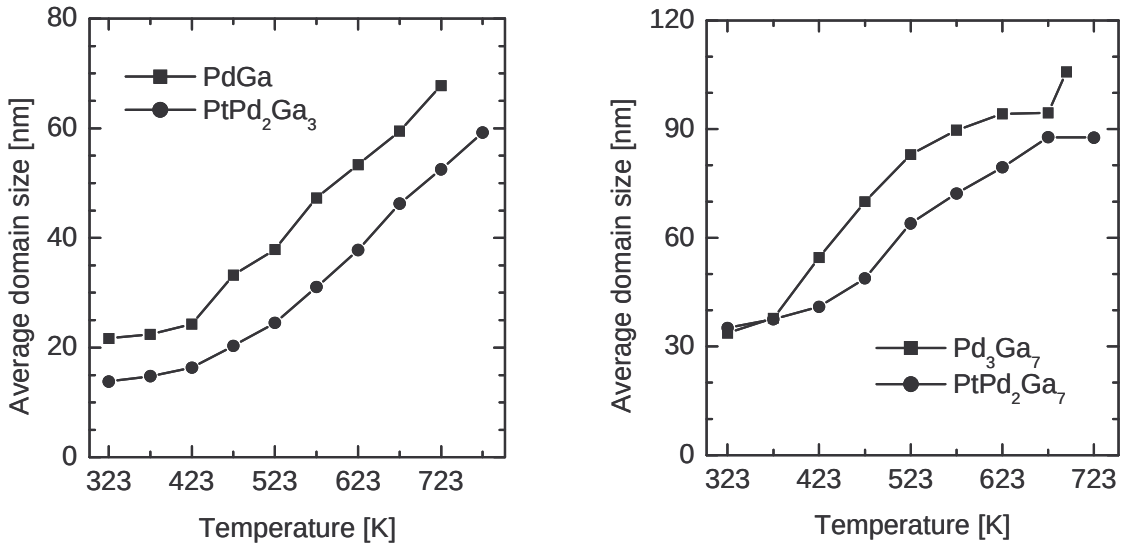

Figure 48: Evolution of average domain sizes of PdGa and $PtPd_2Ga_3$ (left) and Pd_3Ga_7 and $PtPd_3Ga_7$ (right) during thermal treatment in 50% hydrogen in helium obtained by profile analysis

8.1.3 Investigation of the catalytic performance of $PtPd_2Ga_3$ and $PtPd_2Ga_7$

Acetylene hydrogenation

Figure 49 shows the product composition measured during acetylene hydrogenation on $PtPd_2Ga_3$ (condition A). Catalytic activity exhibited a maximum at 480 K (0.495 g_{C2H2}/g_{cat}·h). Composition of the by-products in selective hydrogenation of acetylene was different for Pt- and Pt-free intermetallic compounds. Hydrogenation of acetylene on PdGa resulted in C4 hydrocarbons by oligomerisation as major by-product whereas $PtPd_2Ga_3$ formed more of the total hydrogenation product ethane than C4 hydrocarbons below 480 K. At temperature above 480 K, $PtPd_2Ga_3$ hydrogenated acetylene with high selectivity to ethylene and C4 hydrocarbons as minor products. Only traces of ethane were formed.

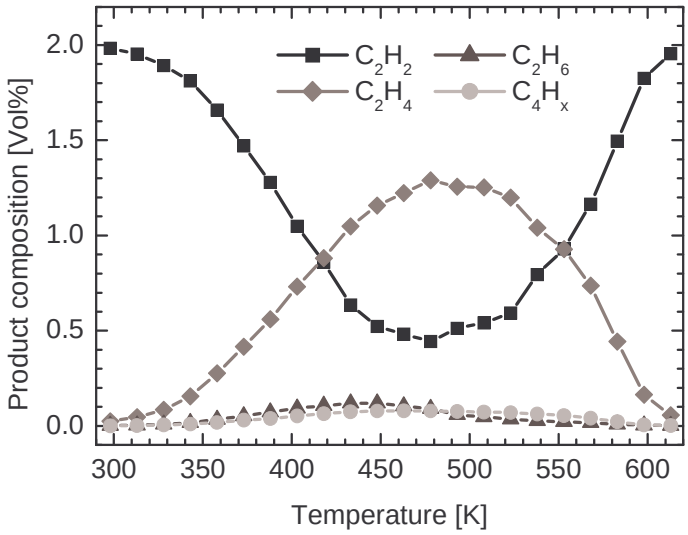

Figure 49: Product composition measured during hydrogenation of acetylene on $PtPd_2Ga_3$ (60 mg) (2% C_2H_2 + 4% H_2, condition A).

Acetylene hydrogenation on $PtPd_2Ga_3$ (60 mg, condition A) versus temperature showed a reduced activity (0.495 g_{C2H2}/g_{cat}·h at 480 K) compared to 50 mg PdGa (0.639 g_{C2H2}/g_{cat}·h at 430 K) (Figure 50) but both sample reached similar acetylene conversion. PdGa (50 mg) was more active in a temperature range from 360 to 460 K compared to $PtPd_2Ga_3$ (60 mg). Only at temperatures above 550 K, the platinum sample showed slightly higher acetylene conversion compared to the Pt free sample. The selectivity of both samples was similar below 450 K taking account that PdGa showed higher acetylene conversion compared to $PtPd_2Ga_3$. Selectivity was significantly higher above 450 K of $PtPd_2Ga_3$ compared to PdGa and Pd/Al_2O_3 (Figure 50).

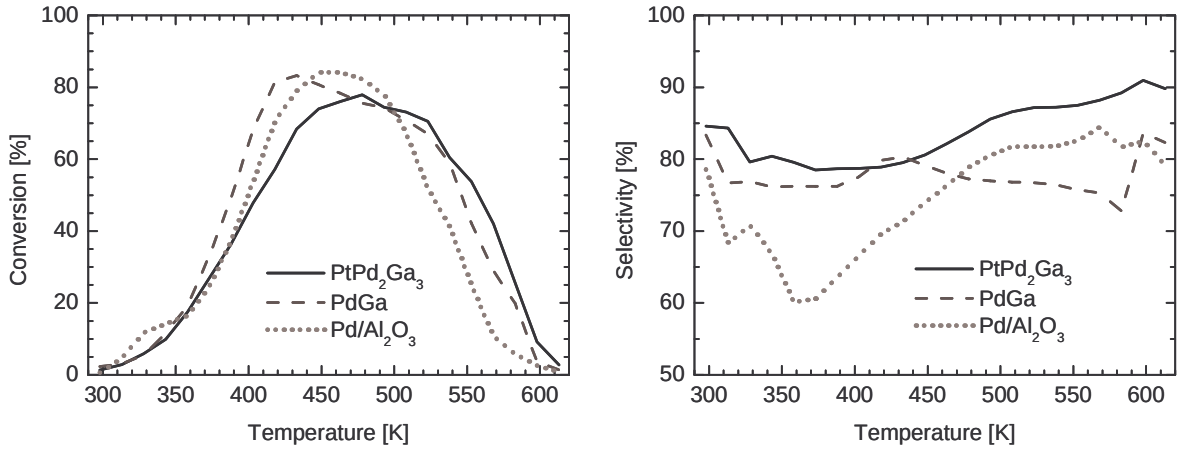

Figure 50: Conversion and selectivity measured during acetylene hydrogenation on $PtPd_2Ga_3$ (60 mg), PdGa (50 mg) and Pd/Al_2O_3 (0.5 mg) in 2% C_2H_2 + 4% H_2 (condition A).

Figure 51 presents acetylene conversion of $PtPd_2Ga_7$ (120 mg) which was significantly lower (activity at 430 K: 0.173 g_{C2H2}/g_{cat}·h) than that of 100 mg Pd_3Ga_7 (activity at 430 K: 0.639 g_{C2H2}/g_{cat}·h). In spite of the low conversion for acetylene hydrogenation, a very low selectivity was observed for $PtPd_2Ga_7$. Similar to $PtPd_2Ga_3$, below 480 K the major by-product of acetylene hydrogenation was the total hydrogenation product ethane.

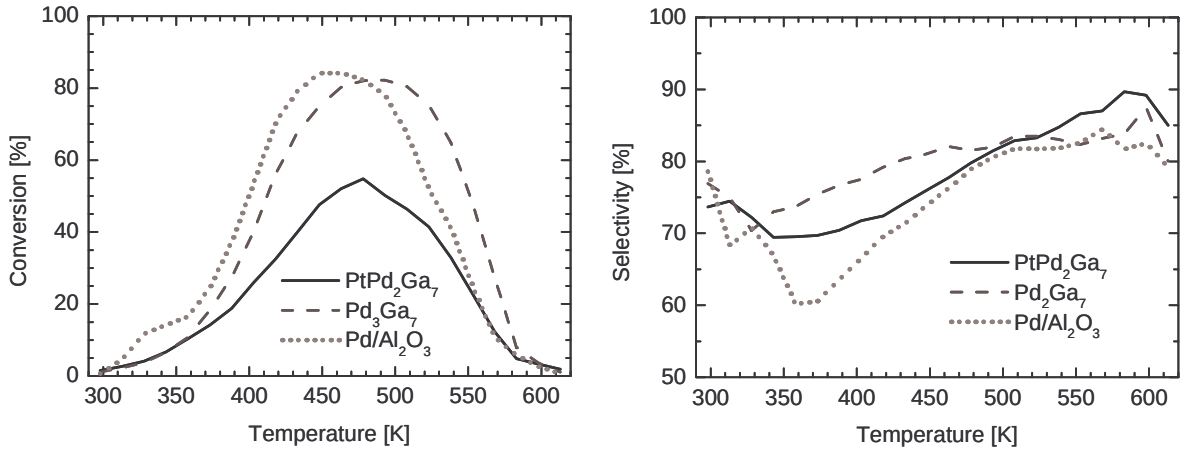

Figure 51: Conversion and selectivity measured during acetylene hydrogenation on $PtPd_2Ga_7$ (120 mg), Pd_3Ga_7 (100 mg) and Pd/Al_2O_3 (0.5 mg) under reaction condition A.

Acetylene hydrogenation in ethylene feed

Catalytic performance of Pt-Pd-Ga intermetallic compounds was measured isothermal at 473 K in ethylene rich feed (condition B). Same amount of sample mass of PdGa and the corresponding Pt sample resulted in higher acetylene conversion of $PtPd_2Ga_3$ (Figure 52). After 20 h acetylene hydrogenation on 40 mg $PtPd_2Ga_3$ resulted in 92% conversion compared to 86% of 40 mg PdGa. Partial substitution of Pd by Pt in the structure of PdGa did not lead to an additional catalytic stability. Both samples showed a slight deactivation during 20 h time on stream. Corresponding selectivity of $PtPd_2Ga_3$ was significantly higher compared to Pd metal supported on alumina. However, the selectivity of $PtPd_2Ga_3$ was much lower compared to the corresponding Pt free sample and lower compared to $Pd_{20}Ag_{80}$.

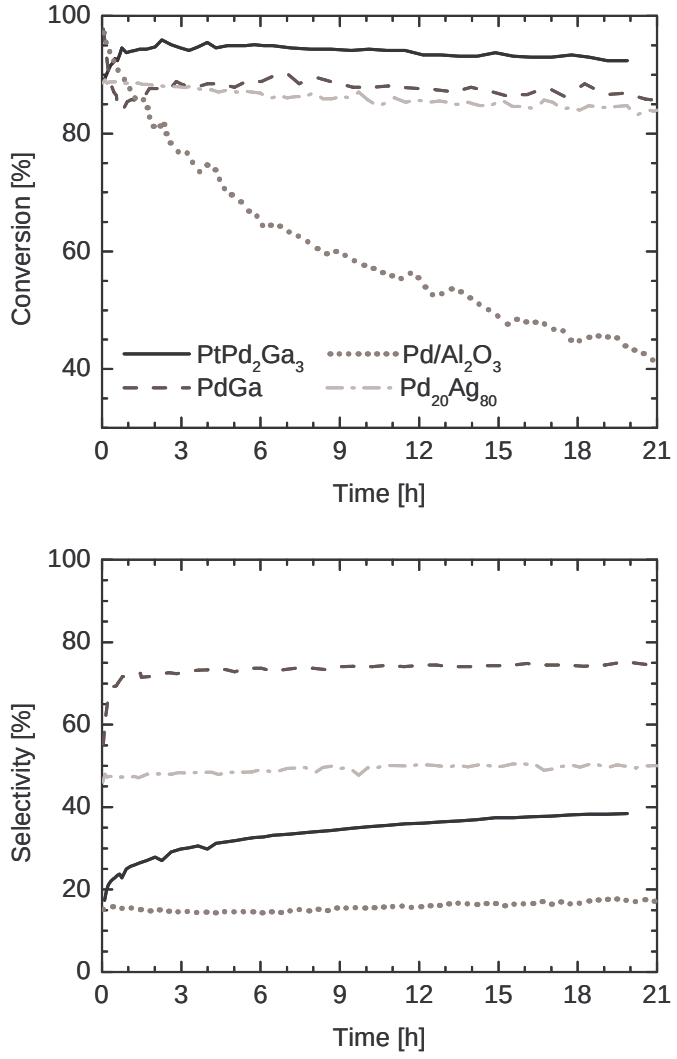

Figure 52: Acetylene conversion and selectivity of $PtPd_2Ga_3$ (40 mg), PdGa (40 mg), Pd/Al_2O_3 (0.15 mg) and $Pd_{20}Ag_{80}$ (200 mg) isothermal at 473 K (condition B).

100 mg of Pd_3Ga_7 and $PtPd_2Ga_7$, resulted in the same acetylene conversion under condition B (Figure 53). Replacement of one third of the Pd by Pt did not lead to an additional an increased catalytic stability. After 20 h time on stream acetylene conversion is 99% respectively 98% for Pd_3Ga_7 and $PtPd_2Ga_7$. Partial replacement of Pd by Pt was accompanied with a loss of selectivity in acetylene hydrogenation in the presence of ethylene. Nevertheless, acetylene hydrogenation over $PtPd_2Ga_7$ resulted in higher selectivity compared to palladium supported on metal oxides.

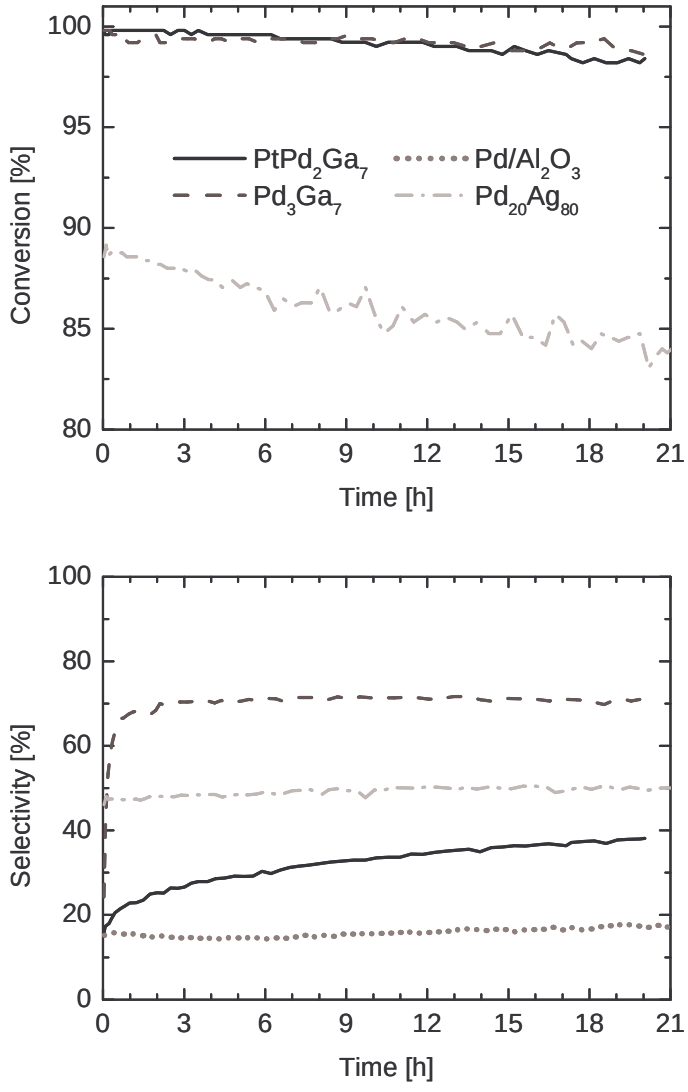

Figure 53: Acetylene conversion and selectivity of $PtPd_2Ga_7$ (100 mg), Pd_3Ga_7 (100 mg), Pd/Al_2O_3 (0.15 mg, only selectivity) and $Pd_{20}Ag_{80}$ (200 mg) isothermal at 473 K (condition B).

Table 10: Acetylene conversion and corresponding selectivity of Pt-Pd-Ga and Pd-Ga intermetallic compounds compared with references Pd/Al_2O_3 and $Pd_{20}Ag_{80}$ after 20 h time on stream at 473 K (condition B).

Sample	sample mass [mg]	acetylene conversion [%]	selectivity [%]	activity [$g/g_{cat}·h$]
PdGa	40	86	75	0.205
$PtPd_2Ga_3$	40	92	38	0.219
Pd_3Ga_7	100	99	71	0.094
$PtPd_2Ga_7$	100	98	38	0.093
Pd/Al_2O_3	0.15	43	17	27.29
$Pd_{20}Ag_{80}$	200	83	49	0.040

8.2 Discussion

8.2.1 Preparation of ternary Pt-Pd-Ga intermetallic compounds

Isomorphic structure and a similar lattice constant of the corresponding Pd-Ga and Pt-Ga intermetallic compounds lead to the conclusion, that preparation of ternary Pt-Pd-Ga intermetallic compounds is possible by a partial replacement of palladium by platinum in the structure of PdGa and Pd_3Ga_7. Homogenous ternary Pt-Pd-Ga intermetallic compounds should show a random distribution of Pt and Pd atoms in their structures. Hence, structural and physical properties of a homogeneous solid solution can be estimated by interpolation from the binary Pd-Ga and Pt-Ga intermetallic compounds. This so-called Vegard's law [76] allows calculation of the theoretical lattice constants of the Pt-Pd-Ga intermetallic compounds and comparison to the experimental values permits to verify Vegard's law. The lattice constant of PdGa [61] from the literature agrees with the experimental lattice constants determined by XRD measurement (Table 8). In contrast, the lattice constant of Pd_3Ga_7 found by Giedigkeit differs significantly from those reported in the literature [57].

Refinement of the XRD pattern of $PtPd_2Ga_3$ resulted in a difference of 0.0038 Å between the experimental and calculated lattice constants and indicated a minor deviation from Vegard's law. The presence of crystals of predominantly Pd or Pt containing intermetallic compounds should result in splitting or broadening of the XRD peaks due to the difference of the lattice constants of the binary PdGa and PtGa. However, the quality of the XRD pattern the ball-milled sample does not allow detecting a peak splitting or broadening (Figure 43). A slightly increased lattice constant of $PtPd_2Ga_3$ compared to the calculated value indicates a distortion and expansion of the structure may be caused by chemical dissimilarity of the Pd-Ga and Pt-Ga bonds. In contrast to $PtPd_2Ga_3$, the deviation of the experimental value from the calculated value of $PtPd_2Ga_7$ was not significant (using lattice constant refined by R. Giedigkeit) and no peak splitting was observed. Hence, a completely random distribution of palladium and platinum can be concluded from the XRD results (Figure 44 + Table 8). From this it follows that the melting point of the ternary $PtPd_2Ga_7$ is between both binary intermetallic compounds. The melting point of the gallium rich Pt-Ga intermetallic compound is 362 K above the melting point of Pd_3Ga_7 and a significantly increased stability can be concluded for the ternary Pt-Pd-Ga compared to Pd_3Ga_7. However, only in an inert

atmosphere an increased structural stability can be deduced from an increased melting point and, hence, does not imply an increased chemical stability against reactive atmosphere under hydrogenation conditions. Chemical stability is important to reduce segregation effects induced by adsorption of reactive gases and is further discussed in the catalysis section.

Nevertheless, with respect to the small differences in lattice constants of the binary Pd-Ga and Pt-Ga intermetallic compounds and the accuracy of the XRD measurements, Vegard's law has to be used very carefully. In contrast to XRD, X-ray absorption measurements are more suitable to distinguish between a ternary Pt-Pd-Ga intermetallic compound and a mixture of binary intermetallic compounds. XAS measurements at the Pd K-edge resulted in absorption exclusively of the Pd containing parts of the sample. A possible PtGa or Pt_3Ga_7 phase could not be detected and lead to an increased background X-ray absorption compared to the binary Pd-Ga intermetallic compounds. Hence, EXAFS refinements of $PtPd_2Ga_3$ and $PtPd_2Ga_7$ using FEFF calculated scattering path from model structure resulting in a proper integration of the Pt shells is indicative of a homogeneous ternary Pt-Pd-Ga intermetallic compound. Deviations from crystallographic interatomic distances and high Debye-Waller factors are indicative of a structural degradation caused by the presence of Pt atoms or the presence of crystals consisting of PdGa and PtGa or Pd_3Ga_7 and Pt_3Ga_7, respectively.

EXAFS refinement of the ball-milled $PtPd_2Ga_3$ resulted in only small (≤ 0.04 Å) deviations from crystallographic interatomic distances and highly ordered structures were deduced from relatively low Debye-Waller factors (Figure 45 + Table 9). The Pt shell at 3.01 Å showed no deviation from the crystallographic distance and the Debye-Waller factor was similar to that of the corresponding Pd shell of $PtPd_2Ga_3$ and the Pt free PdGa. However, the deviation of the interatomic distance of the third Ga shell and its relatively high Debye-Waller factor may indicate a distortion induced by the presence of Pt. Nevertheless, it should take that the same mechanical treatment of PdGa and $PtPd_2Ga_3$ resulted in a reduced average domain size obtained by XRD profile fitting into account. Therefore, increased Debye-Waller factors and deviations are due to an increased structural degradation of $PtPd_2Ga_3$. Hence, from XAS measurements it can be concluded that $PtPd_2Ga_3$ existed as ternary intermetallic compound. In the case of $PtPd_2Ga_7$, a conclusion was not that easy. A deviation from crystallographic structure by 0.04 Å was at the limit of the accuracy of EXAFS, but a low Debye-Waller factor indicated no disordering and no absence of Pt in the structure of the intermetallic compound (Table 9). A possible explanation of the increased Pd-Pt distance is the presence of Pd pairs in the structure of Pd_3Ga_7 with a considerable short interatomic distance of 2.73

Å. The short interatomic distance is reduced compared to cubic closed packed palladium and may lead to Pd-Pd interaction and can result in an increased interatomic Pd-Pt distance or a preferred presence of Pd-Pd pairs and Pt-Pt pairs in the structure of $PtPd_2Ga_7$. Further investigation by XAS at a Pt edge is necessary to obtain reliable results. Moreover, the contradictory results from XRD using Vegard's law and from XAS for both ternary intermetallic compounds did not lead to reliable conclusions about the presence of either a ternary or a mixture of two binary intermetallic compounds.

Higher Debye-Waller factors for $PtPd_2Ga_3$ compared to $PtPd_2Ga_7$ indicated a stronger disordering from ballmilling (Table 9). This is in agreement with the shorted ballmilling procedure used for $PtPd_2Ga_7$ and the different average domain sizes obtained by profile fitting of XRD peaks ($PtPd_2Ga_3$: 14 nm, $PtPd_2Ga_7$: 32 nm) (Figure 48). Partial replacement of Pd by Pt resulted in a significantly decreased average domain size after application of the same mechanical treatment of $PtPd_2Ga_3$ compared to PdGa and indicates an increased brittleness of the ternary intermetallic compound. However, a partial replacement of Pd by Pt of Pd_3Ga_7 did not lead to different average domain sizes and may be caused by the lower Pd or Pt content of Pd_3Ga_7 compared to PdGa.

8.2.2 Thermal stability and hydride formation

In situ XRD experiments during thermal treatment in 50% hydrogen in helium, 100% helium and in 20% oxygen in helium showed high structural stability and indicated that the presence of Pt atoms in the Pd-Ga intermetallic compounds did not lead to destabilization of the structure (Figure 46 + Figure 47). Moreover, a higher final temperature of 773 K and 723 K for $PtPd_2Ga_3$ and $PtPd_2Ga_7$, respectively, resulted in an increased structural stability under the gas atmospheres used compared to PdGa and Pd_3Ga_7. A linear shift of the XRD peaks during thermal treatment in hydrogen indicated a thermal lattice expansion only. No hydride formation was detectable (Figure 46 + Figure 47). In addition, the same XRD peak shift was also observed by experiments in helium and in oxygen and implying the absence of a "kinetic effect" in the selective acetylene hydrogenation [39-45,94].

The influence of Pt in the structure of the Pt-Pd-Ga intermetallic compounds was shown by profile fitting of selected *hkl*-peaks of the XRD pattern. Calculation of the average domain

size by profile fitting of XRD peaks assumes the presence of a homogeneous composition of ternary Pt-Pd-Ga intermetallic compounds ("Vegard's law"). The Pt-Pd-Ga intermetallic compounds exhibited reduced tendencies to sinter compared to the corresponding Pd-Ga intermetallic compounds (Figure 48). Less sintering was more pronounced for $PtPd_2Ga_3$ compared to the gallium-rich $PtPd_2Ga_7$, and may be due to the higher Pt content of the "equiatomic" compound. Pt content of $PtPd_2Ga_7$ (10 at%) was lower compared to $PtPd_2Ga_3$ (17 at%) which resulted in a decreased influence of the presence of Pt. Fewer tendencies of the catalyst to sinter are important because sintering decreases the active-surface area and consequently leads to deactivation.

8.2.3 Acetylene hydrogenation on $PtPd_2Ga_3$ and $PtPd_2Ga_7$

Influence of the presence of Pt on the catalytic performance of Pd intermetallic compounds

Catalytic performance of $PtPd_2Ga_3$ and $PtPd_2Ga_7$ was measured under the same condition as PdGa and Pd_3Ga_7 to show the influence of the partial replacement of Pd by Pt. A slightly reduced activity of $PtPd_2Ga_3$ under acetylene hydrogenation condition A can be deduced from the higher atomic weight of Pt compared to Pd (Figure 50). Platinum is a heavy element and decreases the Pd content of $PtPd_2Ga_3$ compared to PdGa. 50 mg PdGa exhibits a total amount of 30.2 mg Pd whereas 60 mg $PtPd_2Ga_3$ consists of only 20.7 mg Pd and, therefore, the activity per mass of palladium was higher compared to PdGa. A higher surface area can be assumed because of the smaller average domain size obtained by XRD profile analysis of $PtPd_2Ga_3$ compared to PdGa (Figure 48). XRD profile fitting during thermal treatment showed an increasing difference in average domain size between PdGa and $PtPd_2Ga_3$ up to 700 K and may be responsible for the decreased difference in activity between the Pt free and the Pt containing sample at elevated temperature. Acetylene hydrogenation carried out isothermal at 473 K under reaction condition B resulted in a higher activity of $PtPd_2Ga_3$ compared to PdGa indicative of less sintering during long-term application at elevated temperature (Figure 52).

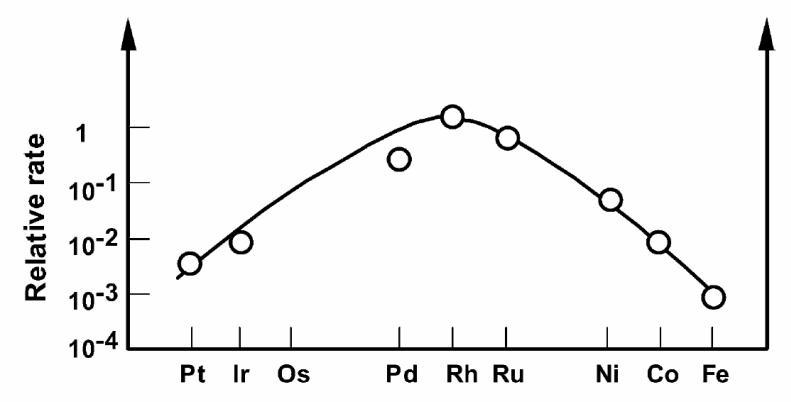

Figure 54: Rate of C_2H_4 hydrogenation on some metal wires relative to Rh [137].

In addition, platinum is known as hydrogenation catalyst and, thus, additional hydrogenation of acetylene can proceed on Pt sites on the catalyst surface. However, platinum exhibits a lower availability to hydrogenate unsaturated hydrocarbons compared to palladium (Figure 54). Further investigations are necessary to obtain an activity per surface area to distinguish between a surface area induced effect and an additional hydrogenation on Pt sites. A synergetic effect of Pd and Pt leading to an increased activity per Pd site due to the presence of Pt is an additional possible explanation. Binary Pt-Pd alloys are more catalytically active in aromatic hydrogenation reactions compared to the monometallic Pd and Pt [138,139], but an increased activity for hydrogenation of unsaturated aliphatic hydrocarbons was not reported.

High selectivity of $PtPd_2Ga_3$ under reaction condition A and lower selectivity under reaction condition B is caused by increased ethylene hydrogenation in the ethylene-rich atmosphere compared to PdGa (Figure 50 + Figure 52). Ethylene hydrogenation under reaction condition A plays a less pronounced role and the oligomerisation to higher hydrocarbons has a pronounced impact on the selectivity. Hence, on the surface of $PtPd_2Ga_3$ less-selective sites compared to PdGa resulted in an enhanced ethane formation. Pt atoms on the catalysts surface may be the less-selective sites according to a by lower selectivity in acetylene hydrogenation of monometallic Pt compared to Pd [6]. Interesting point is the exchange of ethane as major by-product by C4 hydrocarbons at 480 K under condition A (Figure 49). This implies a reduced activity of the less-selective sites at temperature above 480 K. However, the slightly increasing selectivity with time under reaction condition B can be explained by a successive poisoning of the less-selective site at elevated temperature in a

reactive atmosphere and may also be responsible for the change of the by-product relation during temperature programmed experiments under reaction condition A.

Gallium rich $PtPd_2Ga_7$ was less active in acetylene hydrogenation (condition A) compared to Pd_3Ga_7 which can be deduced from the lower Pd content (Figure 51). The Pd content of 100 mg Pd_3Ga_7 is 39.5 mg and therefore considerable higher compared to 28.6 mg of 120 mg $PtPd_2Ga_7$. Ballmilling of the gallium rich Pt sample did not lead to an increased average domain size while during thermal treatment a difference in average domain size appeared (Figure 48). However, the slightly reduced tendencies to sinter could not compensate the lower Pd content of $PtPd_2Ga_7$ compared to Pd_3Ga_7.

The influence of Pt on the selectivity of $PtPd_2Ga_7$ under reaction condition A was more pronounced compared to $PtPd_2Ga_3$. $PtPd_2Ga_7$ led to an increased C4 formation relative to the acetylene conversion. Because of the higher impact of the oligomerisation reaction on the selectivity under condition A, a lower selectivity resulted for $PtPd_2Ga_7$ compared to Pd_3Ga_7 (Figure 51). In contrast to the condition A, $PtPd_2Ga_7$ showed a similar selectivity compared to $PtPd_2Ga_3$ under ethylene-rich condition B (Figure 53). Enhanced ethane formation and similar selectivity of both ternary intermetallic compounds can be attributed to the presence of a similar number of the same less-selective sites on the surface. Nevertheless, both ternary Pt-Pd-Ga intermetallic compounds showed improved catalytic performance like selectivity and long-term stability compared to palladium supported on metal oxides. However, $PtPd_2Ga_3$ and $PtPd_2Ga_7$ were less selective in acetylene hydrogen in the presence of ethylene compared to the corresponding Pd-Ga intermetallic compounds (Table 10).

Increased stability versus reduced selectivity

Maintaining site isolation and preventing sintering of the Pd-Ga intermetallic compounds was the reason for partially replacing Pd by Pt. However, increased structural stability in helium and in hydrogen did not directly lead to an increased catalytic stability. Long-term experiments revealed no increased catalytic stability in acetylene conversion. Furthermore, an increased selectivity under condition B indicates an additional chemical effect induced by the hydrocarbon atmosphere. It can be explained by the presence of less-active sites identified as Pt atoms on the catalyst surface which were poisoned under hydrogenation conditions and, hence, resulted in a slightly increasing selectivity under reaction atmosphere (Figure 52 + Figure 53). Another possibility is the adsorption induced segregation which was

observed on bimetallic catalysts. Segregation of one metal of a bimetallic catalyst often decreases surface energy of a bimetallic catalyst and is influenced by the adsorbed species on the surface [140-144]. Hydrocarbon atmosphere on bimetallic Pd-Pt surfaces leads to segregation of Pd to the surface [140]. A segregation of Pd of the Pt-Pd-Ga intermetallic compounds may be hindered compared to Pt-Pd solid solutions because of the contribution of covalent bonding in the Pd-Ga intermetallic compounds. Nevertheless, under long-time hydrogenation reaction conditions also a reduced tendency to segregate will destabilize the structure in the near-surface region and can lead to Pd clusters on the surface. Slightly increasing selectivity of $PtPd_2Ga_3$ and $PtPd_2Ga_7$ can be attributed to deactivation of less selective-sites like Pd clusters and Pt atoms and the reformation of Pd clusters on the surface by segregation and destabilization of the near-surface region. Surface analysis of the used catalysts with XPS and ISS can be used for further investigation of the surface composition of Pt-Pd-Ga after treatment in hydrocarbon atmosphere.

A potential application of ternary Pt-Pd-Ga intermetallic compounds as industrial catalyst for the selective hydrogenation of acetylene is less likely because the catalytic long-time stability of PdGa and Pd_3Ga_7 under applied reaction condition is sufficient and a partial replacement of Pd by Pt led to no further increase of the catalytic stability but was accompanied by a reduced selectivity due to enhanced ethane formation. Pt-Pd-Ga intermetallic compounds as hydrogenation catalysts may find a potential application under sulphur-rich condition for petrochemical processes. It has been reported, that, bimetallic Pd-Pt catalysts show high catalytic activity for the hydrogenation of aromatic and polyaromatic organic compounds with considerable increased sulphur tolerance compared to the monometallic Pd or Pt catalysts [138,139,145,146].

9 Pd-Sn intermetallic compound

9.1 Results

9.1.1 Preparation and characterization of $PdSn_2$

After preparation $PdSn_2$ was ground by hand and phase purity was confirmed by X-ray diffraction (Figure 55). The experimental pattern showed no deviation from the simulated pattern [65]. The sample was ball-milled to increase surface area. XRD measurements of the ball-milled sample resulted in a pattern with larger FWHM of the peaks which indicates a smaller particles size and a higher surface area. P-Voigt profile fitting resulted in an average crystallite size of 14 nm. No other phase was detected. Nitrogen adsorption measurements resulted in a BET surface area of about 1 m^2/g for $PdSn_2$ after the ballmilling procedure.

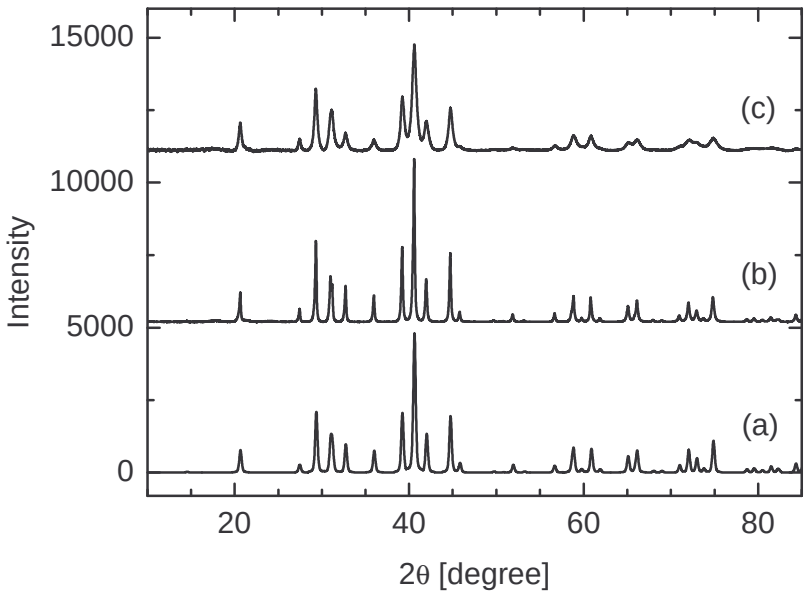

Figure 55: Experimental X-ray diffraction patterns of $PdSn_2$ (b) after grinding in a mortar and (c) after ball milling, together with a simulated pattern of $PdSn_2$ [65].

Ex-situ EXAFS investigation of $PdSn_2$ at the Pd K-edge after the ballmilling procedure resulted in only small deviations of the refined and simulated interatomic distances of the Pd-Sn and Pd-Pd shells. A low Debye-Waller factor resulted for the Pd-Pd shell but relatively high Debye-Waller factors were observed for the Pd-Sn shells of 0.011 $Å^2$. The Pd-Sn shells showed a shift to lower distances and a deviation of the experimental and simulated RDF around 2 Å of the uncorrected distances was observed.

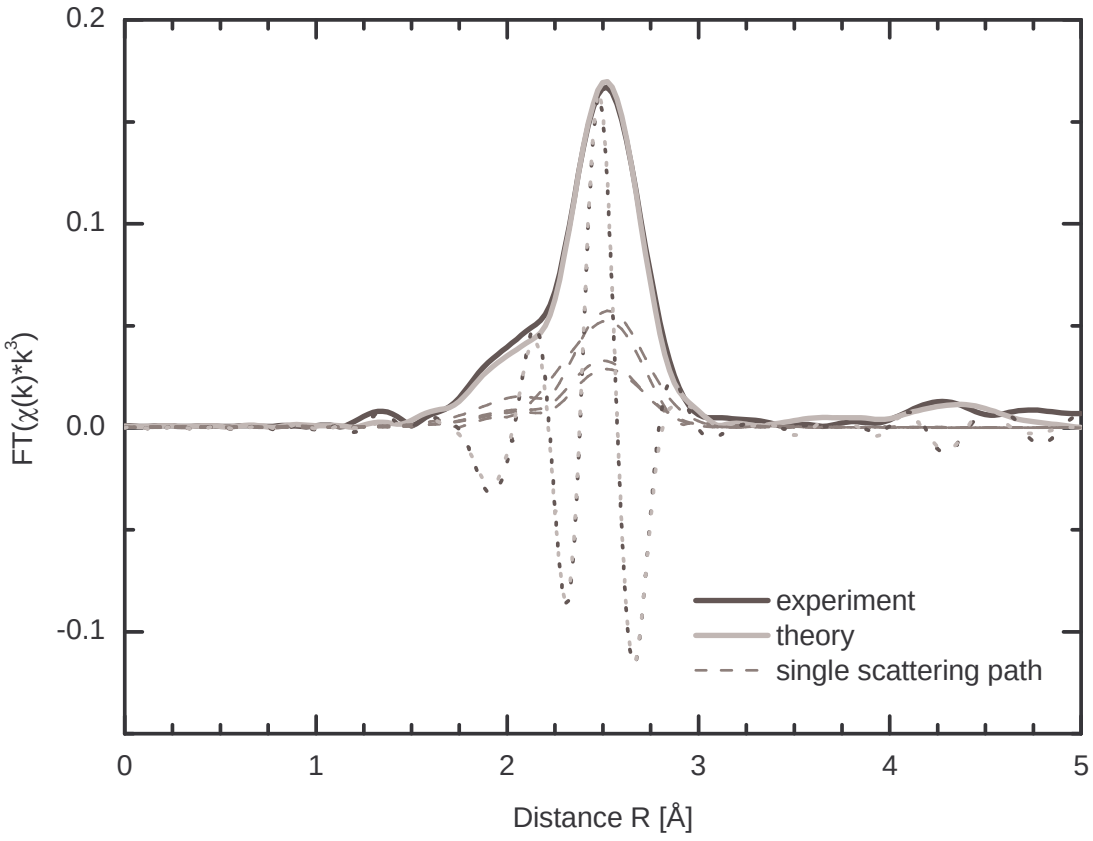

Figure 56: Experimental and theoretical FT(χ(k)*k^3) of $PdSn_2$. Dotted lines refer to imaginary part and dashed lines to the first five single-scattering paths (3x Sn and 1x Pd).

Table 11: Result of EXAFS refinement of $PdSn_2$ at the Pd K-edge measured at 300 K in air. ΔR_c refers to deviation of refined interatomic distances to crystallographic data [65].

$PdSn_2$	CN	R [Å]	ΔR_c [Å]	σ^2 [Å^2]	E_0 [eV]
Sn	2	2.78	-0.03	0.011	-3.70
Sn	2	2.80	-0.03	0.011	-3.70
Sn	4	2.80	-0.03	0.011	-3.70
Pd	1	2.83	-0.01	0.003	-2.03

9.1.2 Structural investigations during thermal treatment

Thermal analysis

TG analysis of $PdSn_2$ in 50% hydrogen showed a mass loss due to water desorption and an additional surface oxide reduction with an onset temperature around 600 K (Figure 57). The corresponding DSC signal showed only small amplitude may be due to exothermic processes like sintering and annealing of the ball-milled sample. The additional mass gain to 100% in helium after water evaporation may be due to surface oxidation by traces of oxygen in the helium flow. The DSC signal showed the similar behavior compared to experiments in hydrogen indicating the presence of sintering and annealing processes independent of the gas atmosphere. In 50% oxygen more surface oxide formation compared to the Pd-Ga intermetallic compounds was observed. An enhanced mass gain to 101.2% at 600 K and less surface oxidation at temperature above 630 K was observed (Figure 57). The DSC signal showed a sharp exothermic maximum at 600 K subsequently followed by a slight exothermic plateau indicating a fast surface oxidation at 600 K. At temperatures above 630 K less oxidation occurred with reduced extension indicating protection of the surface by an oxide formation.

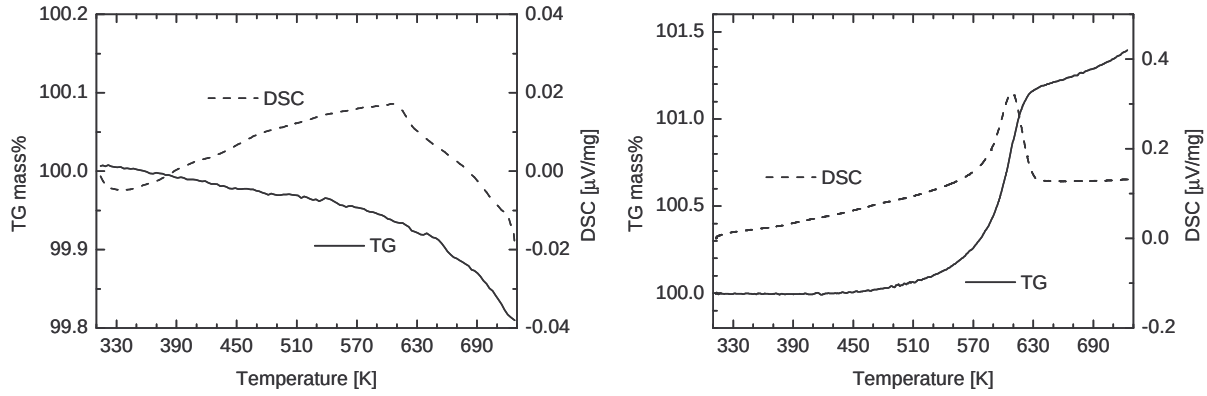

Figure 57: Relative mass (TG) (solid) and DSC signal (dashed) during thermal treatment of $PdSn_2$ in 50% hydrogen in helium (left, 300 K – 723 K at 6 K/min) and in 50% oxygen in He (right, 300 K – 723 K at 6 K/min).

Scanning electron microscopy

$PdSn_2$ was investigated with SEM and EDX after ballmilling and after hydrogen treatment at 573 K to obtain information about particle size, morphology and surface composition (Figure 58). The ball-milled sample showed the expected Pd-Sn ratio, a widely inhomogeneous particle size distribution and rough surfaces.

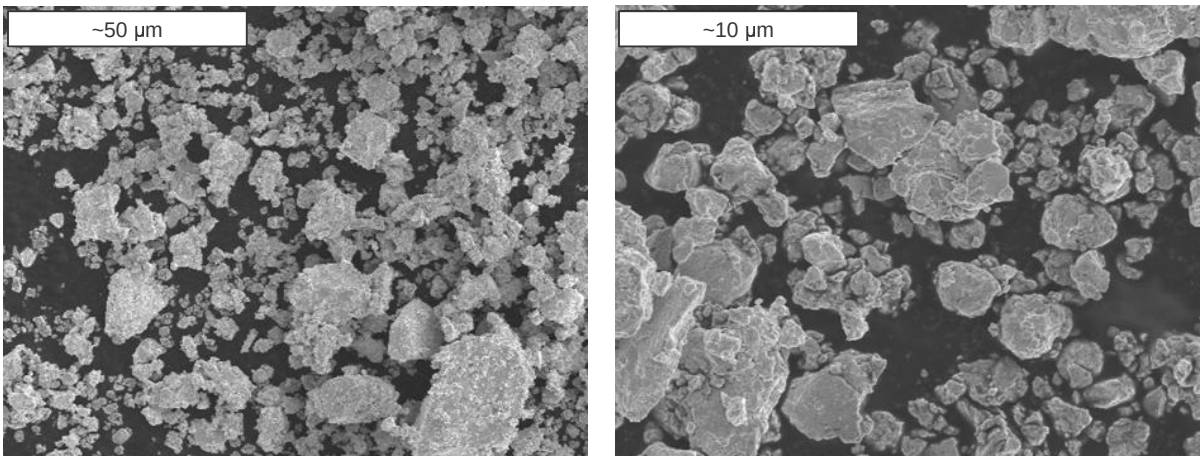

Figure 58: Scanning electron microscopy images of ball-milled $PdSn_2$.

After the hydrogen treatment the particles looked more agglomerated and exhibited smoother surfaces (Figure 59). In contrast to Pd-Ga intermetallic compounds which possess

surface regions with high gallium content, EDX measurements of untreated and treated $PdSn_2$ resulted in the expected Pd-Sn ratio for the whole samples.

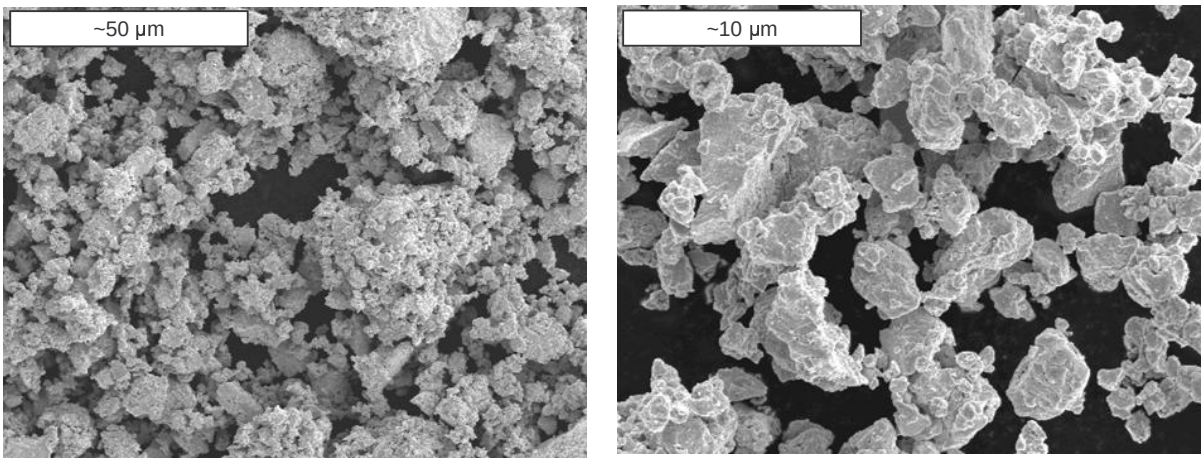

Figure 59: Scanning electron microscopy images of ball-milled $PdSn_2$ after heating in 50% hydrogen in helium to 573 K.

In situ X-ray diffraction

X-ray diffraction measured during thermal treatment of $PdSn_2$ in 50% hydrogen showed no formation of an additional phase from 323 K to 773 K and no incorporation of hydrogen leading to an additional lattice expansion was detectable (Figure 60). Broad peaks in the diffraction pattern were measured at 323 K indicating a small average domain size. During thermal treatment the average domain size increases nearly linear from 17 nm to 80 nm at 723 K (Figure 61).

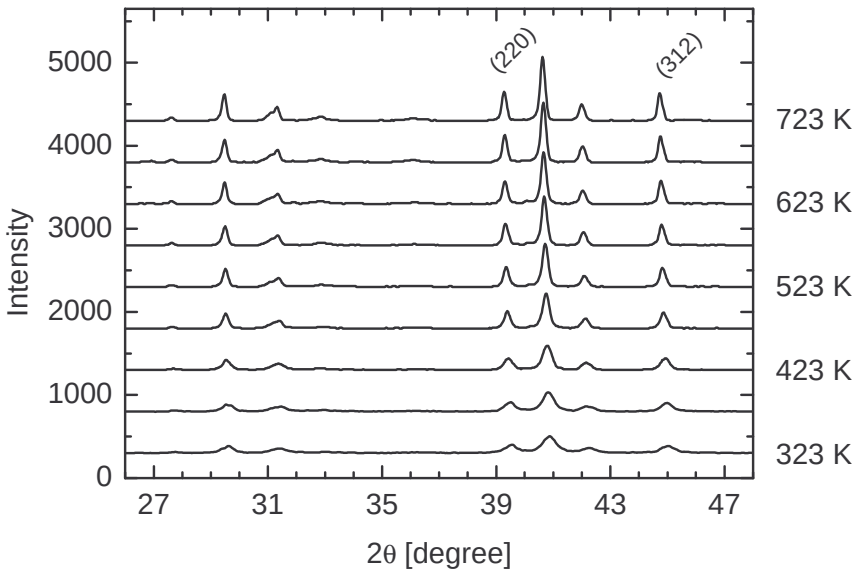

Figure 60: Evolution of X-ray diffraction pattern of $PdSn_2$ during thermal treatment from 323 K to 723 K in 50% H_2 + 50% He.

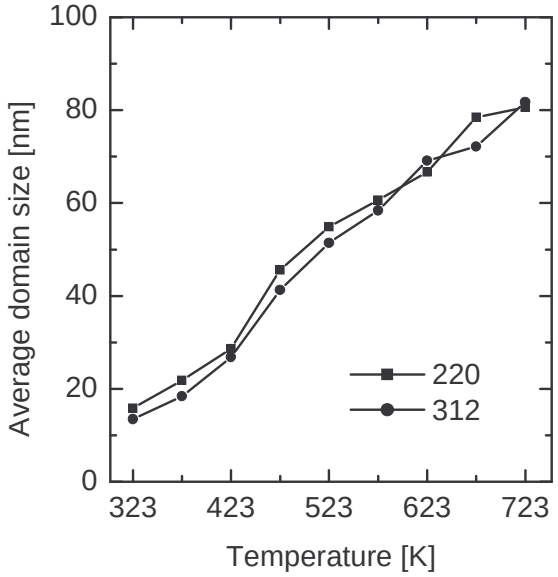

Figure 61: Evolution of average domain size of $PdSn_2$ during thermal treatment in 50% hydrogen in helium obtained by profile analysis of (220) and (312) diffraction lines

A reduced stability of $PdSn_2$ was observed in 20% oxygen in helium. Formation of additional peaks in the diffraction pattern at 523 K indicates the presence of an additional phase. At temperatures above 523 K, more additional peaks were formed and were identified to correspond to PdSn. At 573 K, peaks corresponding to tin dioxide appeared. Nevertheless, at the highest temperature at 723 K $PdSn_2$ was still the major compound. In contrast, thermal treatment in pure helium led to a total decomposition of $PdSn_2$ to PdSn, SnO_2, Pd and unidentified peaks which may belongs to palladium rich or tin rich intermetallic compounds from the Pd-Sn system (Figure 62). The onset of the decomposition was at 573 K with initial formation of small amounts of PdSn.

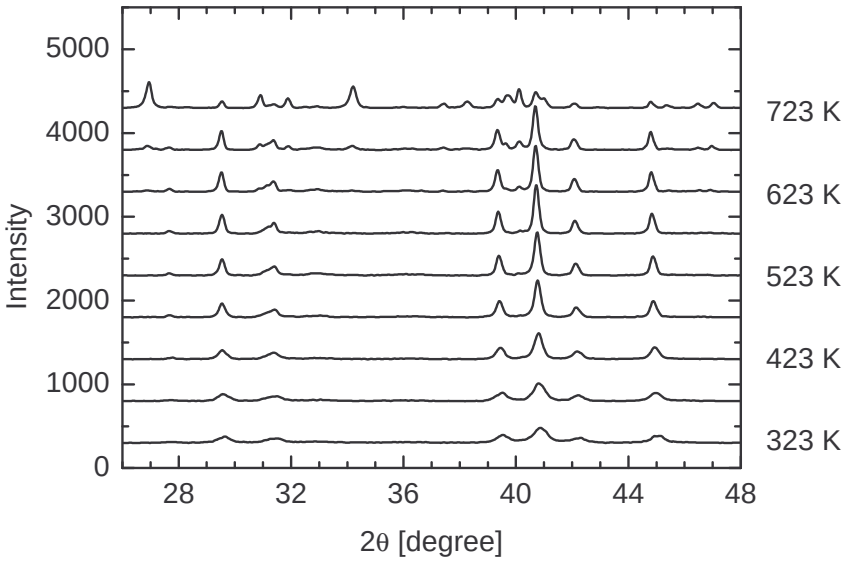

Figure 62: Evolution of X-ray diffraction pattern of $PdSn_2$ during thermal treatment from 323 K to 723 K in 100% helium.

In situ X-ray absorption spectroscopy

In situ XAS measurements at the Pd K-edge of $PdSn_2$ during thermal treatment in different gas atmospheres resulted in a similar behavior compared to the results obtained by in situ XRD measurements. In situ EXAFS in 50% hydrogen resulted in the highest stability of all gas atmospheres applied. Refined interatomic distances of the Pd-Sn shells and the Pd-Pd single shell were similar to the theoretical distances obtained from structural data. The first three Sn shells are very close to each other and were merged to one shell for the refinement. There were no additional significant effects besides the decreasing distances of the Pd-Sn

shells up to 580 K. These decreasing distances were due to the asymmetric peak shape of the Pd-Sn shells at elevated temperature which is not full corrected by the 3rd cumulant and is often observed fore heavy elements like Sn [82]. At temperatures above 500 K the Pd-Pd interatomic distance decreased indicative for initial structural changes. The increasing Debye-Waller factor for the Pd-Sn shells was due to the expected behavior of increasing thermal disordering of $PdSn_2$ during thermal treatment. Additional changes are not observed. In contrast to the Pd-Sn shells, the Pd-Pd shell showed a non-linear behavior with a plateau between 320 and 430 K which is due to annealing and sintering effects and compensates the increasing thermal disordering. A similar behavior was observed for PdGa (Figure 28). At 500 K the Debye-Waller factor increased linearly like expected.

Corresponding experiment in an acetylene feed consisting of 20% hydrogen and additional 10% acetylene resulted in less stability compared to the experiment in 50% hydrogen in helium. Above 460 K the refined interatomic distances started to decrease significantly. The same behavior was observed for experiments in pure helium and in oxygen. The decreasing interatomic distances and high Debye-Waller factors indicate a beginning decomposition of $PdSn_2$. Decreasing Pd-Sn shells can be explained by the a rearrangement to shorter Pd-Sn distances of PdSn and shorter Pd-Pd distances of Pd rich Pd-Sn intermetallic compounds and Pd metal.

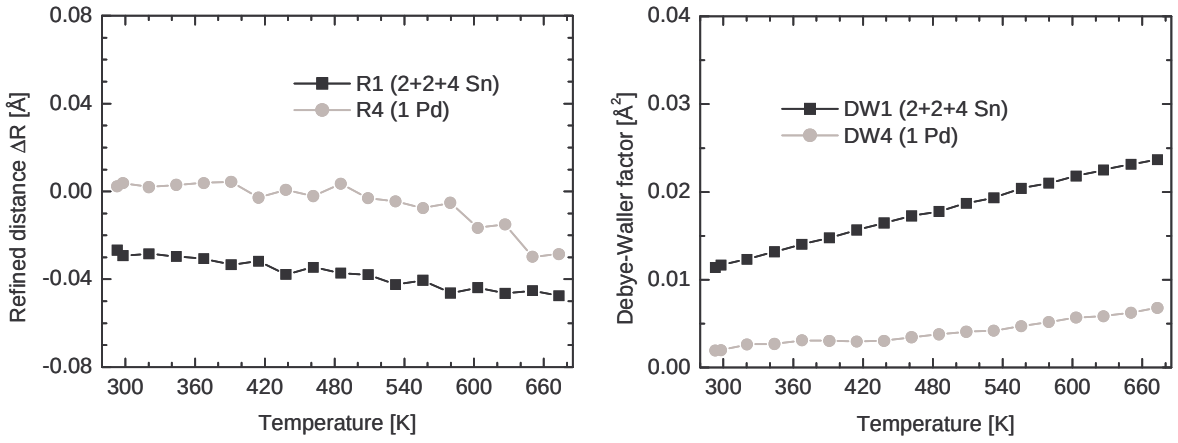

Figure 63: Evolution of selected relative Pd-Sn and Pd-Pd distances and Debye-Waller factors of selected scattering paths of $PdSn_2$ during thermal treatment of $PdSn_2$ in 50% hydrogen in helium from 323 K to 723 K obtained from analysis of the corresponding EXAFS spectra.

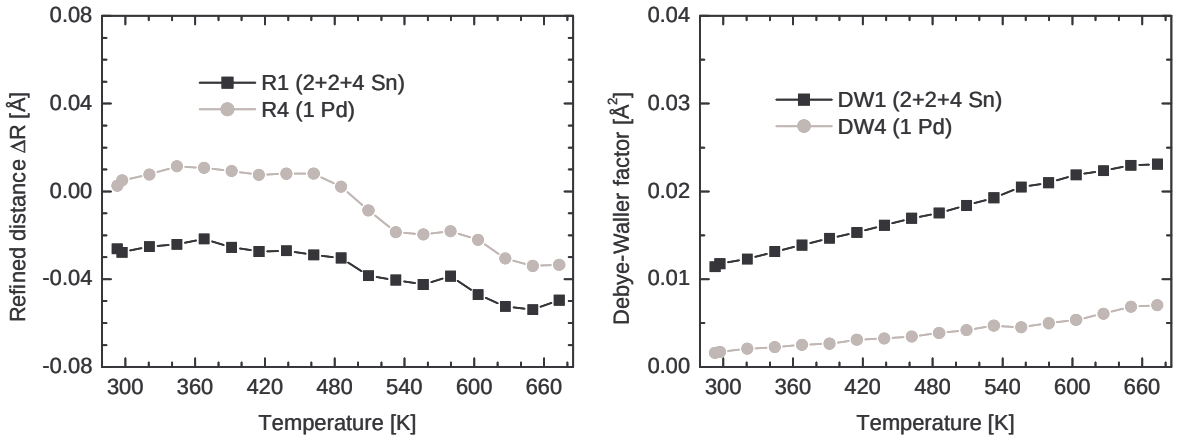

Figure 64: Evolution of selected relative Pd-Sn and Pd-Pd distances and Debye-Waller factors of selected scattering paths of $PdSn_2$ during thermal treatment of $PdSn_2$ in 10% C_2H_2 + 20% H_2 + 70% He from 323 K to 673 K obtained from analysis of the corresponding EXAFS.

9.1.3 Investigation of the catalytic performance of $PdSn_2$

Freshly prepared and ground $PdSn_2$ showed catalytic activity in acetylene hydrogenation. However, ballmilling applied to increase surface area as well as surface oxidation caused by storing under air led to a complete deactivation of $PdSn_2$. A hydrogen treatment of $PdSn_2$ (20% H_2 in He) at 473 K, 573 K, and 673 K did not lead to an increased activity and, therefore, not to a successful removal of the inactive overlayer. A chemical etching procedure was necessary to obtain catalytic activity of $PdSn_2$.

Chemical etching of $PdSn_2$

Chemical etching of $PdSn_2$ by application of a hydrochloric acid solution (pH = 3) led to a full deactivation. More successful was chemical etching with a sodium hydroxide solution. A strong basic solution (pH = 13.5) led to an acetylene conversion of 38% for 100 mg $PdSn_2$ at 510 K under reaction condition A (Figure 65). The corresponding selectivity was 80% with respect to ethylene formation. Small amounts of C4 hydrocarbons were formed by oligomerisation as by-product and only traces of ethane were detected.

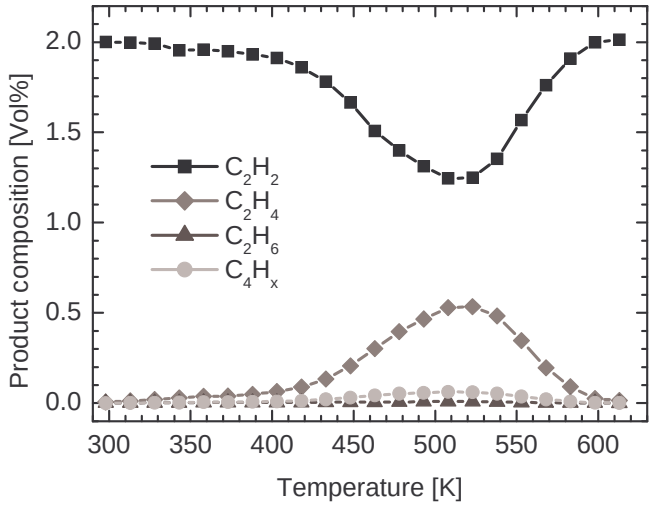

Figure 65: Product composition measured during hydrogenation of acetylene on $PdSn_2$ (100 mg) under condition A.

Further investigation with aqueous solution of sodium hydroxide, ammonia, hydrogen peroxide, and EDTA and etching solutions of combination of the compounds mentioned led to wide variation in activity, selectivity, and long-time stability. The optimal composition with respect to the best catalytic performance of $PdSn_2$ was obtained from an aqueous etching solution containing high amounts of NaOH and EDTA. Figure 66 shows acetylene conversion of 85 mg chemically etched $PdSn_2$ compared with the acetylene conversion of Pd/Al_2O_3 and $Pd_{20}Ag_{80}$. $PdSn_2$ showed 99% acetylene conversion but deactivated with time on stream (activity from 0.111 g_{C2H2}/g_{cat}·h to 0.061 g_{C2H2}/g_{cat}·h after 20h). The plateau in the first three hours in the conversion plot for $PdSn_2$ was due to the high amount of catalyst inside the reactor to obtain a higher acetylene conversion over the entire experiment compared to reference Pd/Al_2O_3. After 20 h in acetylene-ethylene feed, the acetylene conversion decreased to 55%. $PdSn_2$ and Pd/Al_2O_3 showed a similar deactivation behaviour and both compounds did not reach a steady state after 20 hours. High selectivity was obtained for $PdSn_2$. During the entire experiment the selectivity of $PdSn_2$ was higher compared to the supported palladium and the palladium-silver alloy. Selectivity below 60% in the first three hours was due to full acetylene conversion and increased with decreasing activity to 74% after 20 h time on stream. After nine hours, acetylene conversion of both samples, $PdSn_2$ and $Pd_{20}Ag_{80}$, was at 86% and the corresponding selectivity for $PdSn_2$ was 69% and significantly lower for $Pd_{20}Ag_{80}$ (49%). Acetylene hydrogenation on $PdSn_2$ resulted

in less stability compared to $Pd_{20}Ag_{80}$ but in a much higher selectivity compared to Pd/Al_2O_3 and $Pd_{20}Ag_{80}$.

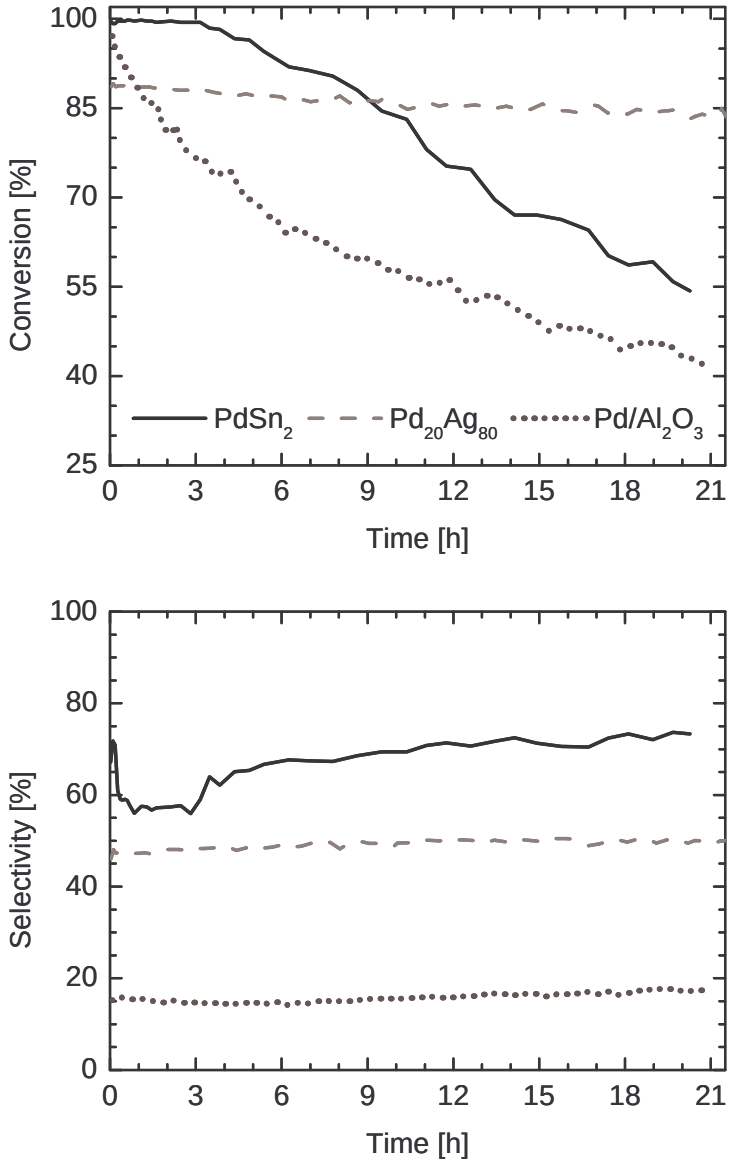

Figure 66: Acetylene conversion and corresponding selectivity of chemically etched (NaOH + EDTA) $PdSn_2$ (85 mg), Pd/Al_2O_3 (0.15 mg) and $Pd_{20}Ag_{80}$ (200 mg) isothermal at 473 K (condition B).

9.2 Discussion

9.2.1 Preparation and structural characteristics

$PdSn_2$ as a representative of Pd-Sn intermetallic compounds was prepared by a standard method [62]. Similar to Pd_3Ga_7, $PdSn_2$ needed an additional annealing to obtain a phase pure compound. XRD patterns of as-prepared $PdSn_2$ and after ballmilling consisted only of diffraction peaks attributed to the structure of $PdSn_2$ (Figure 55). The surface area of $PdSn_2$ was increased by mechanical treatment indicated by peak broadening of the XRD pattern and the average domain size of $PdSn_2$ was lower compared to those of the Pd-Ga intermetallic compound.

Every Pd atom is surrounded by eight Sn atoms and the shortest Pd-Pd interatomic distances is 2.84 Å to a single Pd atom (Figure 7, Table 3) [65]. Consequently, the structure of $PdSn_2$ contains only isolated Pd atoms and allows verifying the validity of the active-site isolation concept additional to the Pd-Ga intermetallic compounds. Similar to Pd-Ga intermetallic compounds increasing the surface area by ballmilling is limited because extended mechanical treatment leads to structural degradation. Furthermore, the presence of sintering effects requires other preparation methods to obtain a high surface area catalyst.

Deviation of the interatomic Pd-Sn distances obtained by refinement of X-ray absorption data and crystallographic data as well as high Debye-Waller factors may be caused by the correlation of interatomic distances and DW factors, which is necessary to reduce the number of free running parameters (Figure 56, Table 11). Nevertheless, the deviation from crystallographic data of the first Pd-Sn shell can also be due to structural degradation induced by ballmilling or an insufficient structural model from the literature [65].

9.2.2 Thermal stability and hydride formation

Palladium-tin intermetallic compound $PdSn_2$ was investigated as an alternative material providing isolated Pd atoms in a tin matrix. Further application as catalytically active intermetallic compounds requires high structural stability to maintain the site isolation under

reaction condition. Therefore, the structural stability of $PdSn_2$ had to be investigated during thermal treatment in inert and reactive gas atmosphere in the same way as the Pd-Ga intermetallic compounds. TG and DSC experiment in hydrogen resulted in similar high thermal stability compared to PdGa and Pd_3Ga_7. SEM measurements of $PdSn_2$ confirm the overall stability of the morphology during treatment in hydrogen with only small increases in the coalescence of the particles and a smoother surface detectable (Figure 58 + Figure 59). EDX measurements resulted in the expected Pd-Sn ratio before and after the hydrogen treatment. A reduced stability was observed under oxidation condition (Figure 57). In addition, in situ XRD and in situ EXAFS measurements resulted in high thermal stability only for experiments in hydrogen (Figure 60 + Figure 63). Nevertheless, further application as hydrogenation catalyst requires only stability under reactive gas atmosphere containing hydrogen and unsaturated hydrocarbons. However, in situ EXAFS investigation of $PdSn_2$ in reactive feed (10% acetylene and 20% hydrogen in helium) led to decomposition comparable to experiments in oxygen and helium above 480 K (Figure 64). Decomposition may be caused by the reduced hydrogen content and additional hydrogen consumption by the hydrogenation reaction. Furthermore, the lower structural stability detected by in situ XRD and in situ XAS in helium and in oxygen (Figure 62) indicated a reduced stability and a long-term application as catalyst may result in decomposition also under hydrogenation conditions. Moreover, in situ XRD and in situ XAS showed the stability of the bulk material while initial structural changes in the near-surface region may not have been detected.

Decomposition of $PdSn_2$ during thermal treatment is less pronounced in 20% oxygen compared to in 100% helium (Figure 62). Hence, it can be concluded that the formation of an oxide layer observed from TG/DSC (Figure 57) led to protection and stabilization of the bulk material. The absence of a full decomposition during XAS measurements in helium and oxygen observed by in situ XRD measurements can be explained by a higher heating rate for the in situ XAS experiments of 6 K/min. In contrast to the XAS measurements, in situ XRD was performed with an average heating rate of 0.3 K/min. The lower heating rate led to longer time of thermal treatment and to an enhanced decomposition already at lower temperature compared to in situ XAS. In general, the comparison of the thermal and structural investigations with TG/DSC, in situ XRD, and in situ EXAFS of $PdSn_2$ with Pd-Ga intermetallic compounds leads to the conclusion, that $PdSn_2$ exhibited less structural stability compared to Pd-Ga intermetallic compounds. The reduced stability at elevated temperature may be caused by a reduced thermodynamical stability of $PdSn_2$ compared to

PdGa and Pd_3Ga_7. Nature and strength of the bonding forces in the structure of $PdSn_2$ have not been fully analyzed and reported in literature. Nylén and co-workers reported only weak Pd-Sn bonding interaction obtained by theoretical calculations and Sn Mössbauer spectroscopy [147].

In situ XRD and in situ XAS were used to investigate $PdSn_2$ in hydrogen atmosphere to elucidate the presence or absence of hydrogen incorporation (Figure 60 + Figure 63). Hydride formation could not be detected by an additional lattice expansion during in situ XRD experiments in hydrogen compared to corresponding experiment in pure helium. Furthermore, no increasing interatomic distances were obtained by refinement of the XAS data from temperature programmed heating of $PdSn_2$ in 50% hydrogen. Hence, a "kinetic effect" in the selective hydrogenation of acetylene can be excluded [39-45,94].

9.2.3 Catalytic performance of $PdSn_2$

In contrast to Pd-Ga intermetallic compounds, as-prepared $PdSn_2$ showed negligible activity. Thus, chemical etching to remove the inactive overlayer was necessary to investigate the catalytic performance of $PdSn_2$. Thermal treatment in hydrogen led to a mass loss detected by TG (Figure 57) indicative of the presence of an oxide layer on the surface of $PdSn_2$. Very low activity for hydrogenation reactions excluded the presence of palladium oxides and, therefore, presence of tin oxides on the surface is concluded. Nevertheless, the mass loss detected by TG (Figure 57) during thermal treatment in hydrogen did not result in the formation of a catalytically active $PdSn_2$ intermetallic surface because of the absence of activity after hydrogen treatment. Treatment under strong reducing condition may reduce tin oxides to tin but did not lead to a re-dissolution of tin in the bulk and a re-formation of a Pd-Sn intermetallic surface. Tin oxides are difficult to dissolve by chemical etching because of their low solubility in many solvents. Only strong complexing agents like EDTA and high pH were sufficient to remove tin oxide from the catalyst surface.

$PdSn_2$ showed activity and selectivity in acetylene hydrogenation similar to Pd-Ga intermetallic compounds (Figure 65 + Figure 66). However, the activity of $PdSn_2$ was lower compared to PdGa and Pd_3Ga_7 and can be explained by the reduced Pd content due to the higher atomic weight of Sn compared to Ga, and by a still insufficient chemical etching.

A remarkably high selectivity in acetylene hydrogenation indicates the presence of only isolated Pd atoms on the surface of $PdSn_2$. Catalytic results of acetylene hydrogenation on $PdSn_2$, PdGa, and Pd_3Ga_7 showed that isolated Pd atoms exhibited a high selectivity in the hydrogenation of acetylene to ethylene independent of the choice of the surrounding atoms. High selectivity in acetylene hydrogenation seems to validate the concept of active-site isolation by selecting well-defined intermetallic compounds.

Isothermal long-time experiments resulted in high selectivity in acetylene hydrogenation. However, a deactivation of $PdSn_2$ with time on stream was observed (Figure 66). The deactivation trends of $PdSn_2$ and Pd/Al_2O_3 looked similar but may be for different reasons. Deactivation of Pd metal under hydrogenation reaction conditions was mainly due to carbon deposit blocking the active Pd sites supposed in the literature [6-8]. It was shown for Pd-Ga intermetallic compounds that active-site isolation prevents deactivation. Carbon deposits by hydrocarbon decomposition can be excluded as the major source of deactivation for site-isolated $PdSn_2$. Deactivation of $PdSn_2$ can be explained by a structural degradation observed by investigation of $PdSn_2$ during thermal treatment in different atmospheres. Less stability compared to Pd-Ga intermetallic compounds may cause the decomposition to Pd rich intermetallic compounds detected and to tin and tin oxide. TG and DSC as well as in situ XRD and in situ XAS experiments suggested a segregation of tin to the surface induced by thermal treatment and may be accelerated by the presence of traces of oxygen in feed. Thermal treatment in helium, oxygen, in reactive feed resulted in palladium enrichment in the bulk and led to the formation of Pd and Pd rich intermetallic compounds whereas tin segregated to the surface and led to deactivation. Long-term experiments could show a complete deactivation to very low acetylene conversion or a steady state can be reached. Nevertheless, $PdSn_2$ was a suitable Pd intermetallic compound to investigate the concept of active-site isolation for improved catalytic performance in hydrogenation reactions. $PdSn_2$ is not a suitable catalyst for a possible industrial application because of the deactivation of $PdSn_2$ under reaction condition. Longer operation time can be obtained by decreasing operating temperature while deactivation by decomposition may be reduced but not stopped.

PdSn is an alternative Pd-Sn intermetallic compound as potential hydrogenation catalyst [148] because of the isolation of Pd atoms in the structure and a higher melting point indicative of a higher thermal stability [58].

10 Summary

In the work described here, intermetallic compounds of palladium with gallium, platinum, and tin (PdGa, Pd_3Ga_7, $PtPd_2Ga_3$, $PtPd_2Ga_7$, $PdSn_2$) are introduced as selective catalysts for the hydrogenation of acetylene. These materials possess well-defined crystallographic structures with Pd centers coordinated to Ga atoms or Sn atoms. Hence, Pd atoms are effectively isolated from each other. Phase-pure Pd intermetallic compounds with gallium, platinum, and tin can be readily prepared by thermal treatment of a stoichiometric mixture of the corresponding metals. The initially low surface area of the as-prepared materials can be increased by careful mechanical treatment without decomposition or a loss of structural order.

Pd-Ga intermetallic compounds

Application of isolated Pd intermetallic compounds under hydrogenation reaction conditions requires a sufficient structural stability also at elevated temperatures under inert and reactive atmospheres. Detailed investigations of PdGa and Pd_3Ga_7 by TG/DSC, in situ XRD and in situ EXAFS during thermal treatment under various inert or reactive gas atmospheres showed a high thermal stability. The long-range and short-range order structures of the materials remained intact up to temperatures of about 600 K with no phase transitions or decomposition detectable. Hence, the structural motive of isolated Pd atoms will be present under hydrogenation reaction conditions and makes Pd intermetallic compounds as ideal model system to investigate the concept of active-site isolation. In addition to high thermal stability, no incorporation of hydrogen in the intermetallic compounds under reducing conditions was detected by in situ structural investigations. The absence of hydride formation will exert an additional positive influence on the selectivity of intermetallic compounds in the hydrogenation of acetylene. Both intermetallic compounds studied exhibit sufficient thermal stability, isolation of Pd centers under reaction conditions, and no incorporation of hydrogen in the bulk. Therefore, besides being interesting model systems, palladium gallium intermetallic compounds may also be promising candidates for technical application as highly selective hydrogenation catalysts.

Catalytic investigation of intermetallic compounds of palladium with gallium resulted in superior catalytic properties in acetylene hydrogenation. PdGa and Pd_3Ga_7 exhibited a higher selectivity in acetylene hydrogenation than commercial supported Pd/Al_2O_3 and a $Pd_{20}Ag_{80}$ alloy. Both PdGa and Pd_3Ga_7 showed no deactivation during long-time acetylene hydrogenation compared to Pd/Al_2O_3. High selectivity and less deactivation can be assigned to the isolation of active Pd sites in the crystallographic structure of Pd-Ga intermetallic compounds. Isolated active sites results in a "geometric effect", which leads to weakly π-bonded acetylene molecules on top of isolated Pd atoms, an "electronic effect" resulting in a modification of adsorption and desorption properties, and a "kinetic effect" due to the decreased availability of hydrogen because of the absence of Pd hydrides.

Chemical treatment with ammonia solution to remove the gallium oxide layer originally present on the intermetallic compounds yielded a ten-fold increase in activity while maintaining the high selectivity and stability of PdGa and Pd_3Ga_7 in the hydrogenation of acetylene.

Pt-Pd-Ga intermetallic compounds

Partial replacement of palladium by platinum of binary Pd-Ga intermetallic compounds resulted in an increased structural stability of $PtPd_2Ga_3$ and $PtPd_2Ga_7$ under inert, reductive, and oxidizing condition. Further analysis of the XRD data yielded to reduced tendencies of sintering and decreased average domain sizes during thermal treatment. Ternary Pt-Pd-Ga intermetallic compounds showed no improved catalytic long-term stability expected from the increased structural stability determined in helium, hydrogen, and oxygen. Acetylene hydrogenation on $PtPd_2Ga_3$ and $PtPd_2Ga_7$ resulted in decreased selectivity in the presence of ethylene. Partial replacement of palladium by platinum led to less-selective sites on the catalyst surface and may consist of Pt atoms and Pd clusters formed by chemical induced segregation.

$PdSn_2$

In contrast to Pd-Ga and Pt-Pd-Ga intermetallic compounds, $PdSn_2$ showed stable isolation of Pd atoms only at reduced temperature. Acetylene hydrogenation on Pd-Sn intermetallic compound $PdSn_2$ showed similar superior selectivity as the Pd-Ga intermetallic compounds. $PdSn_2$ seems to validate the concept of active-site isolation and showed the independence of

the choice of the second metal as surrounding component of the isolated Pd atoms. However, the observed reduced structural stability by in situ XRD and in situ EXAFS investigation corresponds to a reduced catalytic long-term stability under hydrogenation conditions.

Conclusion

“Active site isolation” was the guiding concept of our knowledge-based search for improved acetylene hydrogenation catalysts. The successful application of structurally well-defined palladium containing intermetallic compounds confirms the value of a rational approach to catalyst development. The concept of using intermetallic compounds with strong covalent bonding interactions rather than intermetallic alloys with non-localized chemical interactions is a suitable way to arrive at long-term stable metallic catalyst with pre-selected electronic and local structural properties. The partly covalent bonding between Pd and Ga accounts for the low reactivity to hydrogen and for the remarkable stability against continuous chemical induced segregation. The specificity of the Pd-X interaction will limit the variation of the element X to those metals exhibiting a suitable electron affinity to allow for a metalloid bonding without destroying the metallic character of the Pd required for its hydrogenation reactivity. Pd intermetallic compounds with gallium fulfill these requirements. In contrast, Pd intermetallic compounds with tin and platinum showed a reduced stability under continuous segregation and, therefore, they are not suitable for catalytic long-term application.

Palladium intermetallic compounds with gallium are materials whose preparation, composition, and structure would hardly have been obtained by any high-throughput search in the periodic table of the elements. New preparation techniques and improved chemical treatment procedures will be pursued in the future and will yield high surface area materials with improved activity while maintaining high selectivity and stability in acetylene hydrogenation.

11 Appendix

11.1 References

[1] A.J. Peacock, Handbook Polyethylene: Structures, properties, and applications, Marcel Decker, New York, 2000.

[2] P.M. Morse: Ethylene market stretched thin. *Chemical & Engineering News* 77 (1999) 20-22.

[3] L.L. Bohm: The ethylene polymerization with Ziegler catalysts: Fifty years after the discovery. *Angewandte Chemie - International Edition* 42 (2003) 5010-5030.

[4] E. Groppo, C. Lamberti, S. Bordiga, G. Spoto, A. Zecchina: The structure of active centers and the ethylene polymerization mechanism on the Cr/SiO_2 catalyst: A frontier for the characterization methods. *Chemical Reviews* 105 (2005) 115-183.

[5] A.N. R. Bos, K.R. Westerterp: Mechanism and kinetics of the selective hydrogenation of ethyne and ethene. *Chemical Engineering and Processing* 32 (1993) 1-7.

[6] H. Arnold, F. Döbert, J. Gaube, in: G. Ertl, H. Knoerzinger, J. Weitkamp (Eds.), Handbook of Heterogeneous Catalysis, VCH, Weinheim, 1997, p. pp. 2165-2186.

[7] A. Molnar, A. Sarkany, M. Varga: Hydrogenation of carbon-carbon multiple bonds: chemo-, regio- and stereo-selectivity. *Journal of Molecular Catalysis A - Chemical* 173 (2001) 185-221.

[8] P. Albers, J. Pietsch, S.F. Parker: Poisoning and deactivation of palladium catalysts. *Journal of Molecular Catalysis A - Chemical* 173 (2001) 275-286.

[9] C. Godinez, A.L. Cabanes, G. Villora: Experimental-study of the front-end selective hydrogenation of steam-cracking C2-C3 mixture. *Chemical Engineering and Processing* 34 (1995) 459-468.

[10] N.S. Schbib, M.A. Garcia, C.E. Gigola, A.F. Errazu: Kinetics of front-end acetylene hydrogenation in ethylene production. *Industrial & Engineering Chemistry Research* 35 (1996) 1496-1505.

[11] C. Godinez, A.L. Cabanes, G. Villora: Experimental study of the tail end selective hydrogenation of steam cracking C2-C3 mixture. *Canadian Journal of Chemical Engineering* 74 (1996) 84-93.

[12] C. Godinez, A.L. Cabanes, G. Villora: Experimental study of the selective hydrogenation of steam cracking C2 cut. Front end and tail end variants. *Chemical Engineering Communications* 164 (1998) 225-247.

[13] T. Hill, M. Haake, E. Schwab, A. Frenzel, and H. Worz: Selective catalytic gas-phase hydrogenation of alkynes, dienes, alkenynes and/or polyene impurities in an alkene stream. *US-Patent 20030069458* (2003) to BASF AG (Ludwigshafen), Germany.

[14] F.A. Lewis, The Palladium Hydrogen System, Academic Press, London, 1967.

[15] Periodic table of elements. 3. Edt., Weinheim, Wilye-VCH, 2002

[16] V. Pallassana, M. Neurock: Electronic factors governing ethylene hydrogenation and dehydrogenation activity of pseudomorphic Pd-ML/Re(0001), Pd-ML/Ru(0001), Pd(111), and Pd-ML/Au(111) surfaces. *Journal of Catalysis* 191 (2000) 301-317.

[17] F. Mittendorfer, C. Thomazeau, P. Raybaud, H. Toulhoat: Adsorption of unsaturated hydrocarbons on Pd(111) and Pt(111): A DFT study. *Journal of Physical Chemistry B* 107 (2003) 12287-12295.

[18] E.G. Derouane: 2nd European Symposium on Catalysis by Metals - Multimetallic Catalysts in Synthesis and Transformation of Hydrocarbons - Concluding Remarks, Critical Issues and Perspectives. *Journal of Molecular Catalysis* 25 (1984) 51-58.

[19] B. Coq, F. Figueras: Bimetallic palladium catalysts: influence of the co-metal on the catalyst performance. *Journal of Molecular Catalysis A-Chemical* 173 (2001) 117-134.

[20] L. Guczi: Bimetallic nano-particles: featuring structure and reactivity. *Catalysis Today* 101 (2005) 53-64.

[21] J.W. Medlin, M.D. Allendorf: Theoretical study of the adsorption of acetylene on the (111) surfaces of Pd, Pt, Ni, and Rh. *Journal of Physical Chemistry B* 107 (2003) 217-223.

[22] C.J. Baddeley, A.F. Lee, R.M. Lambert, T. Giessel, O. Schaff, V. Fernandez, K.M. Schindler, A. Theobald, C.J. Hirschmugl, R. Lindsay, A.M. Bradshaw, D.P. Woodruff: Photoelectron diffraction study of a catalytically active overlayer: C_2H_2 on Pd(111). *Surface Science* 400 (1998) 166-175.

[23] A. Valcarcel, A. Clotet, J.M. Ricart, F. Illas: Comparative theoretical study of the structure and bonding of propyne on the Pt(111) and Pd(111) surfaces. *Chemical Physics* 309 (2005) 33-39.

[24] A.M. Doyle, S.K. Shaikhutdinov, H.J. Freund: Alkene chemistry on the palladium surface: nanoparticles vs single crystals. *Journal of Catalysis* 223 (2004) 444-453.

[25] S.K. Shaikhutdinov, M. Frank, M. Baumer, S.D. Jackson, R. J. Oldman, J.C. Hemminger, H.J. Freund: Effect of carbon deposits on reactivity of supported Pd model catalysts. *Catalysis Letters* 80 (2002) 115-122.

[26] W.J. Kim, J.H. Kang, I.Y. Ahn, S.H. Moon: Deactivation behavior of a TiO_2-added Pd catalyst in acetylene hydrogenation. *Journal of Catalysis* 226 (2004) 226-229.

[27] W.J. Kim, E.W. Shin, J.H. Kang, S.H. Moon: Performance of Si-modified Pd catalyst in acetylene hydrogenation: catalyst deactivation behavior. *Applied Catalysis A-General* 251 (2003) 305-313.

[28] N. Sheppard, C. De la Cruz, Vibrational spectra of hydrocarbons adsorbed on metals - Part II. Adsorbed acyclic alkynes and alkanes, cyclic hydrocarbons including aromatics, and surface hydrocarbon groups derived from the decomposition of alkyl halides, etc, Academic Press Inc, San Diego, 1998, pp. 181-313.

[29] E.W. Shin, C.H. Choi, K.S. Chang, Y.H. Na, S.H. Moon: Properties of Si-modified Pd catalyst for selective hydrogenation of acetylene. *Catalysis Today* 44 (1998) 137-143.

[30] S. Leviness, V. Nair, A.H. Weiss, Z. Schay, L. Guczi: Acetylene hydrogenation selectivity control on $PdCu/Al_2O_3$ catalysts. *Journal of Molecular Catalysis* 25 (1984) 131-140.

[31] V. Ponec: Catalysis by alloys in hydrocarbon reactions. *Advances in Catalysis* 32 (1983) 149-214.

[32] W. Palczewska, A. Jablonski, Z. Kaszkur, G. Zuba, J. Wernisch: Study on lead additives in modified palladium catalysts. *Journal of Molecular Catalysis* 25 (1984) 307-316.

[33] Y.M. Jin, A.K. Datye, E. Rightor, R. Gulotty, W. Waterman, M. Smith, M. Holbrook, J. Maj, J. Blackson: The influence of catalyst restructuring on the selective hydrogenation of acetylene to ethylene. *Journal of Catalysis* 203 (2001) 292-306.

[34] J.H. Kang, E.W. Shin, W J. Kim, J.D. Park, S.H. Moon: Selective hydrogenation of acetylene on TiO_2-added Pd catalysts. *Journal of Catalysis* 208 (2002) 310-320.

[35] V. Ponec: Alloy catalysts: the concepts. *Applied Catalysis A-General* 222 (2001) 31-45.

[36] E.W. Shin, J.H. Kang, W.J. Kim, J.D. Park, S.H. Moon: Performance of Si-modified Pd catalyst in acetylene hydrogenation: the origin of the ethylene selectivity improvement. *Applied Catalysis A-General* 223 (2002) 161-172.

[37] D.C. Huang, K.H. Chang, W.F. Pong, P.K. Tseng, K.J. Hung, W.F. Huang: Effect of Ag-promotion on Pd catalysts by XANES. *Catalysis Letters* 53 (1998) 155-159.

[38] P.A. Sheth, M. Neurock, C.M. Smith: First-principles analysis of the effects of alloying Pd with Ag for the catalytic hydrogenation of acetylene-ethylene mixtures. *Journal of Physical Chemistry B* 109 (2005) 12449-12466.

[39] W. Palczewska, in: Z. Paal, P.G. Denon (Eds.) Hydrogen Effects in Catalysis: fundamentals and practical applications, Marcel Decker, New York, 1988, pp. 372-397.

[40] G.C. Bond, P.B. Wells: Hydrogenation of acetylene: 2. Reaction of acetylene with hydrogen catalyzed by alumina-supported palladium. *Journal of Catalysis* 5 (1966) 65-&.

[41] A.M. Doyle, S.K. Shaikhutdinov, S.D. Jackson, H.J. Freund: Hydrogenation on metal surfaces: Why are nanoparticles more active than single crystals? *Angewandte Chemie - International Edition* 42 (2003) 5240-5243.

[42] A.S. McLeod, R. Blackwell: Monte Carlo simulation of the selective hydrogenation of acetylene. *Chemical Engineering Science* 59 (2004) 4715-4721.

[43] C.M. Pradier, M. Mazina, Y. Berthier, J. Oudar: Hydrogenation of acetylene on palladium. *Journal of Molecular Catalysis* 89 (1994) 211-220.

[44] Q.W. Zhang, J. Li, X.X. Liu, Q.M. Zhu: Synergetic effect of Pd and Ag dispersed on Al_2O_3 in the selective hydrogenation of acetylene. *Applied Catalysis A-General* 197 (2000) 221-228.

[45] T. Komatsu, S. Hyodo, T. Yashima: Catalytic properties of Pt-Ge intermetallic compounds in the hydrogenation of 1,3-butadiene. *Journal of Physical Chemistry B* 101 (1997) 5565-5572.

[46] L. Guczi: Mechanism of reactions on multimetallic catalysts. *Journal of Molecular Catalysis* 25 (1984) 13-29.

[47] W.M.H. Sachtler: Selectivity and rate of activity decline of bimetallic catalysts. *Journal of Molecular Catalysis* 25 (1984) 1-12.

[48] O.M. Lovvik: Surface segregation in palladium based alloys from density-functional calculations. *Surface Science* 583 (2005) 100-106.

[49] J.L. Rousset, J.C. Bertolini, P. Miegge: Theory of segregation using the equivalent-medium approximation and bond-strength modifications at surfaces: Application to fee Pd-X alloys. *Physical Review B* 53 (1996) 4947-4957.

[50] J.H. Kang, E.W. Shin, W.J. Kim, J.D. Park, S.H. Moon: Selective hydrogenation of acetylene on Pd/SiO_2 catalysts promoted with Ti, Nb and Ce oxides. *Catalysis Today* 63 (2000) 183-188.

[51] H. Lindlar: Ein neuer Katalysator für Selektive Hydrierungen. *Helvetica Chimica Acta* 35 (1952) 446-456.

[52] R. Schlögl, K. Noack, H. Zbinden, A. Reller: The microstructure of selective palladium hydrogenation catalysts supported on calcium-carbonate and modified by lead (Lindlar catalysts), studies by photoelectron-spectroscopy, thermogravimetry, X-ray-diffraction, and electron-microscopy. *Helvetica Chimica Acta* 70 (1987) 627-679.

[53] H. Zea, K. Lester, A.K. Datye, E. Rightor, R. Gulotty, W. Waterman, M. Smith: The influence of Pd-Ag catalyst for ethylene hydrogenation restructuring on the activation energy in ethylene-acetylene mixtures. *Applied Catalysis A-General* 282 (2005) 237-245.

[54] K.R. Westerterp, A.N.R. Bos, R.J. Wijngaarden, W.C. Kusters, A. Martens: Selective hydrogenation of acetylene in an ethylene stream in an adiabatic packed bed reactor. *Inzynieria Chemiczna I Procesowa* 21 (2000) 7-28.

[55] J. Gislason, W.S. Xia, H. Sellers: Selective hydrogenation of acetylene in an ethylene rich flow: Results of kinetic simulations. *Journal of Physical Chemistry A* 106 (2002) 767-774.

[56] K. Schubert, H.L. Lukas, H.G. Meissner, S. Bhan: Zum Aufbau der Systeme Kobalt-Gallium, Palladium-Gallium, Palladium-Zinn und verwandter Legierungen. *Zeitschrift fur Metallkunde* 50 (1959) 534-540.

[57] K. Khalaff, K. Schubert: Kristallstruktur von Pd_5Ga_2. *Journal of Less Common Metals* 37 (1974) 129-140.

[58] T.B. Massalski, Binary Alloy Phase Diagrams, Second Edition. ASM international, Ohio, USA, 1990.

[59] Y. Grin, K. Peters, H.G. v. Schnering: Refinement of the crystal structure of palladium pentagallide, $PdGa_5$. *Zeitschrift fur Kristallographie-New Crystal Structures* 212 (1997) 6.

[60] E. Hellner, F. Laves: Kristallchemie des In und Ga in Legierungen mit einigen Übergangsmetallen. *Zeitschrift für Naturforschung* 2a (1947) 177-183.

[61] M.K. Bhargava, A.A. Gadalla, K. Schubert: Koexistente Phasen vom FeSi-Typ in den Mischungen Ni-Pd-Ga und Ni-Pt-Ga. *Journal of Less Common Metals* 42 (1975) 76.

[62] R. Giedigkeit, Intermetallische Verbindungen im System Yb-Pd-Ga, Technische Universität Darmstadt, 1998.

[63] G. Phragmen: *Jernkontor.Ann.* 107 (1923) 121.

[64] H. Pfisterer, K. Schubert: Zur Kristallchemie der B-Metall-reichsten Phasen in Legierungen von Übergangsmetallen der Eisen- und Platintiraden mit Elementen der vierten Nebengruppe. *Zeitschrift für Metallkunde* 41 (1950) 433-441.

[65] B. Künnen, D. Niepmann, W. Jeitschko: Structure refinements and some properties of the transition metal stannides Os_3Sn_7, Ir_5Sn_7, $Ni_{0.402(4)}Pd_{0.598}Sn_4$, alpha-$PdSn_2$ and $PtSn_4$. *Journal of Alloys and Compounds* 309 (2000) 1-9.

[66] W. Kraus, and G. Nolze, PowderCell for Windows 2.4. Federal Institute for Material Research and Testing, Germany, 2000

[67] W.W. Wendlandt: Thermal Analysis. *Analytical Chemistry* 56 (1984) 250R-261R.

[68] D. Dollimore: Thermal Analysis. *Analytical Chemistry* 60 (1988) 274R-278R.

[69] C.M. Earnest: Modern Thermogravimetry. *Analytical Chemistry* 56 (1984) 1471A-1486A.

[70] H.W. Williard, L.L. Merritt, J.A. Dean, F.A. Settle, Instrumental Methods of Analysis, Wadsworth, Belmont, 1988.

[71] D.A. Skoog, J.J. Leary, Instrumentelle Analytik, Springer-Verlag, Berlin, 1996.

[72] J.W. Niemantsverdriet, Spectroscopy in Catalysis : An Introduction, VCH, Weinheim, 1993.

[73] T.J. Jenkins, R. P. Soares, Introduction to X-ray Powder Diffractometry, John-Wiley & Sons, New York, 1996.

[74] R. Allmann, Röntgen-Pulverdiffractometrie, Verlag Sven von Loga, Köln, 1994.

[75] R.A. Young: The Rietveld Method, Oxford Univ. Press, Oxford, UK, 1993.

[76] P. Behrens in: B. Cornils, W.A. Herrmann, R. Schlögl, C.H. Wong (Eds.), Catalysis from A to Z - A Concise Encyclopedia, Wiley-VCH, Weinheim, 2000.

[77] T. Ressler, R.E. Jentoft, J. Wienold, M.M. Günter, O. Timpe: In situ XAS and XRD studies on the formation of Mo suboxides during reduction of MoO_3. *Journal of Physical Chemistry B* 104 (2000) 6360-6370.

[78] K. Khalaff, K. Schubert: Kristallstruktur von Pd_5Ga_2. *Journal of Less Common Metals* 37 (1974) 129-140.

[79] T. Ressler: WinXAS: a program for X-ray absorption spectroscopy data analysis under MS-Windows. *Journal of Synchrotron Radiation* 5 (1998) 118-122.

[80] I. Chorkendorff, J.W. Niemantsverdriet: Concepts of Modern Catalysis and Kinetics, Wiley-VCH, Weinheim, 2004.

[81] T. Boon-Keng: EXAFS - basic principles and data analysis, Springer-Verlag, Berlin, 1986.

[82] G. Dalba, P. Fornasini: EXAFS Debye-Waller factor and thermal vibrations of crystals. *Journal of Synchrotron Radiation* 4 (1997) 243-255.

[83] A.L. Ankudinov, B. Ravel, J.J. Rehr, S.D. Conradson: Real-space multiple-scattering calculation and interpretation of X-ray-absorption near-edge structure. *Physical Review B* 58 (1998) 7565-7576.

[84] J. J. Rehr, R. C. Albers: Scattering: matrix formulation of curved-wave multiple-scattering theory - application to X-ray-absorption fine-structure. *Physical Review B* 41 (1990) 8139-8149.

[85] T. Ressler, S.L. Brock, J. Wong, S.L. Suib: Multiple-scattering EXAFS analysis of tetraalkylammonium manganese oxide colloids. *Journal of Physical Chemistry B* 103 (1999) 6407-6420.

[86] J. Chastain: Handbook of X-ray Photoelectron Spectroscopy, Perkin-Elmer, Eden Prairie, Minn., 1992.

[87] D.P. Woodruff, T.A. Delchar, Modern Techniques of Surface Science, Univ. Pr., Cambridge, 1994.

[88] D. Briggs, M.P. Seah: Practical Surface Analysis, 1: Auger and X-ray Photoelectron Spectroscopy, Wiley, Chichester, 1988, p. 635-638.

[89] G. Schön: Auger and direct electron spectra in X-ray photoelectron studies of zinc, zinc oxide, gallium and gallium oxide. *Journal of Electron Spectroscopy and Related Phenomena* 2 (1973) 75-86.

[90] K.I. Hadjiivanov, G.N. Vayssilov, Characterization of oxide surfaces and zeolites by carbon monoxide as an IR probe molecule, Academic Press Inc, San Diego, 2002, p. 307-511.

[91] J. J. F. Scholten, A. Vanmontfoort: The determination of the free-metal surface area of palladium catalysts. *Journal of Catalysis* 1 (1962) 85-92.

[92] C. Sudhakar, M.A. Vannice: Preparation and characterization of palladium dispersed on rare-earth oxide supports. *Applied Catalysis* 14 (1985) 47-63.

[93] M.B. Palmer, M. A. Vannice: The effect of preparation variables on the dispersion of supported platinum catalysts. *Journal of Chemical Technology and Biotechnology* 30 (1980) 205-216.

[94] M. Morkel, G. Rupprechter, H.J. Freund: Finite size effects on supported Pd nanoparticles: Interaction of hydrogen with CO and C_2H_4. *Surface Science* 588 (2005) L209-L219.

[95] F. Delbecq: General trends in the electronic properties of alloys of transition metals: a semi-empirical study of CO adsorption. *Surface Science* 389 (1997) L1131-L1139.

[96] R. Nyholm, N. Martensson: Core level binding-energies for the elements Zr-Te (z = 40-52). *Journal of Physics C-Solid State Physics* 13 (1980) L279-L284.

[97] H. Dropsch, M. Baerns: CO adsorption on supported Pd catalysts studied by adsorption microcalorimetry and temperature programmed desorption. *Applied Catalysis A-General* 158 (1997) 163-183.

[98] H. Unterhalt, G. Rupprechter, H.J. Freund: Vibrational sum frequency spectroscopy on Pd(111) and supported Pd nanoparticles: CO adsorption from ultrahigh vacuum to atmospheric pressure. *Journal of Physical Chemistry B* 106 (2002) 356-367.

[99] D. Teschner, A. Pestryakov, E. Kleimenov, M. Havecker, H. Bluhm, H. Sauer, A. Knop-Gericke, R. Schlögl: High-pressure X-ray photoelectron spectroscopy of palladium model hydrogenation catalysts. Part 1: Effect of gas ambient and temperature. *Journal of Catalysis* 230 (2005) 186-194.

[100] D. Teschner, A. Pestryakov, E. Kleimenov, M. Havecker, H. Bluhm, H. Sauer, A. Knop-Gericke, R. Schlögl: High-pressure X-ray photoelectron spectroscopy of palladium model hydrogenation catalysts. Part 2: Hydrogenation of trans-2-pentene on palladium. *Journal of Catalysis* 230 (2005) 195-203.

[101] A. Rose, S. Maniguet, R.J. Mathew, C. Slater, J. Yao, A.E. Russell: Hydride phase formation in carbon supported palladium nanoparticle electrodes investigated using in situ EXAFS and XRD. *Physical Chemistry Chemical Physics* 5 (2003) 3220-3225.

[102] N.K. Nag: A study on the formation of palladium hydride in a carbon-supported palladium catalyst. *Journal of Physical Chemistry B* 105 (2001) 5945-5949.

[103] A.E. Russell, S. Maniguet, R.J. Mathew, J. Yao, M.A. Roberts, D. Thompsett: In situ X-ray absorption spectroscopy and X-ray diffraction of fuel cell electrocatalysts. *Journal of Power Sources* 96 (2001) 226-232.

[104] C. Bryce, D. Berk: Kinetics of GaAs dissolution in H_2O_2-NH_4OH-H_2O solutions. *Industrial & Engineering Chemistry Research* 35 (1996) 4464-4470.

[105] M.V. Lebedev, D. Ensling, R. Hunger, T. Mayer, W. Jaegermann: Synchrotron photoemission spectroscopy study of ammonium hydroxide etching to prepare well-ordered GaAs(100) surfaces. *Applied Surface Science* 229 (2004) 226-232.

[106] C.C. Chang, P.H. Citrin, B. Schwartz: Chemical preparation of GaAs surfaces and their characterization by auger-electron and X-ray photoemission spectroscopies. *Journal of Vacuum Science & Technology* 14 (1977) 943-952.

[107] J. Margitfalvi, L. Guczi, A. H. Weiss: Reaction routes for hydrogenation of acetylene-ethylene mixtures using a double labeling method. *Reaction Kinetics and Catalysis Letters* 15 (1980) 475-479.

[108] J. Margitfalvi, L. Guczi: Reactions of acetylene during hydrogenation on pd black catalyst. *Journal of Catalysis* 72 (1981) 185-198.

[109] J.M. Moses, A.H. Weiss, K. Matusek, L. Guczi: The effect of catalyst treatment on the selective hydrogenation of acetylene over palladium alumina. *Journal of Catalysis* 86 (1984) 417-426.

[110] T.P. Beebe, J.T. Yates: An insitu infrared spectroscopic investigation of the role of ethylidyne in the ethylene hydrogenation reaction on Pd/Al_2O_3. *Journal of the American Chemical Society* 108 (1986) 663-671.

[111] P. A. Sheth, M. Neurock, C. M. Smith: A first-principles analysis of acetylene hydrogenation over Pd(111). *Journal of Physical Chemistry B* 107 (2003) 2009-2017.

[112] J.A. Gates, L.L. Kesmodel: Thermal evolution of acetylene and ethylene on Pd(111). *Surface Science* 124 (1983) 68-86.

[113] L.L. Kesmodel: Acetylene decomposition on Pd(100) and Pd(111) - EELS evidence for CCH formation. *Journal of Vacuum Science & Technology A-Vacuum Surfaces and Films* 2 (1984) 1083-1084.

[114] L.L. Kesmodel, G.D. Waddill, J A. Gates: Vibrational spectroscopy of acetylene decomposition on palladium(111) and palladium(100) surfaces. *Surface Science* 138 (1984) 464-474.

[115] W.T. Tysoe, G.L. Nyberg, R.M. Lambert: Photoelectron-spectroscopy and heterogeneous catalysis - benzene and ethylene from acetylene on palladium (111). *Surface Science* 135 (1983) 128-146.

[116] W.T. Tysoe, G.L. Nyberg, R.M. Lambert: Selective hydrogenation of acetylene over palladium in ultra high-vacuum. *Journal of Physical Chemistry* 90 (1986) 3188-3192.

[117] R.M. Ormerod, R.M. Lambert, D.W. Bennett, W.T. Tysoe: Temperature-programmed desorption of coadsorbed hydrogen and acetylene on Pd(111). *Surface Science* 330 (1995) 1-10.

[118] E.A. Arafa, G. Webb: A C-14 radiotracer study of the hydrogenation of ethyne over Europt-1. *Catalysis Today* 17 (1993) 411-418.

[119] L. Vattuone, Y.Y. Yeo, R. Kose, D.A. King: Energetics and kinetics of the interaction of acetylene and ethylene with Pd(100) and Ni(100). *Surface Science* 447 (2000) 1-14.

[120] S. Verdier, B. Didillon, S. Morin, D. Uzio: Pd-Sn/Al_2O_3 catalysts from colloidal oxide synthesis - II. Surface characterization and catalytic properties for buta-1,3-diene selective hydrogenation. *Journal of Catalysis* 218 (2003) 288-295.

[121] T.V. Choudhary, C. Sivadinarayana, A.K. Datye, D. Kumar, D. W. Goodman: Acetylene hydrogenation on Au-based catalysts. *Catalysis Letters* 86 (2003) 1-8.

[122] P. Miegge, J. L. Rousset, B. Tardy, J. Massardier, J. C. Bertolini: Pd_1Ni_{99} AND Pd_5Ni_{95} - Pd surface segregation and reactivity for the hydrogenation of 1,3-butadiene. *Journal of Catalysis* 149 (1994) 404-413.

[123] J.A. Rodriguez: Electronic properties of bimetallic surfaces. *Heterogeneous Chemistry Reviews* 3 (1996) 17-32.

[124] J.A. Rodriguez, D.W. Goodman: Surface science studies of the electronic and chemical-properties of bimetallic systems. *Journal of Physical Chemistry* 95 (1991) 4196-4206.

[125] V. Johanek, I. Stara, V. Matolin: Role of Pd-Al bimetallic interaction in CO adsorption and catalytic properties of bulk PdAl alloy: XPS, ISS, TDS, and SIMS study. *Surface Science* 507 (2002) 92-98.

[126] I. Matolinova, V. Johanek, T. Skala, K. Veltruska, V. Matolin: XPS, TDS and static SIMS studies of binary Pd/Al system properties: correlation between Pd-Al bimetallic interaction and CO adsorption. *Applied Surface Science* 245 (2005) 87-93.

[127] P K. Babu, H.S. Kim, J.H. Chung, E. Oldfield, A. Wieckowski: Bonding and motional aspects of CO adsorbed on the surface of Pt nanoparticles decorated with Pd. *Journal of Physical Chemistry B* 108 (2004) 20228-20232.

[128] R. Giedigkeit and Y. Grin, *unpublished work*

[129] A. Sarkany, A. Horvath, A. Beck: Hydrogenation of acetylene over low loaded Pd and Pd-Au/SiO_2 catalysts. *Applied Catalysis A-General* 229 (2002) 117-125.

[130] V.M. Allenger, D.D. Mclean, M. Ternan: Simultaneous polymerization and oligomerization of acetylene on alumina and fluoridated alumina catalysts. *Journal of Catalysis* 131 (1991) 305-318.

[131] G.C. Bond: The role of carbon deposits in metal-catalysed reactions of hydrocarbons. *Applied Catalysis A-General* 149 (1997) 3-25.

[132] E.M. Stuve, R.J. Madix: Bonding and dehydrogenation of ethylene on palladium metal - vibrational-spectra and temperature-programmed reaction studies on Pd(100). *Journal of Physical Chemistry* 89 (1985) 105-112.

[133] H.J. Freund, M. Baumer, J. Libuda, T. Risse, G. Rupprechter, S. Shaikhutdinov: Preparation and characterization of model catalysts: from ultrahigh vacuum to in situ conditions at the atomic dimension. *Journal of Catalysis* 216 (2003) 223-235.

[134] M.M. Johnson, D.W. Walker, and G.P. Nowack: Selective hydrogenation catalyst. *US-Patent 4404124* (1983) to Phillips Petroleum Company (Bartlesville, OK) USA.

[135] B.E. Nieuwenhuys: Chemistry on single crystal surfaces of Pt and Pd alloys. *Surface Review and Letters* 3 (1996) 1869-1888.

[136] K. Schubert, M. Balk, S. Bhan, H. Breimer, P. Esslinger, E. Stolz: Einige strukturelle Ergebnisse an metallischen Phasen-IV. *Naturwissenschaften* 46 (1959) 647-648.

[137] J. Cosyns, in: B. Imelik, G.A. Martin, A.J. Renouprez (Eds), Catalyse par les Métaux, Paris, 1984, p. 971.

[138] H. Yasuda, Y. Yoshimura: Hydrogenation of tetralin over zeolite-supported Pd-Pt catalysts in the presence of dibenzothiophene. *Catalysis Letters* 46 (1997) 43-48.

[139] R.M. Navarro, B. Pawelec, J.M. Trejo, R. Mariscal, J.L.G. Fierro: Hydrogenation of aromatics on sulfur-resistant PtPd bimetallic catalysts. *Journal of Catalysis* 189 (2000) 184-194.

[140] B. Hammer, J.K. Norskov: Theoretical surface science and catalysis - Calculations and concepts. *Advances in Catalysis, Vol 45* 45 (2000) 71-129.

[141] C.J. Baddeley, L.H. Bloxham, S.C. Laroze, R. Raval, T.C.Q. Noakes, P. Bailey: Quantitative analysis of adsorbate induced segregation at bimetallic surfaces: Improving the accuracy of medium energy ion scattering results. *Journal of Physical Chemistry B* 105 (2001) 2766-2772.

[142] C.J. Baddeley, L.H. Bloxham, S.C. Laroze, R. Raval, T.C.Q. Noakes, P. Bailey: The dynamic catalytic surface: probing bimetallic active sites with medium energy ion scattering. *Surface Science* 435 (1999) 827-832.

[143] E. Christoffersen, P. Stoltze, J.K. Norskov: Monte Carlo simulations of adsorption-induced segregation. *Surface Science* 505 (2002) 200-214.

[144] C. Massen, T.V. Mortimer-Jones, R.L. Johnston: Geometries and segregation properties of platinum-palladium nanoalloy clusters. *Journal of the Chemical Society-Dalton Transactions* (2002) 4375-4388.

[145] S.M. Kovach, and G.D. Wilson: Selective hydrogenation of aromatics and olefins in hydrocarbon fractions. *US-Patent 3943 053* (1974) to Ashland Oil, Inc. (Ashland, KY), USA

[146] M. Jacquin, D.J. Jones, J. Roziere, A. J. Lopez, E. Rodriguez-Castellon, J.M.T. Menayo, M. Lenarda, L. Storaro, A. Vaccari, S. Albertazzi: Cetane improvement of diesel with a novel bimetallic catalyst. *Journal of Catalysis* 228 (2004) 447-459.

[147] J. Nylen, G.F.J. Garcia, B.D. Mosel, R. Pottgen, U. Haussermann: Structural relationships, phase stability and bonding of compounds $PdSn_n$ (n=2, 3, 4). *Solid State Sciences* 6 (2004) 147-155.

[148] H. Nowotny, K. Schubert, U. Dettinger: Zur Kenntnis des Aufbaus und der Kristalchemie einiger Edelmetallsysteme (Pd-Pb, Pd-Sn, Ir-Sn, Rh-Sn, Pt-Pb). *Zeitschrift für Metallkunde* (1946) 137-145.

11.2 List of figures

Figure 1: Di-σ bonded acetylene molecule to two neighbouring Pd atoms (left) and a weakly π-bonded acetylene molecule to an isolated Pd atom (right). Only the π-bonded acetylene is hydrogenated in high selectivity to ethylene. 8

Figure 2: Example of isolated Pd atoms by alternated arrangement of Pd and an additional metal like in Pd intermetallic compounds (left) and an example for random distribution of Pd and a second metal like in a solid solution which does not exclude neighbouring Pd atoms (right). 8

Figure 3: Phase diagram gallium-palladium [58]. 8

Figure 4 : 2x2x2 unit cell of PdGa and coordination sphere of Pd atoms in PdGa. 8

Figure 5: Unit cell of Pd_3Ga_7 and coordination sphere of Pd atoms in Pd_3Ga_7 8

Figure 6: Unit cell of $PdSn_2$. 8

Figure 7: Coordination sphere of Pd atoms in $PdSn_2$ 8

Figure 8: Bragg reflection of X-rays at lattice planes. 8

Figure 9: Geometric arrangement of the Bragg-Brentano diffractometer. X-ray beam (F) passes divergence slit (DS) and parallel plate collimator (soller slit SS1) and was scattered at the lattice of a crystalline sample (S) and passes through SS2 and a receiving slit (RS) to a monochromator (C) through a slit (AS) to the detector [73]. 8

Figure 10: Absorption of X-rays as a function of photon energy by a free atom and an atom in a lattice. The fine structure is due to interference of outgoing and backscattered electron waves [80]. 8

Figure 11: Transmission cell for in situ XAS measurements. The cell consists of a gas inlet from a gas mixing unit, a gas outlet to mass spectrometry to monitor product gas composition, and a thermocouple for temperature control of the cell. Inside of the cell a pressed powder pellet is mounted with a screw perpendicular to the X-ray beam. 8

Figure 12: An example for EXAFS data processing: (a) background corrected and normalised absorption spectrum of PdGa, (b) after transformation into k-space, (c) extracted χ(k) and (d) after Fourier transformation of the χ(k). 8

Figure 13: Scheme of the experimental catalysis set-up. The gases were mixed by mass flow controllers (mfc) and a 4-way-valve allowed to introduce the acetylene feed or the helium bypass into the reactor. Temperature of the reactor was controlled by two thermocouples. Inside thermocouple measured the catalyst bed temperature and outside thermocouple was used to control the heating power. Two 2-ways-valves downside of the reactor allowed switching the product gas either to the gas analysis equipment or directly to the exhaust gas. 8

Figure 14: Experimental X-ray diffraction patterns of PdGa (b) after grinding in a mortar and (c) after ball milling, together with a simulated pattern of PdGa (a) [62]. 8

Figure 15: Experimental X-ray diffraction patterns of Pd_3Ga_7 (b) after grinding in a mortar and (c) after ball milling, together with a simulated pattern of Pd_3Ga_7 (a) [62]. 8

Figure 16: Experimental and theoretical Pd K edge FT(χ(k)*k^3) of PdGa at 300 K. 8

Figure 17: Experimental and theoretical Pd K edge FT(χ(k)*k^3) of Pd_3Ga_7 at 300 K.....8

Figure 18: Relative mass (TG) (solid) and DSC signal (dotted) during thermal treatment (300 K – 723 K at 6 K/min) of PdGa in 50% hydrogen in helium (left) and in 50% oxygen in helium (right). 8

Figure 19: Relative mass (TG) (solid) and DSC signal (dotted) during thermal treatment (300 K – 693 K at 6 K/min) of Pd_3Ga_7 in 50% hydrogen in He (left) and in 50% oxygen in He (right). 8

Figure 20: Scanning electron microscopy images of ball-milled PdGa before (left) and after (right) heating in 50% hydrogen in helium to 573 K.....8

Figure 21: Scanning electron microscopy images of ball-milled Pd_3Ga_7 before (left) and after (right) heating in 50% hydrogen in helium to 573 K.....8

Figure 22: Evolution of in situ X-ray diffraction patterns measured during thermal treatment of PdGa in 50% hydrogen in helium from 323 K to 723 K. 8

Figure 23: Evolution of in situ X-ray diffraction patterns measured during thermal treatment of PdGa in 20% oxygen in helium from 323 K to 723 K. Additional peaks at 674 K are due to the formation of Pd metal and an unidentified phase. 8

Figure 24: Evolution of in situ X-ray diffraction patterns measured during thermal treatment of Pd_3Ga_7 in 50% hydrogen in helium from 323 K to 693 K. Formation of PdGa at higher temperature is observable (*). ..8

Figure 25: Evolution of in situ X-ray diffraction patterns measured during thermal treatment of Pd_3Ga_7 in 100% helium from 323 K to 693 K. Formation of PdGa at higher temperature is observable (*). 8

Figure 26: Evolution of average domain size of PdGa (left) and Pd_3Ga_7 (right) during thermal treatment in 50% hydrogen in helium obtained from by profile analysis of diffraction lines.....8

Figure 27: Evolution of RDF of PdGa during thermal treatment from 300 K to 723 K in 50% H_2 + 50% He. 8

Figure 28: Evolution of selected relative Pd-Ga and Pd-Pd distances (left) and Debye-Waller factors (right) of selected scattering paths of PdGa during thermal treatment of PdGa in helium from 323 K to 723 K obtained from analysis of the corresponding EXAFS spectra. 8

Figure 29: Evolution of selected relative Pd-Ga and Pd-Pd distances and Debye-Waller factors (right) of selected scattering paths of PdGa during thermal treatment of PdGa in 50% hydrogen in helium from 323 K to 723 K obtained from analysis of the corresponding EXAFS spectra. 8

Figure 30: Evolution of selected relative Pd-Ga and Pd-Pd distances and Debye-Waller factors (right) of selected scattering paths of PdGa during thermal treatment of Pd_3Ga_7 in 50% hydrogen in helium from 323 K to 693 K obtained from analysis of the corresponding EXAFS spectra. 8

Figure 31: Evolution of selected relative Pd-Ga and Pd-Pd distances and Debye-Waller factors (right) of selected scattering paths of PdGa during thermal treatment of Pd_3Ga_7 in 10% acetylene in 20% hydrogen in helium from 323 K to 693 K obtained from analysis of the corresponding EXAFS spectra.....8

Figure 32: XPS data of the Ga $2p^{3/2}$ peak of PdGa (left) and Pd_3Ga_7 (right): (a) untreated, (b) after H_2 treatment at 573 K, (c) after H_2 treatment at 673 K, and (d) after ISS. A shoulder at lower binding energy that corresponds to reduced Ga species is indicated.....8

Figure 33: ISS data of untreated PdGa (first 2 scans) and Pd_3Ga_7 (first 3 scans) and after H_2 treatment at 673 K. Peaks at 1750 eV (Pd) and 1650 eV (Ga) are indicated. 8

Figure 34: CO chemisorption on Pd/Al_2O_3 (5%wt) after hydrogen pre-treatment at 473 K. First adsorption isotherm (combined) contains the chemisorbed and physisorbed part of CO on Pd/Al_2O_3. Second isotherm was measured after evacuation and resulted in the weak isotherm (only physisorbed CO). The difference of combined and weak isotherm can be used for calculation of the chemisorbed part of the CO on Pd/Al_2O_3.....8

Figure 35: Product composition measured during hydrogenation of acetylene on PdGa (50 mg), Pd_3Ga_7 (100 mg), and Pd/Al_2O_3 (0.5 mg) (2% C_2H_2 + 4% H_2, condition A).....8

Figure 36: Conversion (left) and selectivity (right) measured during acetylene hydrogenation on PdGa (50 mg), Pd_3Ga_7 (100 mg), and Pd/Al_2O_3 (0.5 mg) (condition A). 8

Figure 37: Conversion and selectivity of PdGa (50 mg) and of Pd/Al_2O_3 (0.5 mg) in acetylene hydrogenation (isothermal at 393 K under condition A).....8

Figure 38: Conversion and selectivity (together with the selectivity of Pd/Al_2O_3) of untreated (50 mg) and chemically etched (5 mg, pH= 9.8) PdGa in acetylene hydrogenation (condition A). 8

Figure 39: Conversion and selectivity (together with the selectivity of Pd/Al_2O_3) of untreated (50 mg) and chemically etched (15 mg, pH= 10.5) Pd_3Ga_7 in acetylene hydrogenation (condition A).....8

Figure 40: Acetylene conversion and selectivity of PdGa (40 mg), Pd_3Ga_7 (100 mg), Pd/Al_2O_3 (0.15 mg) and $Pd_{20}Ag_{80}$ (200 mg) isothermal at 473 K (condition B). 8

Figure 41: Conversion (left) and selectivity (right) of untreated PdGa (40 mg), PdGa chemically etched at pH= 9.8 (1.5 mg) and pH= 9.0 (5 mg), and $Pd_{20}Ag_{80}$ (200 mg) in acetylene hydrogenation (isothermal at 473 under condition B).....8

Figure 42: Conversion (left) and selectivity (right) of untreated Pd_3Ga_7 (100 mg), chemically etched Pd_3Ga_7 (pH= 10.5, 7 mg), chemically etched Pd_3Ga_7 (pH= 9.0, 13 mg) and $Pd_{20}Ag_{80}$ (200 mg) in acetylene hydrogenation (isothermal at 473 under condition B).....8

Figure 43: Experimental XRD pattern of $PtPd_2Ga_3$: simulated pattern (a) and after ballmilling (b).....8

Figure 44: XRD pattern of $PtPd_2Ga_7$: Simulated pattern (a), experimental pattern after grinding in a mortar (b) and after ballmilling (c).....8

Figure 45: Experimental and theoretical FT(χ(k)*k^3) of $PtPd_2Ga_3$. Dotted lines refer to imaginary part and dashed lines to first five single-scattering paths (3x Ga, 1x Pd and 1x Pt).....8

Figure 46: Evolution of in situ X-ray diffraction patterns of $PtPd_2Ga_3$ during thermal treatment from 323 K to 773 K in 50% H_2 + 50% He. 8

Figure 47: Evolution of in situ X-ray diffraction patterns of $PtPd_2Ga_7$ during thermal treatment from 323 K to 723 K in 50% H_2 + 50% He. Formation of $PtPd_2Ga_3$ at higher temperature is observable (*). 8

Figure 48: Evolution of average domain sizes of PdGa and $PtPd_2Ga_3$ (left) and Pd_3Ga_7 and $PtPd_3Ga_7$ (right) during thermal treatment in 50% hydrogen in helium obtained by profile analysis 8

Figure 49: Product composition measured during hydrogenation of acetylene on $PtPd_2Ga_3$ (60 mg) (2% C_2H_2 + 4% H_2, condition A). 8

Figure 50: Conversion and selectivity measured during acetylene hydrogenation on $PtPd_2Ga_3$ (60 mg), PdGa (50 mg) and Pd/Al_2O_3 (0.5 mg) in 2% C_2H_2 + 4% H_2 (condition A). 8

Figure 51: Conversion and selectivity measured during acetylene hydrogenation on $PtPd_2Ga_7$ (120 mg), Pd_3Ga_7 (100 mg) and Pd/Al_2O_3 (0.5 mg) under reaction condition A. 8

Figure 52: Acetylene conversion and selectivity of $PtPd_2Ga_3$ (40 mg), PdGa (40 mg), Pd/Al_2O_3 (0.15 mg) and $Pd_{20}Ag_{80}$ (200 mg) isothermal at 473 K (condition B). 8

Figure 53: Acetylene conversion and selectivity of $PtPd_2Ga_7$ (100 mg), Pd_3Ga_7 (100 mg), Pd/Al_2O_3 (0.15 mg, only selectivity) and $Pd_{20}Ag_{80}$ (200 mg) isothermal at 473 K (condition B). 8

Figure 54: Rate of C_2H_4 hydrogenation on some metal wires relative to Rh [137]. 8

Figure 55: Experimental X-ray diffraction patterns of $PdSn_2$ (b) after grinding in a mortar and (c) after ball milling, together with a simulated pattern of $PdSn_2$ [65].....8

Figure 56: Experimental and theoretical FT(χ(k)*k^3) of $PdSn_2$. Dotted lines refer to imaginary part and dashed lines to the first five single-scattering paths (3x Sn and 1x Pd).....8

Figure 57: Relative mass (TG) (solid) and DSC signal (dashed) during thermal treatment of $PdSn_2$ in 50% hydrogen in helium (left, 300 K – 723 K at 6 K/min) and in 50% oxygen in He (right, 300 K – 723 K at 6 K/min). 8

Figure 58: Scanning electron microscopy images of ball-milled $PdSn_2$. 8

Figure 59: Scanning electron microscopy images of ball-milled $PdSn_2$ after heating in 50% hydrogen in helium to 573 K. 8

Figure 60: Evolution of X-ray diffraction pattern of $PdSn_2$ during thermal treatment from 323 K to 723 K in 50% H_2 + 50% He. 8

Figure 61: Evolution of average domain size of $PdSn_2$ during thermal treatment in 50% hydrogen in helium obtained by profile analysis of (220) and (312) diffraction lines 8

Figure 62: Evolution of X-ray diffraction pattern of $PdSn_2$ during thermal treatment from 323 K to 723 K in 100% helium.....8

Figure 63: Evolution of selected relative Pd-Sn and Pd-Pd distances and Debye-Waller factors of selected scattering paths of $PdSn_2$ during thermal treatment of $PdSn_2$ in 50% hydrogen in helium from 323 K to 723 K obtained from analysis of the corresponding EXAFS spectra. 8

Figure 64: Evolution of selected relative Pd-Sn and Pd-Pd distances and Debye-Waller factors of selected scattering paths of $PdSn_2$ during thermal treatment of $PdSn_2$ in 10% C_2H_2 + 20% H_2 + 70% He from 323 K to 673 K obtained from analysis of the corresponding EXAFS.....8

Figure 65: Product composition measured during hydrogenation of acetylene on $PdSn_2$ (100 mg) under condition A. 8

Figure 66: Acetylene conversion and corresponding selectivity of chemically etched (NaOH + EDTA) $PdSn_2$ (85 mg), Pd/Al_2O_3 (0.15 mg) and $Pd_{20}Ag_{80}$ (200 mg) isothermal at 473 K (condition B).....8

11.3 List of tables

Table 1: Some physical properties of palladium [15]. 8

Table 2: Crystallographic data of PdGa, Pd_3Ga_7 and $PdSn_2$ [60,62,64,65]....8

Table 3: Coordination of Pd atoms in PdGa, Pd_3Ga_7 and $PdSn_2$. 8

Table 4: Result of EXAFS refinement of PdGa and Pd_3Ga_7 ex-situ at the Pd K-edge. ΔR_c refers to the deviation of the refined interatomic distance to the crystallographic data. 8

Table 5: Surface composition as calculated from XPS data (in atom-%) of untreated PdGa, after hydrogen treatment at 573 K and 673 K, and after ISS. 8

Table 6: Amount of oxidized and metallic Ga at the surface of untreated PdGa and Pd_3Ga_7, and after H_2 treatment as calculated from a Ga $2p^{3/2}$ XPS peak refinement (in atom-%). 8

Table 7: Acetylene conversion and corresponding selectivity of untreated and chemically etched PdGa, Pd_3Ga_7, Pd/Al_2O_3 and $Pd_{20}Ag_{80}$ after 20 h at 473 K under condition B. 8

Table 8: Crystallographic lattice constants of PdGa [61], Pd_3Ga_7 [62], PtGa [61] and Pt_3Ga_7 [136] from literature and obtained by refinement of experimental XRD pattern in Å. Lattice constants of the ternary Pt-Pd-Ga intermetallic compounds were calculated by assuming of the validity of Vegard's law. 8

Table 9: Results of EXAFS refinement of $PtPd_2Ga_3$ and $PtPd_2Ga_7$. ΔR_c refers to the deviation of refined interatomic distances to crystallographic data of PdGa and Pd_3Ga_7. 8

Table 10: Acetylene conversion and corresponding selectivity of Pt-Pd-Ga and Pd-Ga intermetallic compounds compared with references Pd/Al_2O_3 and $Pd_{20}Ag_{80}$ after 20 h time on stream at 473 K (condition B). 8

Table 11: Result of EXAFS refinement of $PdSn_2$ at the Pd K-edge measured at 300 K in air. ΔR_c refers to deviation of refined interatomic distances to crystallographic data [65]. 8

11.4 Publications

11.4.1 Patent application

Jürgen Osswald, Rainer Giedigkeit, Marc Armbrüster, Kirill Kovnir, Rolf E. Jentoft, Thorsten Ressler, Yuri Grin, Robert Schlögl:

Palladium-Gallium Intermetallic Compounds as Catalysts for the Selective Hydrogenation of Acetylene.

Submitted to European Patent Office 2006

11.4.2 Publications

Jürgen Osswald, Rainer Giedigkeit, Kirill Kovnir, Rolf E. Jentoft, Marc Armbrüster, Thorsten Ressler, Yuri Grin, Robert Schlögl:

Pd-Ga Intermetallic Compounds: Active-Site Isolation for the Selective Hydrogenation of Acetylene.

Angewandte Chemie – International Edition, in preparation

Jürgen Osswald, Rainer Giedigkeit, Rolf E. Jentoft, Marc Armbrüster, Frank Girgsdies, Kirill Kovnir, Thorsten Ressler, Yuri Grin, Robert Schlögl:

Palladium Gallium Intermetallic Compounds for the Selective Hydrogenation of Acetylene, Part I: Preparation and Structural Investigation Under Reaction Conditions.

Journal of Catalysis, ready for submission

Jürgen Osswald, Kirill Kovnir, Marc Armbrüster, Rainer Giedigkeit, Rolf E. Jentoft, Ute Wild, Thorsten Ressler, Yuri Grin, Robert Schlögl:

Palladium Gallium Intermetallic Compounds for the Selective Hydrogenation of Acetylene, Part II: Surface Characterization and Catalytic Performance.

Journal of Catalysis, ready for submission

Jürgen Osswald, Kirill Kovnir, Marc Armbrüster, Rolf E. Jentoft, Yuri Grin, Robert Schlögl, Thorsten Ressler:

$PdSn_2$ – an active-site isolated intermetallic compound for selective hydrogenation of acetylene.

Catalysis letters, in preparation

Jürgen Osswald, Rainer Giedigkeit, Kirill Kovnir, Marc Armbrüster, Rolf E. Jentoft, Thorsten Ressler, Yuri Grin, Robert Schlögl:

Ternary Pd-Pt-Ga Intermetallic Compounds for the Selective Hydrogenation of Acetylene

Catalysis letters, in preparation

11.4.3 Oral presentations

Jürgen Osswald, Rainer Giedigkeit, Kirill Kovnir, Marc Armbrüster, Rolf E. Jentoft, Yuri Grin, Robert Schlögl, Thorsten Ressler:

Structural and Catalytic Investigation of Active-Site Isolation in Pd-Ga Intermetallic Compounds.

19. North American Meeting of the North American Catalysis Society, Philadelphia, 22.-27.05.05

Jürgen Osswald, Rainer Giedigkeit, Kirill Kovnir, Rolf E. Jentoft, Marc Armbrüster, Yuri Grin, Robert Schlögl, Thorsten Ressler:

Structural and Catalytic Investigation of Active-Site Isolation in Pd-Ga Intermetallic Compounds

EuropaCat VII, Sofia, 28.08.-01.09.05

Zhong Zhao, Andreas Männig, Dirk Rosenthal, Jürgen Osswald, Sven L.M. Schroeder, Klaus Christmann, Hubert Rauscher und Rolf-Jürgen Behm:

Structure and thermal stability of TiO_x films on Ru(0001) and Au/TiO_x/Ru(0001) model catalysts.

Frühjahrstagung der Deutschen Physikalischen Gesellschaft, Dresden, 24.-28.03.03

11.4.4 Reports

Jürgen Osswald, Rainer Giedigkeit, Marc Armbrüster, Rolf E. Jentoft, Frank Girgsdies, Yuri Grin, Robert Schlögl, Thorsten Ressler:

Structural and Catalytic Investigation of Active-Site Isolation in Pd-Ga and Pd-Sn Intermetallic Compounds.

Hasylab Jahresbericht 2004, Hamburger Synchrotronstrahlungslabor HASYLAB at Deutsches Elektronen-Synchrotron DESY, p. 537-538.

Jürgen Osswald, Rolf E. Jentoft, Frank Girgsdies, Rainer Giedigkeit, Yuri Grin, Robert Schlögl, Thorsten Ressler:

Structural and Catalytic Investigation of Palladium-Gallium Intermetallic Compounds.

Hasylab Jahresbericht 2003, Hamburger Synchrotronstrahlungslabor HASYLAB at Deutsches Elektronen-Synchrotron DESY, p. 443-444.

11.4.5 Poster

XXXVIII. Jahrestreffen Deutscher Katalytiker, Weimar, 16.-18.03.05

Hamburger Synchrotronstrahlungslabor HASYLAB – Usermeeting 2005

13. International Congress on Catalysis, Paris, 11.-16.07.04

XXXVII. Jahrestreffen Deutscher Katalytiker, Weimar, 17.-19.03.04

Hamburger Synchrotronstrahlungslabor HASYLAB – Usermeeting 2004

GDCh-Jahrestagung Chemie, München, 06.-11.10.03

12th International Conference on X-ray Absorption Fine Structure; Malmö, 22.-27.06.03

11.5 Acknowledgement / Danksagung

Die vorliegende Arbeit wurde vom Oktober 2002 bis Dezember 2005 in der Abteilung Anorganische Chemie des Fritz-Haber-Institutes der Max-Planck-Gesellschaft unter Leitung von Prof. Dr. R. Schlögl und Prof. Dr. T. Ressler angefertigt.
Ich möchte allen danken, die zum Gelingen dieser Arbeit beigetragen haben.
Insbesondere bedanke ich mich bei:

Prof. Dr. Robert Schlögl
Prof. Dr. Thorsten Ressler
Dr. Rolf. E. Jentoft
Dr. Kirill Kovnir
Dr. Frank Girgsdies
Rainer Giedigkeit
Dr. Marc Armbrüster
Prof. Dr. Y. Grin
Edith Kitzelmann
Eva Rödel
Dr. Benjamin Kniep
Dr. Alexandara Szizybalski
Ute Wild
Jutta Kröhnert
Dr. Genka Tzolova-Müller
Gisela Weinberg

ganz besonderen Dank gilt meiner Frau Elena und meinen Eltern.